Corneal epithelial cell responses to tensile stress and compressive stress

by

Yiran Zhou

A thesis

presented to the University of Waterloo

in the fulfillment of the

thesis requirements for the degree of

Master of Applied Science

in

Chemical Engineering

Waterloo, Ontario, Canada, 2020

AUTHOR'S DECLARATION

This thesis consists of material all of which I co-authored or contributed: see Statement of Contributions included in the thesis. This is a true copy of the thesis, including any required final revisions, as accepted by my examiners.

I understand that my thesis may be made electronically available to the public.

Statement of contributions

Sections 2.1.1 and 2.1.2 of this thesis are co-authored with Mr. Young Ju Son, Mr. John W. Tse, and Mr. Wei Mao as a review paper. Sections 3.2 and 4.2 are issue from collaborative with Ms. Moyosoluwa Akinbola, Ms. Shimona Esmail, Ms. Uchenna Mbanefo and Ms. Taniya Sebastiampillai from University of Waterloo when I mentored their Capstone project in Professor Yim's lab. In section 3.2 where the cell stretcher design is presented, I selected the reference cell stretcher model and provided dimensions needed for the cell stretcher. The Capstone group helped in drawing SolidWork images used for 3D printing. In section 4.2 presenting the fluidic cell stretcher calibration, I led the Capstone group in assembling the device and taking images. Images were analyzed by the Capstone group. In section 4.2 presenting the electric cell stretcher calibration, preliminary work was done by Johnathan Rasmussen, a former master student co-supervised by Professors Gorbet and Yim. He contributed to the stretcher assembly and wrote the codes used to control the electric cell stretcher.

Citation for section 2.1.1 and 2.1.2: Y. J. Son, J. W. Tse, Y. Zhou, and W. Mao, "Biomaterials Science Biomaterials and controlled release strategy for epithelial wound healing," Biomater. Science, vol. 7, pp. 4444–4471, 2019.

Abstract

Eye rubbing is a commonly adopted habit that is frequently happening in our daily life. However, the mechanical stress generated by long term chronic abnormal eye rubbing could lead to keratoconus (KC) with the symptoms of central protrusion, high astigmatism and impaired vision, affecting 57-229/100,000 people in their twenties to forties in Asians and Caucasian population. Therefore, ophthalmologists have advised people to avoid eye rubbing to prevent KC. To better understand why eye rubbing could lead to KC, researchers have attempted to investigate corneal change under mechanical stress. However, there are two limitations in the current work: (1) the lack of a mechanical system which can simulate eye rubbing stress; (2) the lack of study on human corneal epithelial cells (HCEpCs) behavior under mechanical stimuli.

To solve these challenges, we designed three models to mimic eye rubbing generated stress. The actual eye rubbing stress can be divided into in-plane tensile stress, out-of-plane- compressive stress and shear stress. To study the effect of tensile stress on HCEpCs, two customized cell stretchers were fabricated: a fluidic stretcher and an electric stretcher. The stretchers were designed to enable HCEpCs culture on a stretchable membrane or mounting of a cornea tissue, both of which can be stretched under control. The cell culture chamber size was designed to be 1cm in diameter, similar to that of human cornea. This is of great importance because it enables better mimicking of the corneal microenvironment. Calibration and cell viability test were conducted on the fabricated cell stretchers. Our results showed that the lab-built fluidic cell stretcher and electric cell stretcher were able to apply tensile stress on the cell culture membrane with the control of air pressure and linear actuator, respectively. The HCEpCs seeded on cell membrane showed altered cell viability after stretching, indicating cell response to in-plane tensile stress.

To investigate how compressive stress could contribute to the development and progression of KC, a customized polydimethylsiloxane (PDMS) stamp was used to introduce compressive stress to HCEpCs. Different cyclic compressive stress (0 N/cm^2, 0.03 N/cm^2, 0.05 N/cm^2, 0.10N/cm^2 before forming tight junction and 0 N/cm^2, 50.03 N/cm^2, 0.93 N/cm^2 after forming tight junction, a 3-minute compression was applied every 30 minutes twice and then repeated one hour later) were applied on HCEpCs monolayer. Cell behavior including cell viability, apoptosis, cytoskeleton rearrangement and cellular tight junction (Zonula occludens-1, ZO-1) expression were characterized. Cell viability and cell apoptosis analyses were conducted to determine whether the cells were alive or dead and whether they were going through programmed death, respectively. Cytoskeleton rearrangement was conducted by staining F-actin, a filamentous protein indicating how the cells would remodel themselves in response to mechanical stimuli. ZO-1 is an important protein for cellular adhesion and cell barrier function. Our results revealed that HCEpCs were sensitive to out-of-plane compressive stress in that increased cell death rate and apoptosis, change in cell membrane permeability, rearranged F-actin and loss of ZO-1 were observed under compression. Additionally, ZO-1 could protect HCEpCs against compressive stress. This was proved by the finding that 9 times higher loading could be tolerated for ZO-1-expressing cells compared with the cells without ZO-1 and cell membrane stability was also maintained by ZO-1-expressing cells upon compression.

Our results provide *in vitro* evidence on the potential impacts from rubbing-related stress, and may shed light on understanding and prevention of keratoconus.

Acknowledgements

I would like to thank my supervisors, Associate Professor Evelyn Yim, and Associate Professor Maud Gorbet, for their enormous support and advice throughout my Master study. Their patience and trust are what kept me motivated to obtain the best possible outcome in my research.

I would like to also thank the group members in Yim lab and Gorbet lab for their help in research setup and advice. Especially, thank you to John for his mentorship on lab skills and for his help with reviewing cornea anatomy. Thank you to Johnathan Rasmussen and Yejin Jeong for their help in designing and understanding the code needed for controlling the electric cell stretcher. Thank you to Adrian Chee and Yejin Jeong for their help in 3D printing the fluidic cell stretcher mold's prototype. Thank you to Aung Moe Zaw, Yuan Yao, Sabrina Mattiassi, Sarah Wenhui Chan, Deepak Jain for help with lab organization and cleaning.

I would like to also thank Moyosoluwa Toluwalope Akinbola, Shimona Esmail, Taniya Sebastiapollai and Uchenna Mbanefo for designing the mechanical devices used in this thesis.

And thank you to my families who have encouraged me in overcoming difficulties during the study.

Table of Contents

List of Figures

List of tables

List of Abbreviations

KC: Keratoconus

HCEpCs: Human corneal epithelial cells

CEpCs: Corneal epithelial cells

PDMS: Polydimethylsiloxane

ZO-1: Zonula occludens-1

CHAR: Chronic abnormal eye rubbing

MMPs: Matrix metalloproteinases

ECM: Extracellular matrix

TIMP: Tissue inhibitor metalloproteinase

IL: Interleukin

TNF: Tumor necrosis factor

IOP: Intraocular pressure

CH: Corneal hysteresis

CRF: Corneal resistance factor

AFM: Atomic force microscopy

ORA: Ocular Response Analyzer

ICRS: Intra corneal rings segment

IOL: Intraocular lens

PRK: Photorefractive keratectomy

CXL: Collagen crosslinking

PKP: Penetrating keratoplasty

DLK: Deep lamellar keratoplasty

CH: Corneal hysteresis

CRF: Corneal resistance factor

YAP/TAZ: Yes-associated protein/transcriptional coactivator with PDZ-binding motif

TGF-β: Transforming growth factor-β

LEC: Limbal epithelial cells

FEM: Finite element method

EthD-1: Ethidium Homodimer-1

PFA: Paraformaldehyde

TCPS: Tissue culture polystyrene

HPV: Human papillomaviruses

FAM: fluorochrome

FLICA: Fluorochrome-Labeled Inhibitors of Caspases

1.0 Introduction

The cornea is responsible for 70 % of the eye's refractive power as well as protecting the underlying structures from the external environment and preventing pathogens from entering [1]. As is the anterior most portion of the eye, the cornea is most susceptible to external damages including mechanical stimuli, chemical irritation, and ultraviolet exposure. Mechanical stimuli applied on the cornea have been thought to be one of the leading causes of corneal aberration due to its common sources including eye rubbing [2], contact lens wearing [3], and trauma [4].

Either too long or too often repetitive mechanical stimuli have been shown to be a contributing factor of several cornea-related diseases such as keratoconus (KC), which is characterized by corneal degeneration with corneal thinning and protrusion, leading to high myopia, irregular astigmatism and other impaired vision. Among various sources of mechanical stimuli, chronic abnormal eye rubbing (CHAR) has been determined to be a crucial risk factor to KC [5]. Research has found that over half of KC patients have CHAR habits [6] and avoiding eye rubbing has been adopted by several ophthalmologists as clinical management to prevent KC [7]. Several clinical studies have demonstrated that eye rubbing could trigger several keratoconus-related symptoms including increased release of protease and inflammatory markers, resulting in the degradation of collagen fibrils in the stroma and thinning of the cornea with altered corneal mechanical properties in terms of decreased rigidity, stress or strain to failure and hysteresis [8], [2], [9], [10].

Eye-rubbing results in different kinds of mechanical stresses applied on the cornea and comprises in-plane shear stress, tension, and out-of-plane compressive stress [11]. Although the effect of eye-rubbing on the cornea has been investigated clinically, the understanding of how human corneal epithelial cells (HCEpCs) respond to different kind of mechanical stress still remains poor due to the lack of systematic investigation on epithelial behavior under rubbing-related mechanical stress and the lack of a mechanical model to simulate rubbing stress on HCEpCs. Such investigation will be of great significance to understand the pathogenesis of KC and to provide evidence for clinical prevention management.

Our research team hypothesized that eye rubbing related mechanical stimuli including tensile stress and compressive stress could lead to changes in epithelial cell behaviors, which will in turn contribute to keratoconus-progression. In order to understand the effect of mechanical stress in the formation and progression of KC *in vitro*, I aim to build lab-based mechanical stretching system and compressive system to introduce in-plane tensile stress and out-of-plane compressive stress to HCEpCs and characterize HCEpCs response under those stresses.

1.1 Objective and Research Question

This thesis focuses on the hypothesis whether mechanical forces generated by eye rubbing would affect corneal epithelial cell behavior. According to several pathologists' claims that eye rubbing is a main risk factor to KC due to the commonly adopted habit of CHAR in KC patients, we hypothesize that the mechanical forces generated in eye rubbing process stimulate changes in corneal epithelial cells, which can contribute to the onset and progression of KC. Specifically, the corneal deformations caused by in-plane tensile stress and out-of-plane compressive stress arising from eye rubbing could lead to a

keratoconus-like phenotype in HCEpCs.

Based on this research question, this thesis can be divided into two aims:

(a) Aim 1: Design of cell stretching system and characterization of cell response to in-plane tensile stress

Previous research lacks a standard mechanical system that can introduce tensile stress to cultured corneal cell monolayer, and mimic elements of the eye rubbing stress applied on corneal epithelium to observe *in vitro* corneal epithelial cell mechanoresponse. It is also important to keep the cell culture container dimension similar to that of human cornea (which is around 1cm in diameter) to better mimic eye rubbing process. Hence, it is necessary to build a customized cell stretching system. In this thesis, two cell stretchers were built using two different approaches to investigate corneal response upon tensile stress: a fluidic cell stretcher and an electric cell stretcher. As part of this work, I led a Capstone group, in the design and fabrication of a fluidic cell stretcher and an electric cell stretcher. The calibration of the fluidic cell stretcher was completed together with the Capstone group, and the preliminary calibration of the electric cell stretcher was performed by another master student in our group, who drafted the code for controlling the device and developed the method for detecting membrane deformation.

(b) Aim 2: Design of cell compressing system and characterization of cell response to out-of-plane compressive stress

Another aspect of eye rubbing related stress is out-of-plane compressive stress. In the present study, I built a compressing system which could apply loading on cell monolayer. Specifically, two studies with compressive stress were performed: 0 N/cm^2, 0.03 N/cm^2, 0.05 N/cm^2 and 0.10 N/cm^2 for HCEpCs before forming tight junction; and 0 N/cm^2, 0.52 N/cm^2 and 0.93 N/cm^2 for HCEpCs layer with tight junction. HCEpCs response to compressive stress was characterized. Specifically, cell viability, cell apoptosis, cytoskeleton arrangement and ZO-1 expression were assessed after compression.

2.0 Background

2.1 The Cornea

The anterior chamber of the eye is in the front part of the eyeball. The cornea is the outmost layer of the anterior chamber which is in direct contact with tear film on the anterior /external surface. The cornea is an avascular tissue and consists of three cellular layers with two non-cellular layers in between. Both the cellular and non-cellular components are responsible for maintaining the physiological activity and biomechanical properties of the cornea.

2.1.1 Structure of the cornea

The cornea can be further divided into epithelium, Bowman's membrane, stroma, Descemet's membrane, and the corneal endothelium [12], [13] as shown in Figure 1 A.

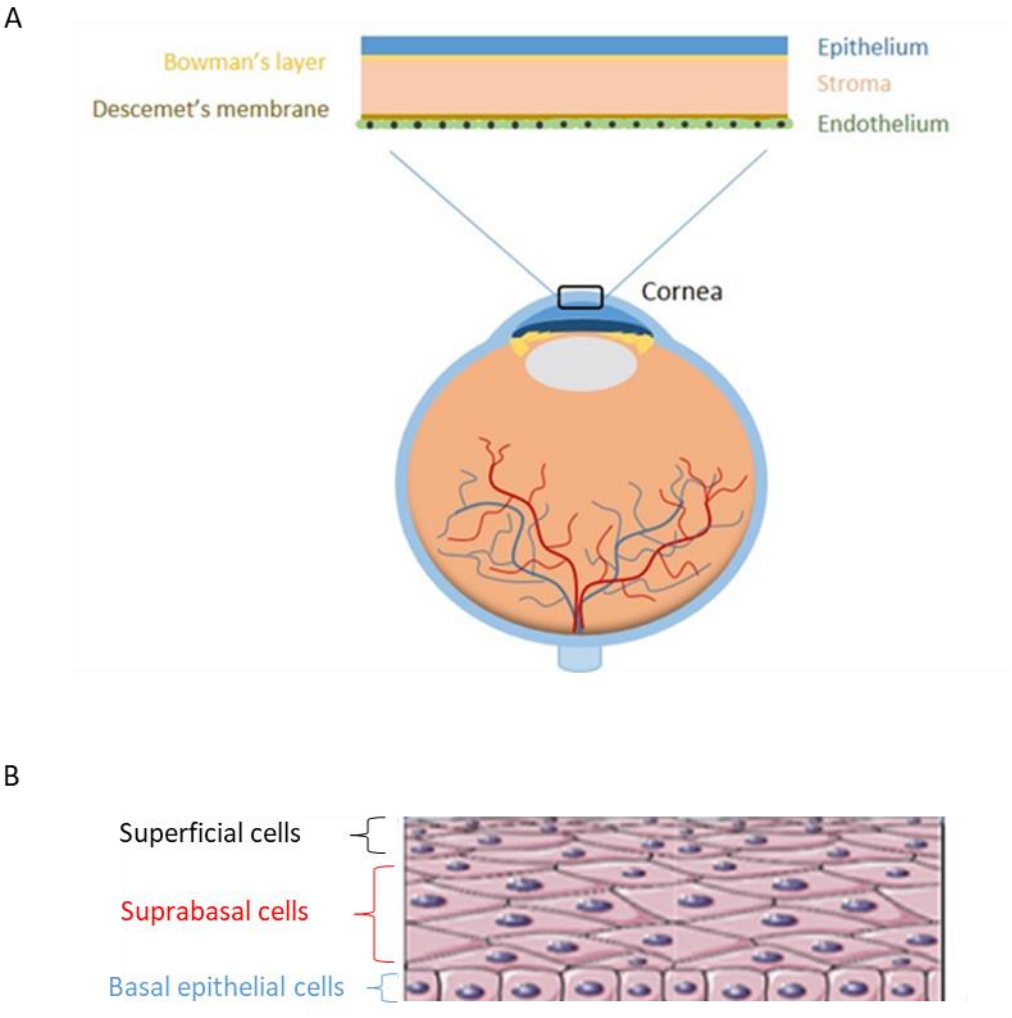

Figure. 1 Diagram of cornea and corneal epithelium.

A, Structure of the cornea [14]. B, Structure of corneal epithelium [15].

The corneal epithelium consists of 5-6 layers of three types of epithelial cells (Figure 1 B) [12]. Moving anteriorly from the Bowman's basement membrane, one layer of columnar basal epithelial cells is

attached to the Bowman's membrane, with 2-3 layers of suprabasal or wing cells above the basal cells, and the outermost layer is comprised of 2-3 layers of superficial squamous cells [13]. Basal cells secrete the necessary components for the formation of the underlying basement membrane called the Bowman's membrane to which they are attached via hemidesmosomes, multiprotein complexes facilitating epithelial cell adhesion [16][17]. The basal cells are the only cells which possess mitotic activity in the corneal epithelium and are the source of both the suprabasal and superficial cells [12]. Above the basal cells and underneath the superficial cells are the suprabasal cells, or wing cells (based on their wing-like appearance). The cells are attached through interdigitations and are linked through desmosomes, gap junctions and adherens junctions. Interdigitations are finger-like-protruded cell membrane foldings which stabilize the cellular adhesion [18]. Desmosomes are junctional complexes providing cellular adhesion [17]. Gap junctions are intercellular cell membrane connections allowing the transportation of ions and metabolites [19]. Adherens junctions are intercellular proteins that are significant for cell adhesion and barrier function [20]. The suprabasal cells are in an intermediate state of differentiation between the basal and superficial cells. The superficial corneal epithelial cells are flat and polygonal terminally differentiated cells that are in direct contact with the tear fluid, which provides nutrients and removes wastes from the cornea. To maximize the uptake of oxygen and nutrients in the tear fluid, each of these cells are covered with microvilli for increased surface area.

The corneal stroma, which is posterior to the Bowman's membrane, constitutes approximately 85 % - 90 % thickness of the cornea, and about 70 % of the corneal dry weight [21]–[23]. The corneal stroma is a controlled three-dimensional structure composed of collagen lamellae with a diameter of 0.2-2.5 nm which consist of transversely oriented collagen fibrils of 25-35 nm diameter (Figure 2 A) [24]. The small diameter and highly organized structure of the collagen fibrils are essential for the transparency of the corneal stroma. The density and alignment of collagen fibrils have been shown to differ in both axial direction and radial direction [25], [26]. The anterior stroma has been shown to be more intertwined than the posterior stroma [25]. Collagen fibers are well aligned with an orthogonal organization in the central area while aligned circumferentially in the limbal area (Figure 2 C) [26]. Various collagen molecules are known to exist in the corneal stroma by either forming collagen fibrils or binding the fibrils together. Collagen type I, type III, type V are found to form human stromal fibrils, while collagen type VI and type XII are found to be non-fibril forming collagens [27]. In addition to collagen, proteoglycans are also believed to play a role in maintaining the structural properties of the stroma by regulating the diameter and spacing of collagen fibrils [28]. Keratocytes, as the main cell type in corneal stroma, are populated parallel to collagen lamellae (Figure 2 B). They are capable of secreting collagen molecules and matrix metalloproteases (MMPs) [29]. The integrity and stability of the corneal stroma are maintained with a regular turnover of keratocytes every 2-3 years [30]. Apart from the maintenance of stromal structure, some studies have found that keratocytes may contribute to the transparency of the cornea by minimizing the refractive index inhomogeneities [31]. The corneal stroma lacks blood and lymphatic vessels; it contains a dense network of autonomic and sensory nerve fibers that do not have myelin sheaths in the central corneal axons [29], [32]. These features also contribute to the transparency of the cornea.

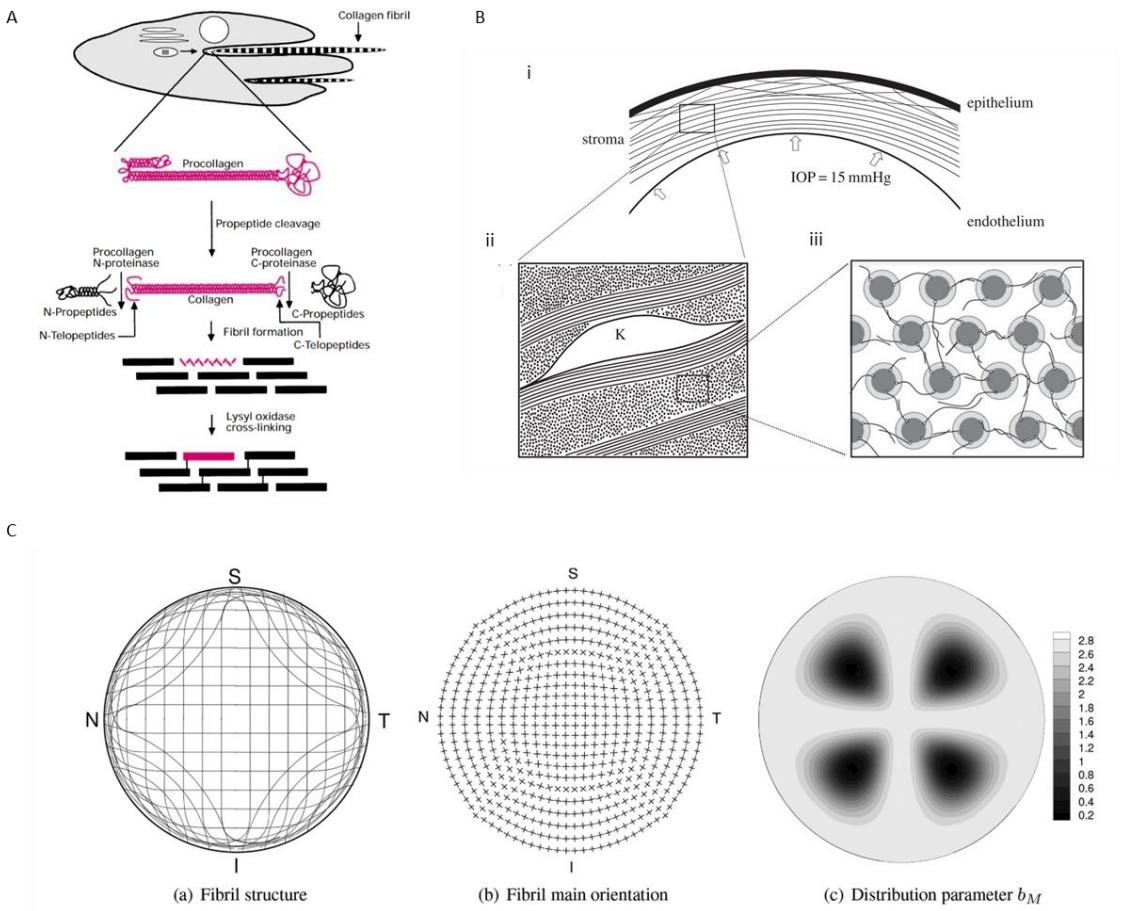

Figure. 2 Collagen lamellae in the cornea.

A, Expression of collagen fibrils and formation of fibril bundle (collagen lamellae) [33]. B, Orientation of collagen lamellae in the stroma (i), the interaction of collagen lamellae and keratocytes (ii) and the linkage between lamellae (iii) [34]. (C), Structure, orientation and distribution of collagen lamellae in the cornea [26].

The endothelium is a cell monolayer that rests on the posterior side of cornea attaching Descemet's membrane which is responsible for the regulation of cornea hydration [35] so as to maintain transparency of the cornea by keeping structural integrity [36]. Unlike other cell types in cornea, the corneal endothelium doesn't recover well from injuries such as immunologic rejection due to highly limited mitotic activity [37].

Bowman's membrane and Descemet's membrane are the two non-cellular layers in the cornea serving as barriers for separating epithelium, stroma and endothelium, and are believed to play a role in keeping the normal metabolic activity of the three cell types [38] as well as in maintaining the rigidity of cornea [11].

2.1.2 Molecules secreted in corneal microenvironment

Multiple molecules secreted by epithelial cells, stromal keratocytes and endothelial cells including matrix metalloproteinases (MMPs), protease inhibitors and pro-inflammatory cytokines act collaterally in maintaining the integrity of the cornea. MMPs, mainly secreted by epithelial cells and stromal

keratocytes, are a group of endo-peptidases that can degrade extracellular matrix (ECM) and induce keratocyte apoptosis. Several groups of MMPs have been detected in the corneal matrix including gelatinases (MMP-2 and -9), collagenases (MMP-1 and -13), and stromelysins (MMP-3, -10, and -11) [39]. Protease inhibitors such as tissue inhibitor metalloproteinase (TIMP) can inhibit the activity of MMPs [40]. The balance of MMPs/TIMP is crucial in keeping the right amount of ECM and keratocytes in the cornea and an imbalance has been found to be related to several diseases such as keratoconus [39]. Pro-inflammatory cytokines include interleukin 1, 6 (IL-1, 6) [41], [42] and tumor necrosis factor alpha (TNF-α) [43] acting as modulator of cell growth, death and differentiation. IL-1 and its receptor are produced by the corneal epithelium, stromal keratocytes and endothelium [44]. The presence of IL-1 can stimulate the expression of IL6 in human corneal epithelial cells and stromal keratocytes [44]. The IL-6 receptor is mainly expressed by corneal epithelial cells [45]. TNF-α and TNF-α receptors have been postulated to be secreted by all three cell types in the cornea [46].

2.1.3 Biomechanical properties

Corneal biomechanical properties is thought to be essential for resisting intraocular pressure (IOP), thus maintaining corneal curvature, corneal shape stability and sensitivity to curvature change upon stimuli [47][48]. The cornea itself is a viscoelastic material [49]. Each component of the cornea contributes to its biomechanical properties. As the thickest layer, the stroma mainly defines the biomechanical strength of the cornea [11], thereby changes in the number and distribution of stromal collagen lamellae lead to altered corneal biomechanical properties. Due to the special alignment of stromal collagen fibrils stated above, the central part of stroma is usually strongest under pressure [50]. However, in abnormal conditions such as keratoconus, the central stroma is thinned and shows altered biomechanical properties [8]. Bowman's membrane and Descemet's membrane accounts for 20 % of corneal bending rigidity [11]. The epithelium and endothelium do not contribute directly to the cornea biomechanical properties, instead, they regulate corneal biomechanical strength by modulating hydration [47].

Several parameters have been adopted clinically as an indicator of corneal biomechanical strength. These mainly include Young's modulus (or elastic modulus), corneal hysteresis (CH), corneal resistance factor (CRF) [49]. The *ex vivo* testing of corneal Young's modulus can be measured with tensile testing [48], atomic force microscopy (AFM) [51] and bulging-induced inflation test [52]. Among the five layers, epithelium accounts for the minimum impact on elastic modulus whereas Bowman's layer and Descemet's membrane contribute most to corneal elasticity [51], [53]. It has been found that the stroma is heterogeneous giving that its elasticity decreases from the anterior to posterior location [25]. CH and CRF can be measured with the Ocular Response Analyzer (ORA) in which air-pulsed pressure is applied to the cornea. The cornea is flattened during the inward applanation and outward applanation as a response to the pressure. The pressure leading to the two applanations is due to the viscoelasticity of the cornea. CH and CRF are calculated by the pressure difference of the two applanations or the pressure difference with a corrected value [49], [54].

Research has shown that weakened cornea is present in corneal degenerative diseases, such as keratoconus (KC), in which elastic modulus, CH and CRF are significantly lower compared to those in healthy cornea. The altered mechanical properties are believed to weaken the cornea so that it cannot hold IOP, thus inducing a conical distension of the cornea in KC [55].

2.2 Keratoconus

Keratoconus (KC) is a corneal disorder characterized by localized corneal thinning and protrusion where the cornea is weakened and fails to resist intraocular pressure. Keratoconus cornea often manifests itself as a conical shape and is usually associated with some visual problems such as myopia and high astigmatism [39].

2.2.1 Epidemiology

Other than some rare congenital cases, KC is typically discovered during puberty and will progress steadily until patients' forties before arrest [39]. KC affects both genders and all ethnicities. While there's no gender preponderance, some studies have reported a higher prevalence of KC in Asian people compared with Caucasians [56], [57]. The prevalence and incidence of KC has been calculated to be 57-229/100,000 and 4.5-19.6/100,000, respectively in Asian and Caucasian population [57]–[59].

2.2.2 Aetiology and risk factors

It has been proposed that KC is caused by genetic disposition [60], [61], biochemical alteration [62] and mechanical stimuli [2]. The effect of mechanical stimuli has arisen researchers' interest over the past few decades due to the evidence of chronic corneal injuries induced in KC. The common practice leading to chronic corneal injury, eye rubbing, has been observed in KC patients and is believed to be one of the most common risk factors of KC by ophthalmologists [2], [5].

2.2.3 Clinical features and treatments

Ocular symptoms of KC are highly variable depending on the stages and severity of the disease [63]–[65]. Three main stages have been proposed with increasing severity: subclinical (initial), moderate and severe [39]. In the subclinical stage, no symptoms are experienced by the patient. Diagnosis may be made with the test of corneal topography when increased keratometry and densitometry are detected, indicating steepened corneal curvature and decreased cell density, respectively [66]. The disease is often noted at a progressed stage when the patient presents irregular astigmatism and decreased vision acuity which can no longer be compensated for with spectacle [67]. Moderate stage often manifests single or combination of *Fleischers' ring* and *Vogt's striae*. The former is characterized with a circle line on the cornea base due to corneal curvature change resulting from iron accumulation and deposition from the tear film [68]; the latter is a feature with the presence of vertical lines caused by compression of the Descemet's membrane [69]. Other signs accompanying the progression of KC may include dryness [70], increased corneal nerves [71], corneal opacity [72], and subepithelial fibrillary lines [73]. In severe stages, common symptoms might show as *Munson's sign*, *Rizzutis sign*, and Hydrops. *Munson's sign* is a V-shaped distortion of the lower lid [74]. *Rizzutis sign* is bright reflection of the nasal limbus [74]. Hydrops is an acute stromal oedema caused by breakage of Descemet's membrane and can induce temporary vision loss [75].

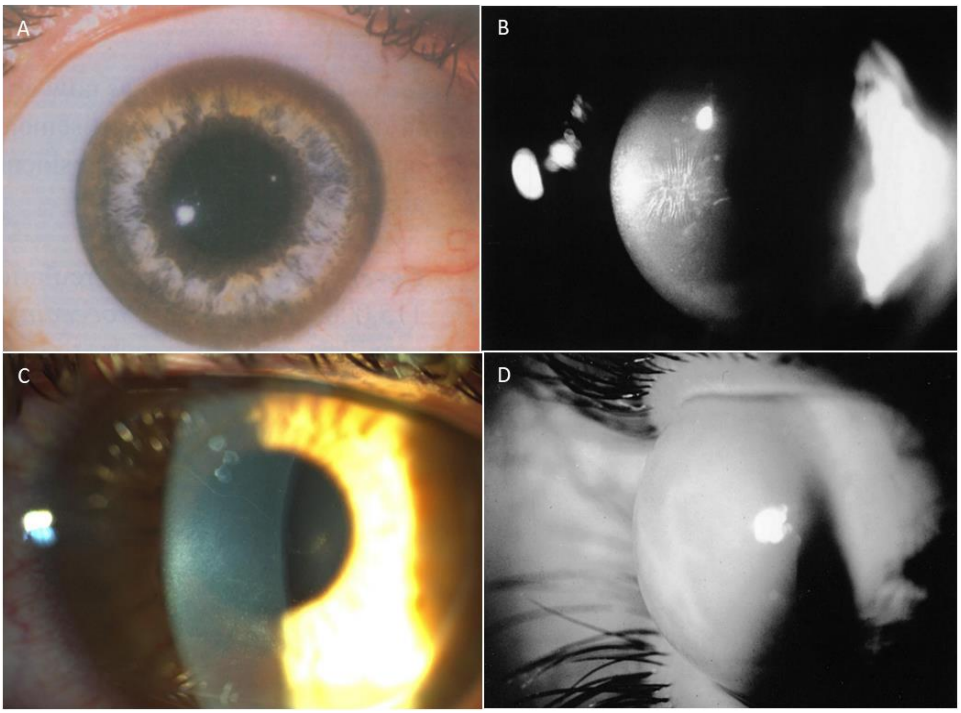

Figure. 3 Clinical features of keratoconus.

A, *Fleischers' ring* [76]. B, *Vogt's striae* [39]. C, Increased corneal nerves [77]. D, hydrops [39].

Treatments for keratoconus vary according to severity of the disease. For the subclinical stage of KC, spectacles are usually applied for vision correction. As the disease progresses to moderate stage when spectacles will still suffice, customized contact lenses would be the ideal option to achieve vision acuity because they allow to adjust the distorted corneal curvature. For others who cannot tolerate contact lens, surgeries such as implantation of intra corneal rings segment (ICRS) [78], [79] or intraocular lens (IOL) [80], photorefractive keratectomy (PRK) [81] and collagen crosslinking (CXL) [82] may be considered. In the most severe cases of KC, a cornea graft may be the only effective treatment.

2.2.4 Changes in KC cornea

Researchers have found that several structural and molecular changes are associated with the formation and progression of KC, which would lead to altered biomechanical properties of the cornea. The structural changes occur in both cellular and non-cellular component of the cornea, including epithelium deformities [83], reduced stroma thickness [83]–[85], rupture of the endothelium [86], breaks in Bowman's membrane [87], and Descemet's membrane damage [87]. These abnormalities have been suggested to be caused by molecular changes including altered enzyme expression and pro-inflammatory markers expression together with oxidation accumulation. As a result, the cornea is weakened, showing cellular degeneration, delayed wound healing activity and decreased mechanical strength, which eventually lead to its central protrusion [88]–[90].

2.2.4.1 Structural changes

Epithelium deformities accompanying heterogeneous thickness [91]–[94], cellular morphological changes [95], decreased cell density [66], cell barrier disruption [82], [96], cytoskeleton changes [97]

have been discovered in KC cornea. Epithelium irregularity has been found in KC cornea; however, contradictory results have been shown with change in epithelium thickness. Some studies reported thinned epithelium in KC patients [91], [92] whereas others have found a thickened epithelium [93], [94]. Confocal images revealed elongated epithelial superficial cells in a whorl-like manner [95] and enlarged basal epithelial cells [98] in KC cornea. Decreased epithelial cell density in the center area of cornea has also been observed as a result of increased cell apoptosis and cell death [66]. Furthermore, the loss of epithelial cells is often irreversible because the differentiating and proliferating activity of basal epithelial cells is limited in KC cornea [83]. Together with the reduced cell density, the epithelial cell barrier has also been found to be disrupted with the evidence that Zonula occludens-1 (ZO-1), a protein contributing to cellular tight junctions, has been found to be decreasingly expressed or even absent in adjacent epithelial cells in the cone area of KC cornea [56], [96]. Although not intensively investigated, the cytoskeleton has been proposed to change in KC corneal epithelial cells as the gene of several cytoskeleton components, such as α_1-actinin, α_1-tropomyocin, tropomyosin-binding protein troponin T1 and α_3-tubulin show an increased expression [97].

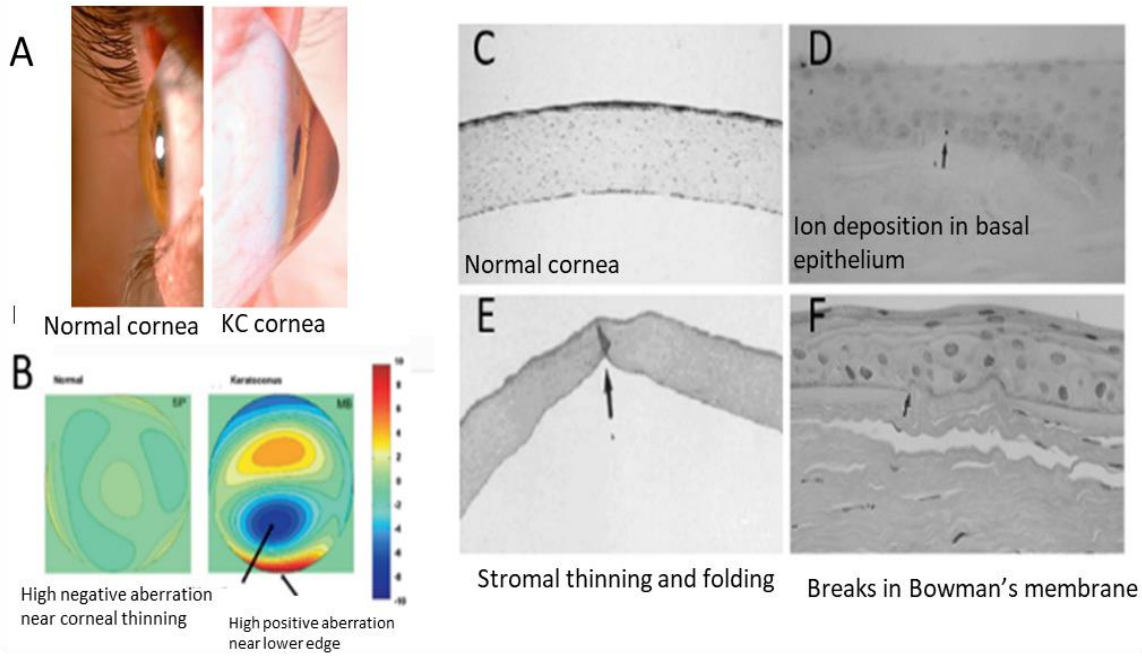

Figure. 4 Changes in KC cornea.

A, Illustration of healthy cornea (left) and KC cornea (right) [99]. B, Wave aberration map of healthy cornea and KC cornea. C-E, Optical image of healthy cornea (C) and KC cornea (D)-(F): (D) Ion deposition in basal epithelium; (E) Stromal thinning and folding; (F) Breaks in Bowman's membrane [39], [100].

Stromal thinning in KC cornea occurs with the decreased number of keratocytes and degradation of collagen lamellae compared to healthy cornea [84], [85]. Notably, research shows that although stromal thinning has been observed in the early stage of KC [91], [92], flattening and spreading instead of degrading collagen lamellae may be associated in this stage since no change in amino acid composition was found in subclinical KC corneal stroma [101].

Rupture of the endothelium has been observed with increased cellular pleomorphism and cell

degeneration [86], [102]. This is not common in KC patients and is believed to occur only in severe cases of KC [103].

The two non-cellular layers, Bowman's membrane and Descemet's membrane have also manifested abnormalities in KC cornea. Breaks and ridges in Bowman's membrane or sub-Bowman's membrane (K-structures) occur commonly in KC cornea [104]. They are often a result of down-growth of epithelial basal cells, eruption of stromal collagen or accumulation of other molecules [39], [87]. Descemet's membrane damage is only seen in acute hydrops [87].

2.2.4.2 Molecular changes

Epithelium deformities and stromal thinning have been suggested to be caused by molecular changes taking place in the corneal microenvironment and characterized by an altered expression of protease and pro-inflammatory markers and intense oxidative damage.

MMPs are the most important enzymes regulating corneal function and have been found to be increased in KC cornea [105]. Increased MMP9 activity has been shown to result in a disrupted corneal cell barrier function and increased cell permeability in corneal epithelium accompanying dryness [106], indicating the potential MMP-induced cellular change in KC corneal epithelium. At the same time, TIMP, the inhibitor of MMPs, is decreasingly expressed in KC cornea [107], resulting in a decreased MMPs / TIMP ratio hence an accelerated degradation of stromal collagen fibrils.

Pro-inflammatory markers have also been demonstrated to play a critical role in maintaining the healthy state of the cornea through the regulation of cell apoptosis, cell death, cell differentiation and cell adherence, thereby modulating the function of the cornea. Elevated expression of TNF and IL cytokine families has been found in KC cornea. It is postulated that TNF-α not only disrupts the barrier function of corneal epithelial cells with the disappearance of ZO-1 expression at cell interface [108] but also promotes stroma degradation by stimulating MMP9 expression [84]. It has been proposed that IL-1 receptors on KC keratocytes are four times higher compared with normal cells, indicating its role in KC-related stroma thinning and mass loss [109], [110].

Oxidation products accumulation in the cornea has been proposed to occur in KC cornea with defects in the ability to process reactive oxygen species which leads the KC cornea to undergo oxidative damage [77]. This is accompanied with decreased expression of aldehyde dehydrogenase (ALDH) Class 3 and superoxide dismutase enzymes which result in cytotoxic malondialdehyde and peroxynitrites deposition and further damage the cornea [62].

2.2.4.3 Biomechanical changes

Research has shown that corneal biomechanical properties change significantly with the onset of KC including the reduction in elastic modulus, maximum stress to failure, corneal hysteresis (CH), and corneal resistance factor (CRF) [88], [101], as is listed in table 1. The Young's modulus value of healthy cornea published in papers shows a wide range from 2 to 4000 kPa (Table 1). This is a result from the different measuring methods, *in-vivo*-indentation or *ex-vivo*-uniax test, and calculating methodologies being used. The calculating methodologies mainly include the involvement of true IOP impact or the selection of applanation dimension and location [25], [111], [112]. In KC cornea, the modulus of elasticity decreases significantly ranging from 1 to 1000 kPa (table 1). Accordingly, the maximum

tensile stress to failure of KC cornea is much lower than that of healthy cornea (Figure 5), indicating that KC cornea is more vulnerable to mechanical stress CH value of healthy cornea have been reported to vary within an individual with a range of 5-14 mmHg [113]. The mean CH values measured in healthy corneas are listed in table 1, showing a range from 10.2 to 11.0 mmHg. The mean CRF values in selected researches are also shown in the table which shows a range from 9.4 to 11.1 mmHg. In comparison, the CH values and CRF values in KC cornea are 8.06-8.1 mmHg and 6.4-7.1 mmHg, respectively, much lower than those in healthy cornea.

Table. 1 Biomechanical properties comparisons of healthy cornea and keratoconus cornea.

Young's modulus / kPa		**Corneal hysteresis (CH) / mm Hg**		**Corneal resistance factor (CRF) / mm Hg**	
Healthy cornea	KC cornea	Healthy cornea	KC cornea	Healthy cornea	KC cornea
2000 [114] 1600 [46] 3810±400 [45]	1000 [114]	10.6±1.4 [115]	8.1±1.4 [115]	10.6±1.6 [115]	7.1±1.6 [115]
4.2±1.2 anterior 2.3±0.7 posterior [112]	1.67±0.44 anterior 0.970±0.30 Posterior [116]	10.2±1.3 [117]	8.06±1.36 [118]	11.1±1.6 [90]	6.89±1.56 [118]
9.03 [119]	7.26 [119]	9.6 ±1.5 [120]	8.1±0.9 [120]	9.4±1.6 [120]	6.4±1.0 [120]

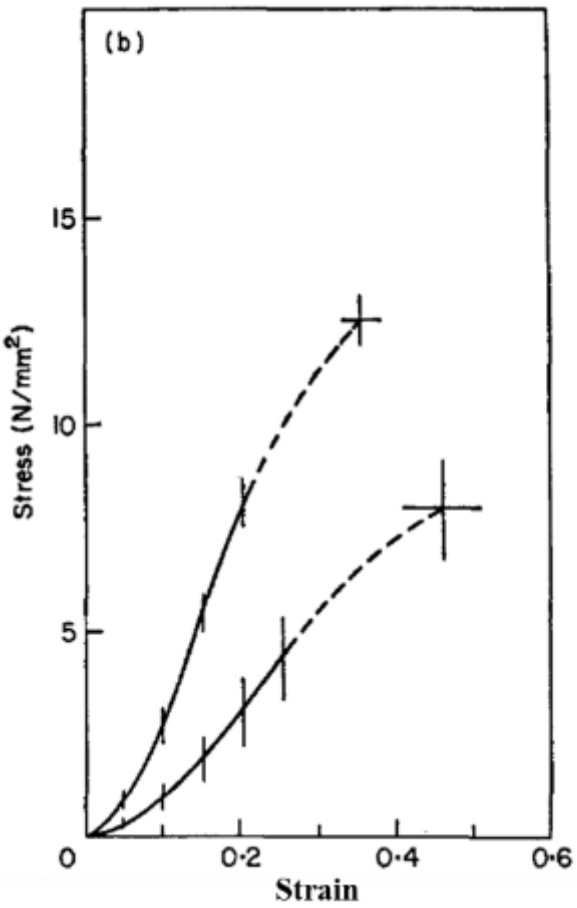

Figure. 5 Maximum stress / strain to failure comparison of healthy cornea and KC cornea and stress-strain curves for KC cornea (upper) and healthy cornea (lower) [88].

2.2.5 Mechanical stimuli and KC

The reduced biomechanical strength in KC cornea is caused by the structural and molecular changes in the cornea which results in a thinner, weaker and eventually bulged cornea upon the load of IOP. It is not only a direct leading factor to the protrusion of the cornea, but also a trigger to the mechanosensing of corneal epithelial cells, which will affect cell behaviors [121]–[123]. The latter process, known as mechanotransduction, is triggered by mechanical stimuli or matrix changes. Mechanotransduction has been suggested to play a critical role in corneal epithelial cells [96]. Among various external mechanical stimuli, eye rubbing has been considered a risk factor of KC [2], [124], [125] and KC patients have been advised by ophthalmologists to avoid vigorous eye rubbing [126].

2.2.5.1 Mechanotransductive effects of corneal epithelial cells

The cornea is subjected to a wide range of mechanical stimuli that are mainly from eye blinking, tight eye closure, eye rubbing, contact lens wear and trauma [10], [96]. Sufficient biomechanical strength is essential to withstand any applied forces and to maintain the bio-physiological activity of corneal cells. External mechanical forces and the weakened corneal stroma observed in KC patients have been proposed to induce the mechanotransductive process of corneal epithelial cells and keratocytes [127].

Several cellular structures or molecular pathways such as actin filaments, integrins, tight junction proteins and yes-associated protein/transcriptional coactivator with PDZ-binding motif (YAP/TAZ) have been recognized as mechanosensors and mechanotransduction has been demonstrated to regulate cell morphology, differentiation, migration, proliferation and death, gene or protein expression [121], [127]–[129].

Corneal cells have been reported to respond to mechanical forces by modulating morphology, cytoskeleton, gene/protein expression, apoptosis, wound healing ability or other cell responses. It has been shown that corneal fibroblasts [130] and epithelial cells [131] rearrange their morphology and cytoskeleton to balance cellular tension homeostasis upon matrix stretching. These changes have also been displayed in HCEpCs under flow-generated shear stress. HCEpCs tend to gather together with reduced extracellular space [132] and rearrangement in actin filaments (F-actin) were also displayed with the accumulation of disorganized F-actin around the cell perimeter [123]. Altered gene expression profile has also been observed in corneal fibroblasts in response to local mechanical stress [133] and in HCEpCs upon shear stress. Examples of the latter include the change in the expression of tight junction protein1β [132] and transforming growth factor-β (TGF-β) [134] observed in HCEpCs under shear stress. Increased cell apoptosis has also been regarded as a mechanoresponsive effect of corneal epithelial cells as increased HCEpCs apoptosis was identified under both flow-induced shear stress [123] and friction-induced shear stress [135]. An *ex vivo* model of rabbit cornea also illustrated the accumulation of DNA fragments on the surface of the cornea due to increased cell apoptosis after exposure to shear stress [136]. Shear stress has also been demonstrated to affect the wound healing ability of HCEpCs. After exposure to shear stress of 12 dyn/cm^2, HCEpCs elicited reduced migration speed and delayed wound healing rate after scratch [134], indicating the close association between wound healing and mechanotransduction in corneal epithelial cells.

Corneal epithelial cellular response to substrate stiffness has also been acknowledged as an important mechanosensing process [137]. Rabbit CEpCs cultured on different matrices with altered stiffness showed change in cytoskeleton protein (F-actin) and adhesion proteins distribution [138]. Limbal epithelial cells (LEC) were cultured on collagen substrates with different stiffness (stiffer 2.9 kPa and softer 0.003 kPa). The higher elastic modulus utilized was similar to the anterior cornea [139]. Results showed higher ZO-1 expression, cytokeratin 3 expression and higher cell number on stiffer matrix, revealing the essential role of substrate stiffness in maintaining corneal epithelial behavior [139]. Human corneal epithelial cells (HCEpCs) seeded on polyacrylamide substrate displayed changes in apoptotic activity, migration speed and cytoskeleton structure (actin fibers) with tuned substrate stiffness (compliant 1.3 kPa, medium 3.2 kPa and stiff 9.2 kPa), indicating the mechanosensing activity of HCEpCs [122]. Increased cell necrosis and lower migration speed were observed when cells were seeded on compliant substrates, which supports well the case in KC cornea [122]. The assessment of cytoskeletal structure showed that cells on compliant substrates were lacking stress fibers. As F-actin helps cells to exert pulling force, this may explain the low migration speed of HCEpCs and the delayed wound healing in KC.

2.2.5.2 Eye rubbing and KC

The potential correlation of chronic abnormal eye rubbing (CHAR) and the formation and progression of keratoconus was first proposed in 1961 [124], and it was proved later with more evidence [7], [125],

[140]. A collaborative longitudinal evaluation of KC study reported that over 50 % KC patients were associated with CHAR for years [6]. For patients with genetic disposition of KC, CHAR has been thought to potentially increase rubbing-related trauma and may be the reason of early onset, rapid development or severe display of KC [141]. The significance of CHAR was further validated by a multivariate case study which concluded that eye rubbing was the only critical risk factor of KC [5]. Both bilateral [140] and unilateral [142], [143] KC have been reported and the dominant hand appears to correspond with the worse eye or the affected eye, respectively. Despite clinical evidence, the etiology and histopathology of KC due to eye rubbing has not been well established. It is postulated that the pressure applied on the cornea during rubbing may result in cell membrane rupture, epithelium thinning, Bowman's membrane ridges and lost regularity of corneal curvature, as signs of the formation of KC [144]. Additionally, rubbing on damaged cornea would further decrease its mechanical stability and accelerate corneal degeneration [7], which may explain why acute hydrops often occur with vigorous rubbing in KC patients [145].

The rubbing activity of KC patients differs significantly from healthy people. A survey illustrated that the rubbing patterns adopted by KC patients are not significantly different with others, although they tend to rub their eyes in a circular mode using their fingertips or knuckles [2], [146]. However, rubbing vigor, intensity, lid tightness and rubbing duration are much higher in KC patients than those of healthy subjects [147]. The mean rubbing stress generated by KC patients has been estimated to be 10 times greater than that of non-KC subjects [148]. Severe eye rubbing stress can be as high as 1.77 kg/cm^2 (17 N/cm^2) [149]. The intensity of eye rubbing for KC patients has been reported to range from 10 to 180 seconds, and it is not uncommon that KC patients would rub their eyes for hundreds of times a day. Furthermore, KC patients tend to rub their eyes more often and much longer during sleep [147], which means that the rubbing activity of KC patients is often underestimated since they could happen unconsciously.

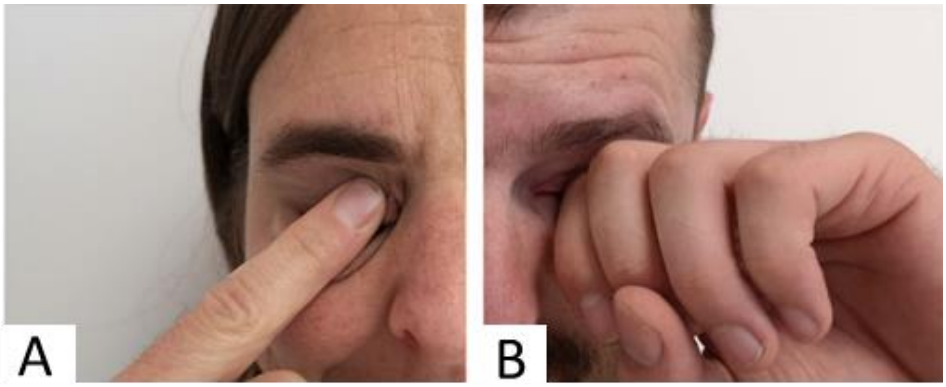

Figure. 6 Eye rubbing patterns found in keratoconus patients.

KC patients rub their eyes with finger tips or (A) knuckles (B) in circular motion to apply mechanical forces on the cornea [150].

Eye rubbing has been suggested to induce intraocular fluid displacement which results in IOP spike. The increased IOP could contribute to conical formation of KC cornea when it lasts over 20 seconds per episode frequently (as is seen commonly in CHAR) or when the spiked IOP is double more than normal level (10-20 mmHg) [151]. Eye rubbing induced IOP elevation has been regarded as very high

level (up to 400 mmHg) thus influencing corneal epithelium greatly daily [152]. The squeeze from compressive rubbing forces anterior to epithelium and elevated IOP distending forces inferior to the cornea, enhance the risk of significant corneal trauma, which may contribute to the onset or progression of KC [147].

The role of eye rubbing in KC progression has been well established as a decrease in the rate of corneal thickness loss was observed in KC patients after stopping eye rubbing [153]. However, whether eye rubbing contributes to the development of KC has remained a controversy. As the outmost corneal layer, epithelium has been proposed to be affected most by rubbing-generated mechanical forces. Thus, researches have been focused on epithelium thickness change and molecules (protease and pro-inflammatory markers) expression. Attempts to detect the temporary corneal changes after eye rubbing have been conducted in some *in vivo* studies and contradictory results have been reported. A study involved 12 healthy subjects for the assessment of corneal reaction to circular rubbing. Surprisingly, an 18.4 % reduction of corneal epithelium thickness was detected after only 15 seconds of rubbing and it took around 30 minutes for baseline recovery [9], showing a KC-like corneal thinning caused by eye rubbing. Another study, however, showed no significant change in epithelium thickness after 30 seconds of eye rubbing using the same method [154]. Increased expression of MMP13, IL-6 and TNF-α in tears were detected in the eyes of volunteers without KC after 60 seconds eye rubbing [10]. Since these proteins are also elevated in KC cornea, this may indicate that rubbing stimuli could possibly induce the development of KC through the regulation of HCEpCs protein expression profile. The observations stated above demonstrate the potential contribution of eye rubbing to the onset of KC due to the KC-related changes in healthy cornea.

2.2.5.3 Eye rubbing related mechanical stress

Although the cornea has been shown to be influenced by eye rubbing in the perspective of KC development, the corneal epithelial change upon eye rubbing introduced mechanical stress has not been systematically investigated. As the rubbing process is a combination of multidirectional forces, it is critical to distinguish each component of these forces so as to investigate their effects on corneal cells separately. Several studies have focused on simulating the stress induced on the cornea upon applanation [11], [155], [156]. Since eye rubbing would pose similar compression on cornea, this may shed light on understanding the stresses generated from rubbing. A recent study adopted a finite element method (FEM) for the simulation of applanation-generated stress on cornea as is shown in Figure 7) [11]. It was concluded that the cornea would be subjected to in-plane tensile stress and out-of-plane compressive stress [11]. Eye rubbing differs from simple applanation. In this study, we studied the effect of in-plane tensile force and out-of-plane compressive force on HCEpCs. The remaining deformations as well as multiaxial stress state will be the subject of future research.

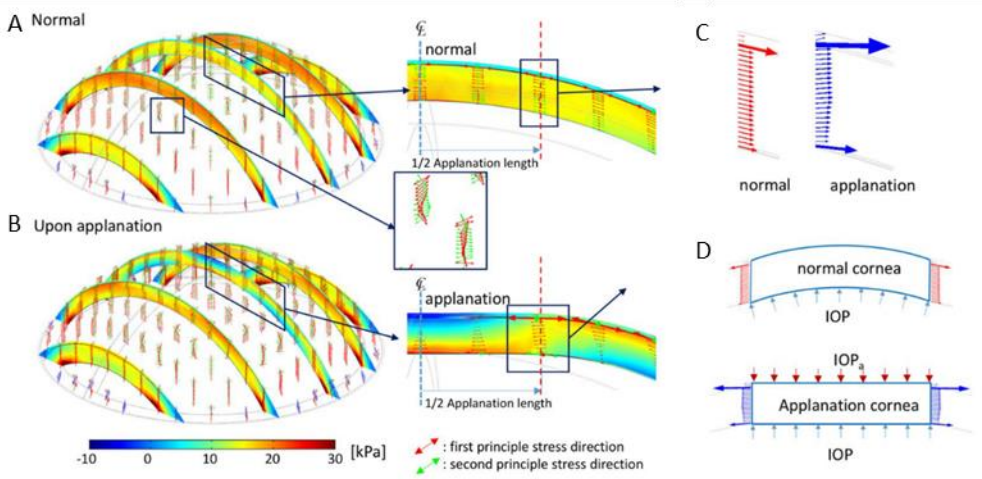

Figure. 7 Stresses applied on cornea under normal state, upon applanation.

Comparison of stress (C, D) on cornea without (A) and with (B) applanation [11].

Severe eye rubbing stress has been reported as 1.77 kg/cm^2 (17 N/cm^2) [149] and it was shown that eye rubbing force is much higher than normal IOP of 10-20 mm Hg [7]. However, the tensile stress and compressive pressure applied on cornea during eye rubbing have not been reported. It has been regarded that the rubbing-compression was several times more than that in normal eye blink, which was estimated to be about 5-37.5 mmHg [9], [157]. For people with CHAR, the compressive force applied on the corneal epithelium was postulated to be maintained for up to 5 minutes during eye rubbing and the induced effect on cornea would last for 30-45 minutes [141]. Several researches have been focused on the corneal cellular response to tensile force and compressive force, most of which being on stromal fibroblasts [130], [158], [159]. A study examined human and rabbit corneal stromal fibroblasts in a 3D collagen matrix and exerted compression (push) and stretch (pull) through a micro-needle [130]. Morphology change and cytoskeleton rearrangement of the cells were observed as a result of the maintenance of cellular tension homeostasis. Increased expressions of MMP and TIMP were found in rabbit corneal fibroblasts as a response to tensile forces [158]. As the imbalance of MMP / TIMP is a characteristic sign of KC, this observation may help explain the close association of eye rubbing and KC formation.

2.3 Mechanical stimulation devices for corneal behavior research

To better understand corneal epithelial cell response to mechanical stress, it is vital to include the use of mechanical stimulation devices in corneal behavior research. Various mechanical stimulation devices which could apply different mechanical stimuli have been designed, fabricated and improved to closely mimic cellular physiological mechanical forces. In the following section, mechanical stretching devices and compressive devices will be introduced, corresponding to the nature of eye rubbing mimicking forces.

2.3.1 Mechanical stretching devices

Mechanical stretching device (or mechanical cell stretcher) is a system that can introduce stretching force to cells. Traditional mechanical stretching devices include AFM [160], optical micro tweezers [161], and magnetic microposts [162]. However, the application of these devices is limited due to the

technical difficulties including the manipulation of single cells and the complexity of device setup. In the past few decades, cell stretchers which stretch the cell culture substrate instead of manipulate cells directly have been developed. Both commercially available (FX 6000™ Tension System (Figure 9 A), [163]–[165] and custom-built mechanical stretching systems (Figure 9 B, C, Figure 8) have been reported. Commercial stretchers are well designed with characterized strain profile and have been used for the studies that are not fastidious about cell culture membrane material, desired strain and experimental expense [164], [165]. However, since most studies are constrained by the factors listed above, the application of commercial cell stretcher is limited. Recently, more and more studies have focused on the design of lab-based cell stretchers because of the needs for customized substrate, stretching pattern, stretching forces and lower cost.

2.3.1.1 Design considerations

Several factors are to be considered when designing a cell stretcher. These include biocompatibility, control strategies, stretching direction, substrate properties and others [166].

It is crucial to keep the device biocompatible to keep viable and sterile cells in culture during or after stretching, which means that a cell culture well containing medium should be incorporated and that the whole device should be able to be sterilized [166]. Control strategy, namely actuation method, is another important factor for the design of the device. Commonly adopted actuation systems include pneumatic actuation [167], [168], piezoelectric actuation [169], [170] and optical actuation [171]. Among these, pneumatic actuation and piezoelectric actuation have been the most commonly used actuation systems due to their simple setup, high resolution and homogeneously induced strain [166]. Another significant factor to be considered is stretching direction of which equibiaxial stretching instead of uniaxial stretching is preferred. The main advantages of equibiaxial stretching is the strain homogeneity so as to reproduce physiological mechanical stress in cells seeded on the stretching membrane to better mimic *in vivo* conditions [172]. Substrate properties such as stiffness and wettability should also be considered in designing the stretching device to promote cell attachment and proliferation. This is of significance for corneal epithelial cells as HCEpCs showed different cell behavior when seeded on substrate with various stiffness [122].

2.3.1.2 Lab-based equibiaxial cell stretcher

Current researches on mechanoresponsive properties of corneal cells are mainly conducted with either commercial cell stretchers [158], [159], [173] or traditional cell stretching techniques [130] as stated in section 2.3.1. Few customized devices have been used for corneal behavior research [50], [174]. A stretching device with the mounting of bovine cornea has been reported recently [50]. The device included a stainless steel pressurization chamber in which the cornea was fixed (Figure 8 A). The pressure was induced by fluid infusion controlled with a syringe, allowing linear deformation of the loaded cornea. This device was successful in achieving a certain stretching strain of the cornea with the apex displacement of cornea ranging from 0 to 1 mm. However, due to the direct contact of the pressurization fluid with the cornea, undesirable deformation of the loaded cornea was observed where the use of silicone oil as pressurization fluid led to a shrinkage of the cornea and saline solution resulted in swelling of the cornea [50]. Another device utilized a conical shaped chamber to induce stretching deformation on the cornea with vacuum [174]. The device was initially designed to correct refractive

errors for the cornea *in vivo* by positioning it onto the patient's eyes and adjust corneal curvature by tuning the shape of the vacuum chamber. While designed for in vivo studies, the structure and mechanism of this device provides valuable information for designing an in vitro corneal cell stretcher.

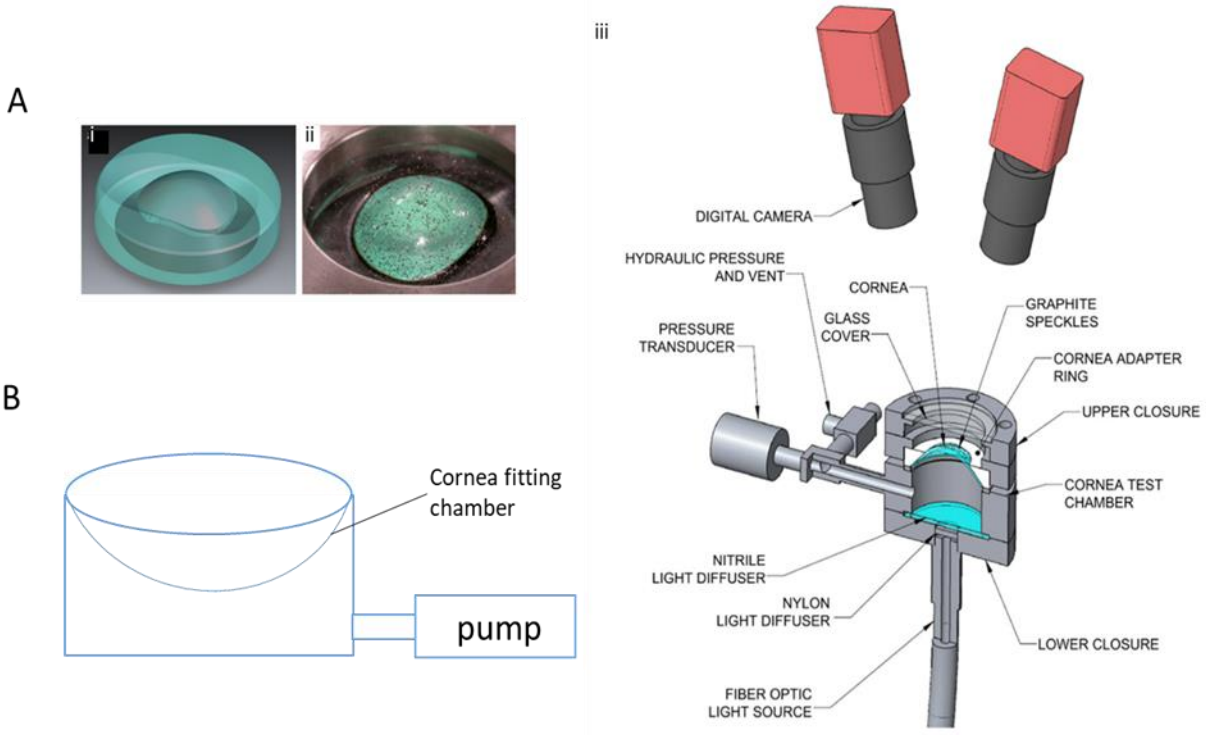

Figure. 8 Equibiaxial stretching devices used in cornea research.

A, Fluid-infused stretcher, (i)-(ii), cornea loaded pressurization chamber; (iii), schematic of the device [50]. B, Vacuum stretching device, adapted from [174].

Other devices have also been built for cell behavior research [167], [170]. Cui *et al* fabricated a cyclic stretching device made of polydimethylsiloxane (PDMS) with pneumatic actuation [167]. The stretching unit was fabricated by soft lithography, which comprised three layers: cell culture layer, post loading layer and actuation cavity layer (Figure 9 C). The cell culture layer was designed with a thin stretchable PDMS cell culture membrane at the bottom and wall around the well to contain cell culture medium. The loading post was designed with a slightly lower diameter than the cell culture membrane so that it could be indented into the stretchable membrane. In working condition, positive air pressure inflates the actuation cavity layer, which pushes the loading post upward, achieving a stretched cell culture membrane. The device utilized a nanopillar patterned PDMS cell culture membrane and was able to stretch the membrane with 0-15 % strain over 6 hours [167]. Another piezoelectrically controlled cell stretcher was designed recently (Figure 9 D) [170]. The device was made from aluminum and a PDMS cell culture membrane fixed by a membrane holder mounted on top of an indenter. Deformation of the membrane was achieved when indented as the membrane holder was moving up and down. Unlike most of the other stretching devices, this device confined the cell culture wall in the stretching region (Figure 9 D-i) so that all cells seeded could sense the tensile force. This design is of high importance to ensure cell homogeneity, however, it demands precise calculation on the dimension of the wall height and thickness to achieve strain homogeneity over the membrane.

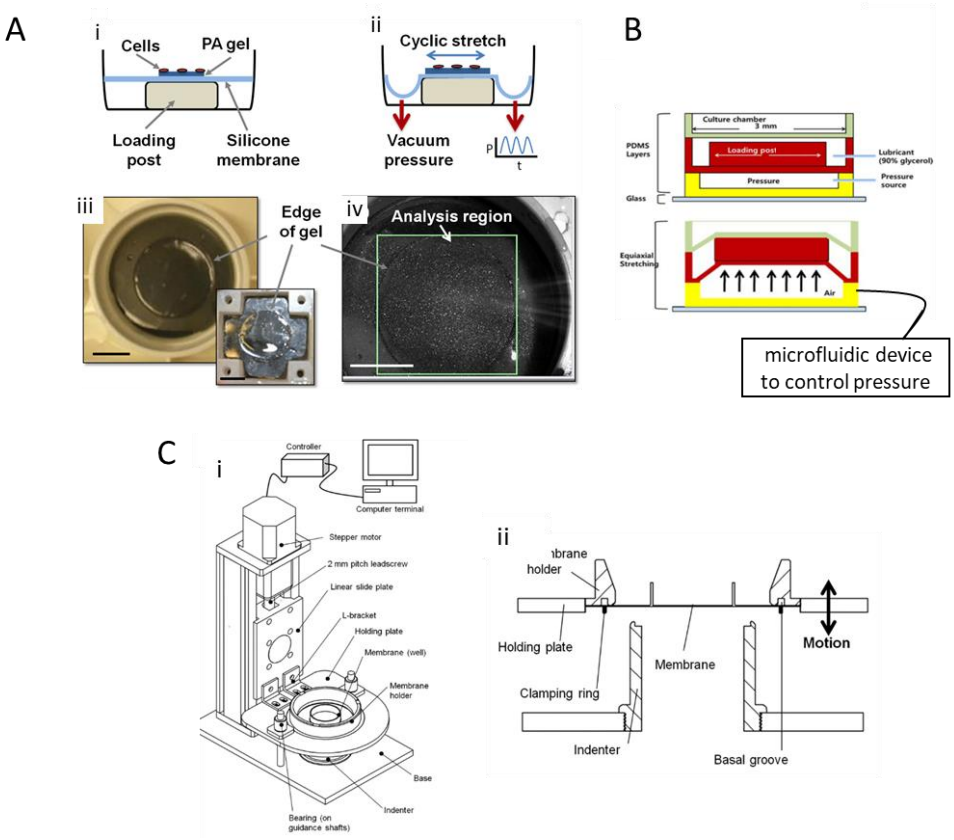

Figure. 9 Other equibiaxial stretching devices for cellular studies.

Commercial (A) and lab-based (B)-(C) equibiaxial cell stretcher. A, Stretching well of FX-6000™ Tension System: i, ii, cross-sectional image of the stretching well; iii, top view of the stretching well; iv, analysis region [175]. B, Microfluidic stretcher [167]. C, Electronic cell stretcher, schematic of the stretcher (i) and cross-section of membrane holder and indenter (ii) [170].

2.3.2 Compressive device

Devices that can apply a compressive force on cells have been used for investigating cellular response to compression. Like the application of tensile force, traditional methods such as the manipulation by microneedles have also been used to induce compression on corneal cells [130]. However, due to the limited availability of such method, other commercial devices [176] or lab-made devices [177]–[185] have been utilized in current research. Commonly adopted lab-built devices include centrifugation [177], [178] and load-induced compression [179]–[183]. The latter is conducted by placing the loading weight on top of the seeded cell layer directly, which has been commonly used due to its easy setup. This method has also been applied in corneal mechanoresponse investigation by Hatami-marbini *et al.*, who reported the compression of corneal stroma by using a strain-controlled rheometer [184], [185].

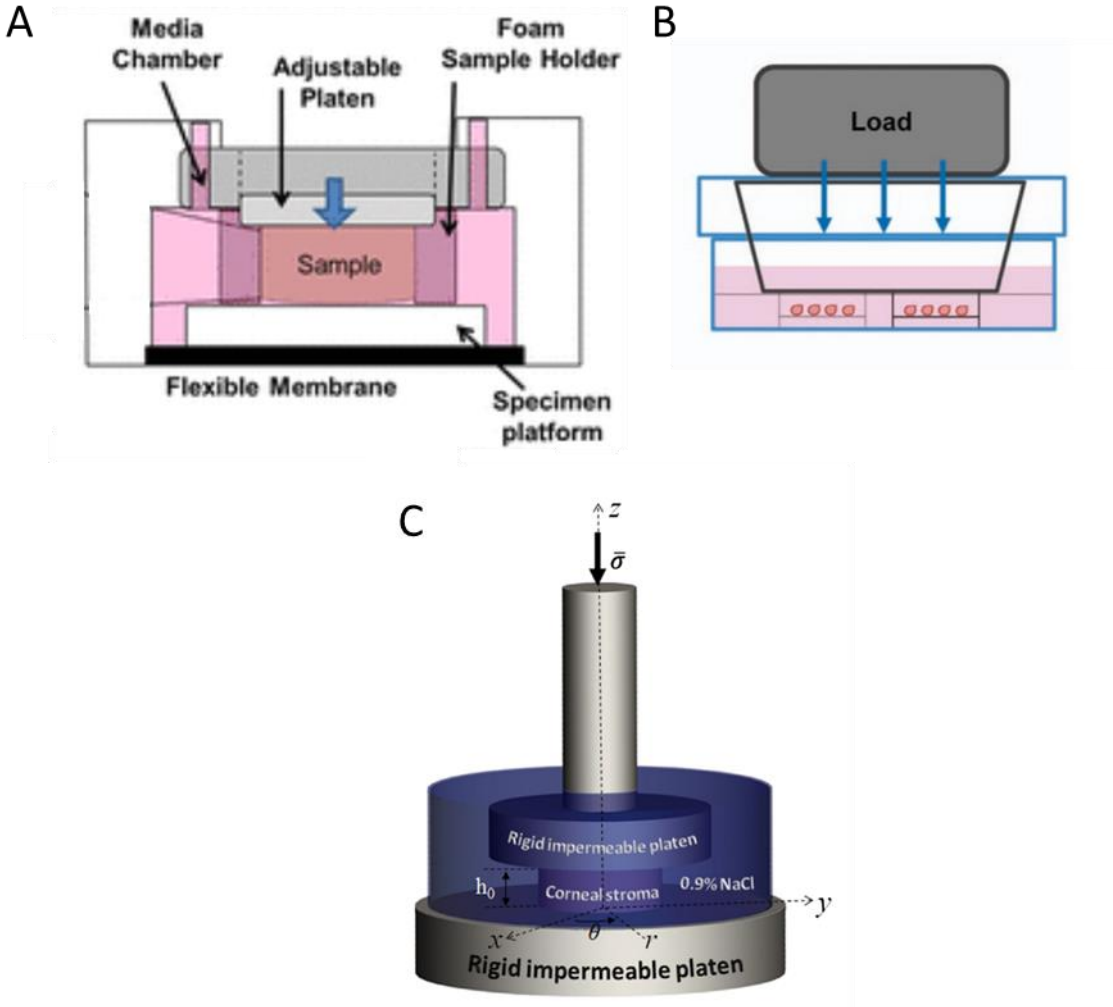

Figure. 10 Compression devices.

A, Cross-sectional image of FX-5000C™ Compression System [186]**. B, Load-based compression system** [183]**. C, Compressive system for cornea research** [184]**.**

3.0 Materials and Methods

3.1 Fabrication and uniaxial stress-strain test of cell culture membrane

The cell culture membrane was spin coated with PDMS. Briefly, 3 ml of PDMS curing agent mixture was aliquoted on top of a petri dish, which was fixed on a spin coating machine (SCS G3 Spin Coater, Specialty coating systems). A thin PDMS membrane was achieved after spinning at 300 rpm for 20 seconds and crosslinking for 3 days at 60°C. The thickness of the spin-coated PDMS membrane was about 500 μm.

Uniaxial stress-strain curve of the cell culture membrane was tested with Universal Macro-Tribometer (UNMT-2MT, T1377 by Centre for Tribology, Inc.). Tensile testing was performed using a 10 kg load cell at the speed of 2 mm/s. Tensile stress was calculated by dividing tensile force with cross-sectional area of the PDMS membrane.

3.2 Protein coating

Gelatin A (Sigma), gelatin B (Sigma) and FNC coating mix (AthenaES, containing fibronectin, collagen and albumin) were selected as coating reagents to promote cell adherence and cell growth on PDMS.

To coat gelatin A and gelatin B, 10 mg/ml gelatin A and gelatin B solutions were made with PBS separately. The gelatin solutions were autoclaved after reconstitution. 500 μl gelatin A and gelatin B solution were added onto PDMS membrane separately and were incubated at 37 °C overnight. Before seeding, the gelatin coated PDMS membrane was washed with PBS three times and UV-irradiated for 30 minutes. Then 500 μl of solution containing 10 % P/S and 1 % amphotericin in deionized water (diH_2O) was added onto PDMS membrane and incubated at 37 °C for 30 minutes to avoid bacteria and fungus growth. The PDMS membrane was then washed with PBS ten times and 500 μl FBS was added on the PDMS membrane. The PDMS membrane was incubated with FBS for 1 hour, washed with PBS and UV-irradiated before seeding.

To coat FNC coating mix, 0.2 ml/ cm^2 of solution was added to wells containing UV-irradiated plasma-treated PDMS. Various incubation time was tested on coating outcome. The selected incubation times include 30 seconds, 10 minutes and 30 minutes. After incubation, FNC coating mix was removed and cells were seeded directly on PDMS membrane.

3.3 Cell culture

Immortalized HCEpCs

Human papillomaviruses (HPV) is commonly used in the immortalization of epithelial cells [187]. Immortalized HPV-HCEpCs, a former gift from Dr. M. Griffith, were used. Cells were seeded on a T25 flask (Falcon) with 5 ml serum-free medium (Keratinocyte medium supplemented with Keratinocyte growth factors and penicillin-streptomycin, KM, ScienCell). The flask was kept in the incubator (Thermo Scientific) with 5 % CO_2 at 37 °C. The medium was changed every other day until a confluence of 80 %. To sub-culture the cells, medium was removed and the cells were washed with 3 ml phosphate buffered saline (PBS, Sigma). Then 3 ml TrypLE Express (Thermofisher Scientific) was added to the flask and the flask was transferred to the incubator for 10 minutes. After incubation, 10 ml of trypsin

neutralization solution containing 89 % of Dulbecco's modified eagle medium (DMED, Gibco), 10 % of Fetal Bovine Serum (FBS, Gibco) and 1 % penicillin- streptomycin (P/S, Sigma) was added to terminate cell dissociation. The cell suspension was harvested in a 15 ml conical tube (VWR) and was then spun down in the centrifuge (Beckman Coulter) at 1500 rpm for 6 minutes. The medium was aspirated and cells were resuspended in KM. Cell counting was done with a hemocytometer. Cell number was calculated and 0.5 million cells were seeded in a new T25 flask.

To characterize cell growth on different substrates, HCEpCs were seeded on tissue culture polystyrene (TCPS) and PDMS. To characterize cell growth with different coating proteins, cells were seeded on the protein-coated PDMS membrane. The seeding density was 20,000 cells/cm^2 and cell number was counted after 3 days of culture. To characterize cell response to in-plane tensile force and out-of-plane compressive force, cells were seeded on FNC-coated PDMS membrane, the seeding density was 20,000 cells/cm^2. Medium was changed every other day until confluence (6 days) or till expressing ZO-1 (11 days) for characterization.

Primary HCEpCs

Primary HCEpCs were purchased from Cell Applications Inc. Cells were seeded on a T25 flask upon arriving. To subculture the cells, the culture medium (HCEpC Growth Medium (serum free), Cell Applications Inc) was removed and the cells were washed with 3 ml of Hanks' Balanced Salt solution (HBSS, Sigma). 0.05 % Trypsin-EDTA solution was added into the flask and cell dissociation was conducted at room temperature for 2 minutes. When cells were detached from the flask, 5 ml of Trypsin Neutralizing Solution (TNS, Sigma) was added to the flask. The cell suspension was transferred to a 15 ml conical tube. Another 5 ml of TNS was then added to the flask to remove the remaining cells and cell suspension was transferred to the same conical tube. Cells were centrifuged at 1500 rpm for 5 minutes and supernatant was aspirated. Cells were resuspended in a 15 ml conical tube with HCEpC Growth Medium. Cell number was counted and calculated before seeding. To seed the cells on PDMS membrane, 7500 cells/cm^2 were added into wells containing PDMS membrane. Medium was changed every other day until confluence (6 days) or till expressing ZO-1 (11 days) for characterization.

3.4 Cell stretcher design

The design and fabrication process of the cell stretchers are shown in Figure 11. Our design was based on the reported stretcher [167], [170] and was modified for corneal research purpose [188]. In brief, the mold of the fluidic cell stretcher and the parts of the electric cell stretcher were designed with SolidWorks. Appropriate material for 3D printing the cell stretcher or the mold was selected before printing. The fabricating material was then selected to fabricate the cell stretchers. After fabrication, calibration was conducted on the cell stretchers to determine the correlation between the controlling factor and cell culture membrane deformation (Figure 11).

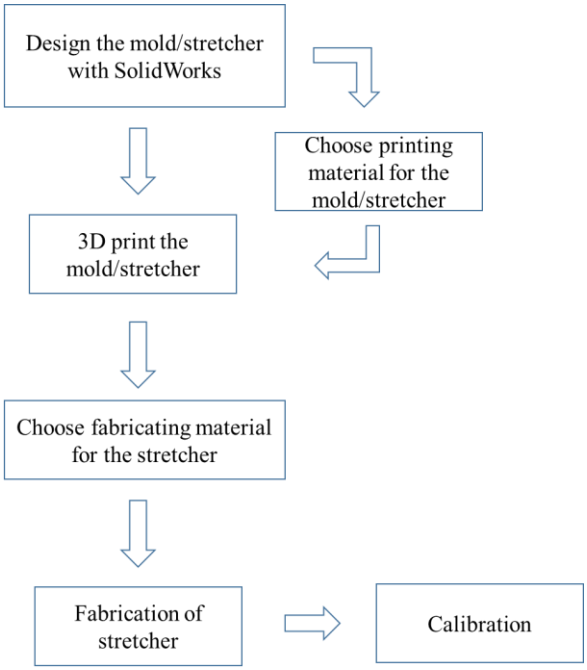

Figure. 11 Schematic of cell stretcher design, fabrication and calibration.

The fluidic cell stretcher including the cell culture membrane was fabricated using PDMS because of its stable properties in the physiological environment, its ability to stretch and its wide application in cell stretching systems [166], [189]. The mold used to fabricate the PDMS cell stretcher was printed with Acrylonitrile butadiene styrene (ABS) due to its chemical stability under 100 °C which would prevent mold deformation during PDMS curing. The mold of the fluidic cell stretcher was designed with SolidWorks followed by 3D print. Three layers including top layer (cell culture layer), middle layer (loading layer) and bottom layer (inflation layer) were implemented for the cell stretcher. For effective demolding, each layer of the mold consisted of multiple parts as shown in Figure 12 A-C. When gas flows and inflates the bottom layer, the loading post in the middle layer is pushed upwards and indents the cell culture membrane to expose cells to tensile force. The gas inlet in the bottom layer should be able to be tuned so as to expose cells to different stress. In an initial prototype, a gas tank was used for gas inflation (Figure 12 D). The detailed dimension of each fluidic cell stretcher layer is listed in Table 2.

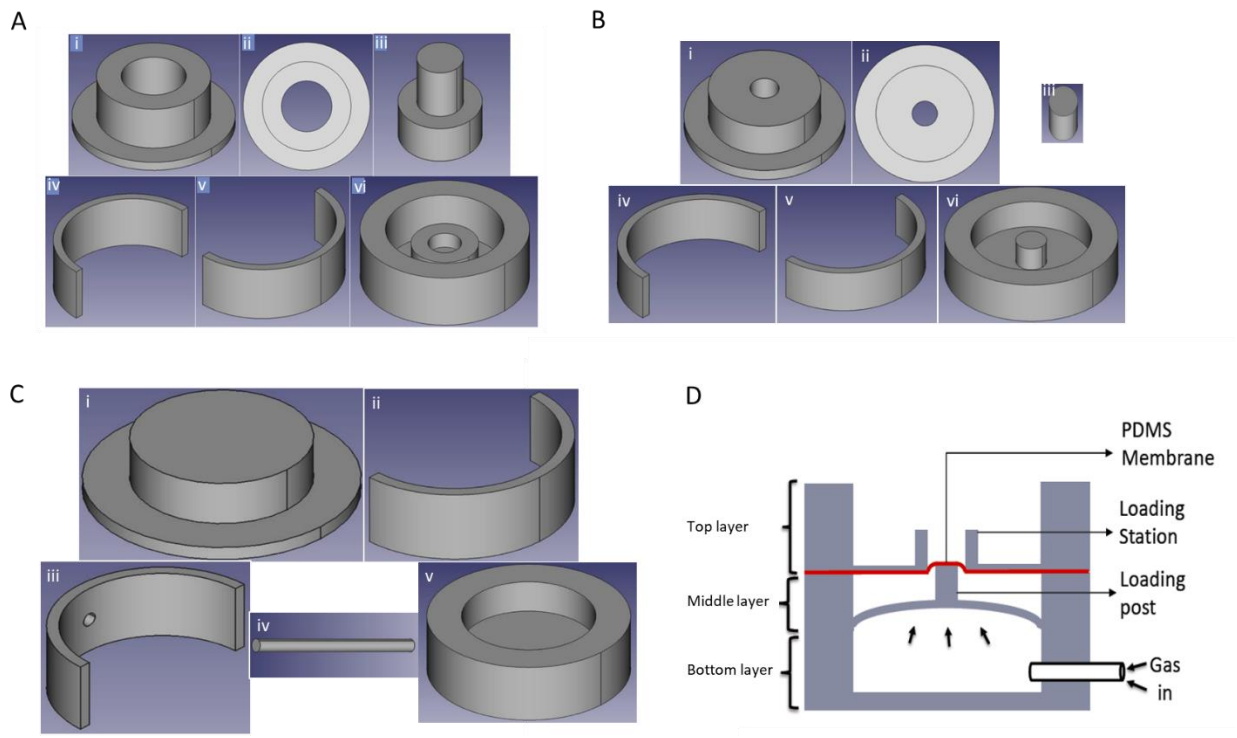

Figure. 12 Fluidic cell stretcher mold design.

SolidWorks image of fluidic cell stretcher layer mold. A, Top layer: (i), inner part; (ii), aerial view of inner part; (iii), inner peg part; (iv), outer part 1; (v), outer part 2; (vi), fabricated PDMS top layer. B, Middle layer: (i), inner part; (ii), aerial view of inner part; (iii), inner peg part; (iv), outer part 1; (v), outer part 2; (vi), fabricated PDMS middle layer. C, Bottom layer: (i), inner part; (ii), outer part 1; (iii), outer part 2; (iv), tube part; (v), fabricated PDMS middle layer. D, Cross-section of assembled fluidic cell stretcher [188].

Table. 2 Dimension of fluidic cell stretcher parts.

Top Layer		Middle Layer		Bottom Layer	
Height	17 mm	Height	15 mm	Height	15 mm
Outer diameter	50 mm	Outer diameter	50 mm	Outer diameter	50 mm
Wall thickness	5 mm	Wall thickness	5 mm	Wall thickness	10 mm
Cell culture chamber height	10 mm	loading post diameter	8 mm	Base thickness	3 mm
Cell culture chamber inner diameter	10 mm	Base thickness	3 mm		
Cell culture chamber wall thickness	5 mm				
Cell culture membrane thickness	0.5 mm				

The electric cell stretcher was mainly made of Aluminum 6061 because of its resistance to corrosion and compatibility to 3D printing. The indenter was made of PC-ABS with enhanced resolution. The O-ring used to fix the cell culture membrane was made of rubber. The cell culture membrane was made of PDMS. The electric cell stretcher was designed with a height / length / width of 270 mm / 200 mm / 350 mm, respectively. It mainly consists of two components: cell culture chamber (Figure 13 A) and linear actuator (Figure 13 B). The linear actuator was incorporated in the electric cell stretcher and programmed to control the movement of the indenter so as to introduce deformation of the cell culture membrane (Figure 13 C). The detailed dimension of each part is displayed in Table 3.

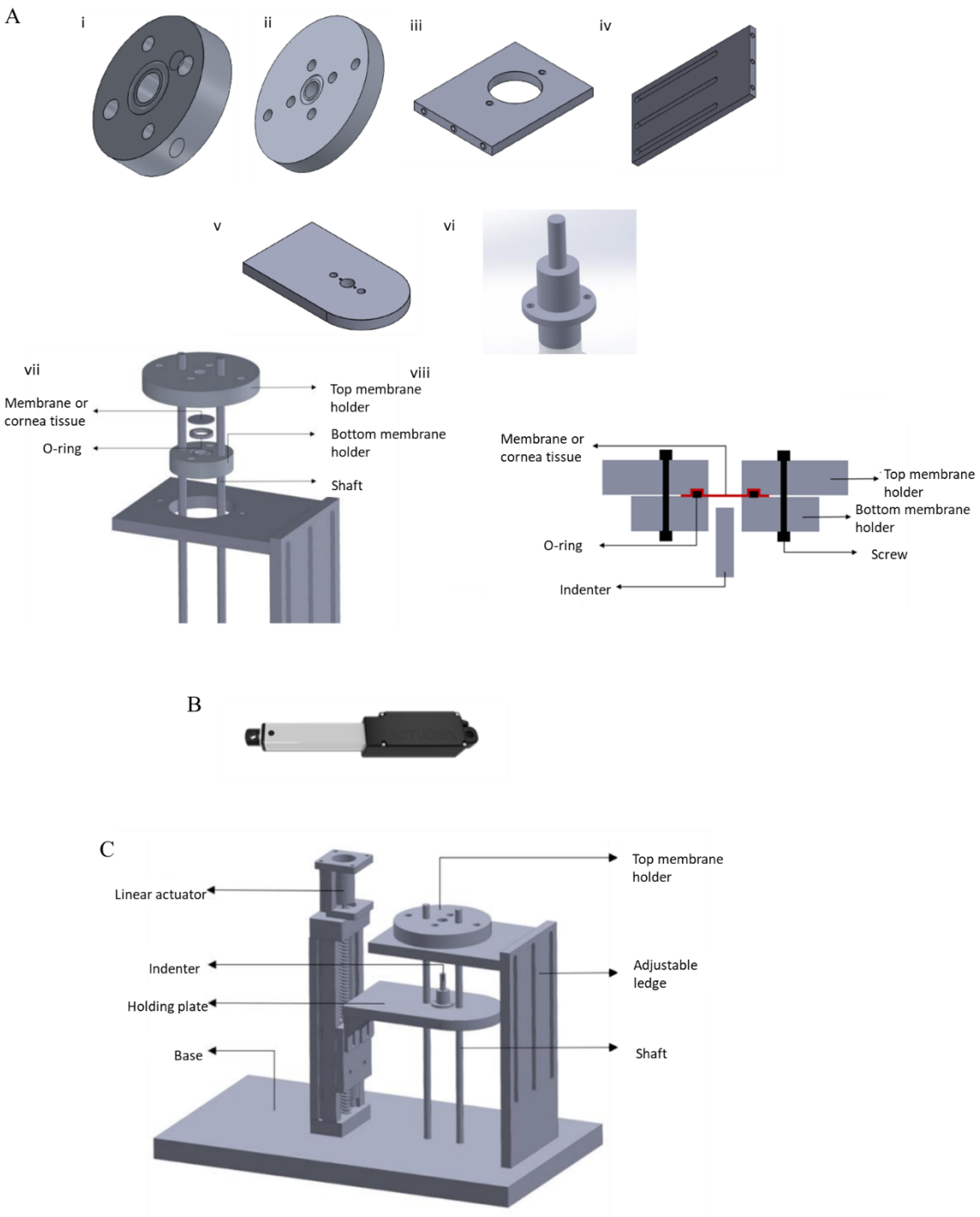

Figure. 13 Electric cell stretcher mold design.

A, SolidWorks image of electric cell stretcher part. (i), Top membrane holder; (ii), Bottom membrane holder; (iii), L-shaped ledge - top; (iv), L-shaped ledge - bottom; (v), Indenter plate; (vi), Indenter; (vii), Combination of cell culture chamber parts; (viii), Cross-sectional view of cell culture chamber with indenter. B, Linear actuator. C, The assembled device [188].

Table. 3 Dimension of electric cell stretcher parts.

Cell culture membrane and membrane holder		L-shaped ledge		Indenter holding plate	
Cell culture membrane diameter	10 mm	L-shaped ledge (top) length	130 mm	Length	137 mm
Bottom membrane holder diameter	47.6 mm	L-shaped ledge (top) width	100 mm	Width	80 mm
Bottom membrane holder height	12 mm	L-shaped ledge (top) height	10 mm	Height	10 mm
Top membrane holder diameter	87.6 mm	L-shaped ledge (bottom) length	200 mm	Indenter diameter	5 mm
Top membrane holder height	12 mm	L-shaped ledge (bottom) width	100 mm		
O-ring diameter	12.4 mm	L-shaped ledge (bottom) height	10 mm		
O-ring thickness	2.6 mm				

3.5 Fluidic cell stretcher fabrication, setup and calibration

3.5.1 Fabrication of fluidic cell stretcher cell culture chamber

The fluidic cell stretcher mold was 3D printed with Acrylonitrile butadiene styrene (ABS). Then the mold was used to fabricate the three layers of fluidic cell stretcher with PDMS (Dow SYLGARD™ 184 Silicone Elastomer Clear, base/curing agent of 10:1). Specifically, the mold of each layer was assembled and tightened with a rubber band. PDMS curing agent mixture was then poured into the stretcher mold and put in an oven at 60 ℃ for 24 hours to crosslink followed by careful demolding (Figure 14).

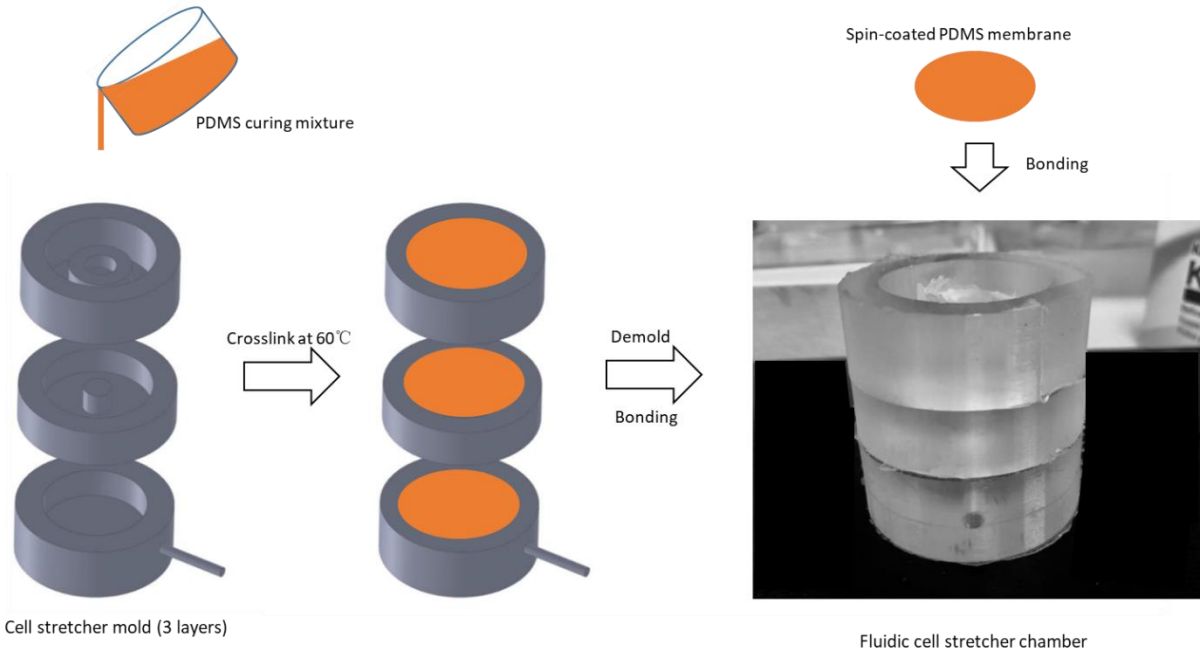

Figure. 14 Fluidic cell stretcher chamber fabrication [188].

3.5.2 Fluidic cell stretcher setup

To setup the fluidic cell stretcher, the cell culture membrane was bonded with the top layer of the fluidic cell stretcher through PDMS gluing. Then the bonded top layer was assembled with the other two layers of the cell stretcher by the same method. A tube was inserted into the bottom layer for gas inlet.

For cell stretching investigation, the fluidic cell stretcher was sterilized by UV irradiation and then HCEpCs were seeded on the membrane in the cell culture chamber. After cells reached confluence, a nitrogen gas cylinder was connected to the fluidic cell stretcher, allowing air-induced pressure to stretch the cell culture membrane (Figure 15).

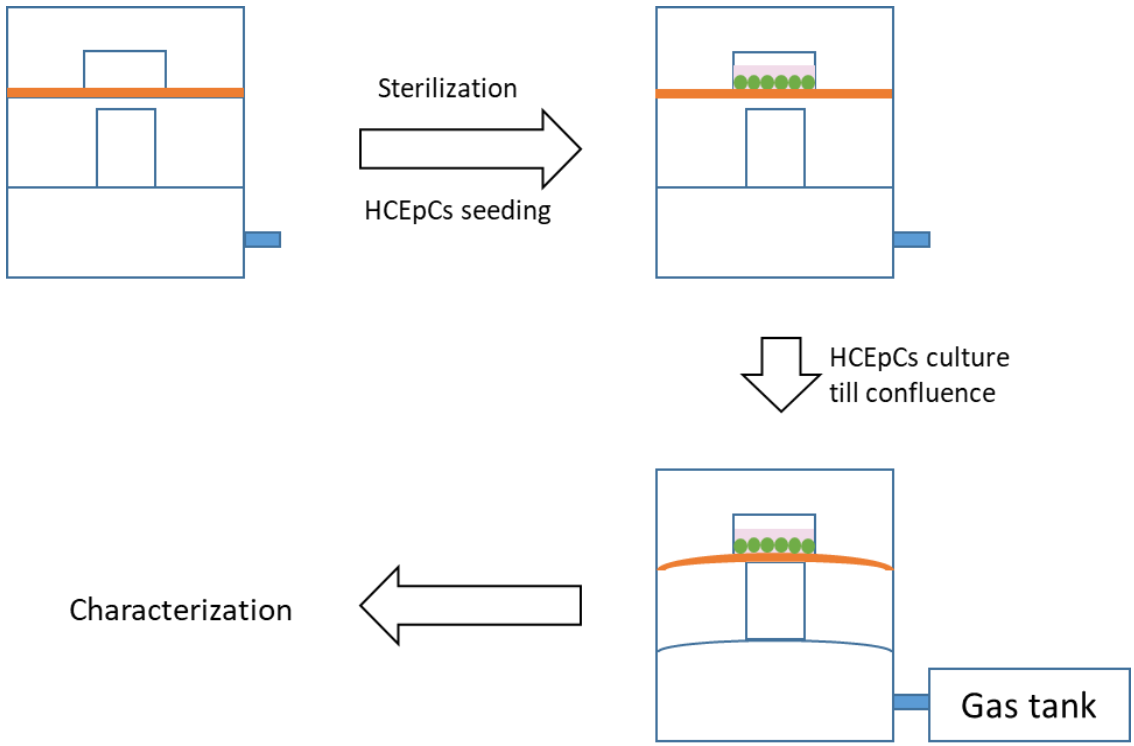

Figure. 15 Fluidic cell stretcher setup.

3.5.3 Fluidic cell stretcher calibration

Calibration was conducted in order to measure the strain of cell culture membrane under pressure. The assembled fluidic cell stretcher was connected to a nitrogen gas tank for air inlet. A weight ring was placed on top of the stretcher to hold it stable under pressure. A microscope which allows image tracking on the computer was used to observe the deformation of the PDMS membrane (Figure 16 A). Gas was released to inflate to the fluidic cell stretcher for 1 minute, then the gas valve was closed and images were taken for strain calculation. To investigate the stability of the system, it was left undisturbed for 4 more minutes after closing the gas valve. Images were taken every minute for strain analysis. To calculate the strain of the membrane, specific markers were made on the cell culture membrane to trace point-to-point displacement after stretching (Figure 16 B). The strain calculation was conducted with ImageJ. Fitted linear correlation of the strain - inlet air pressure was calculated in Origin 8.

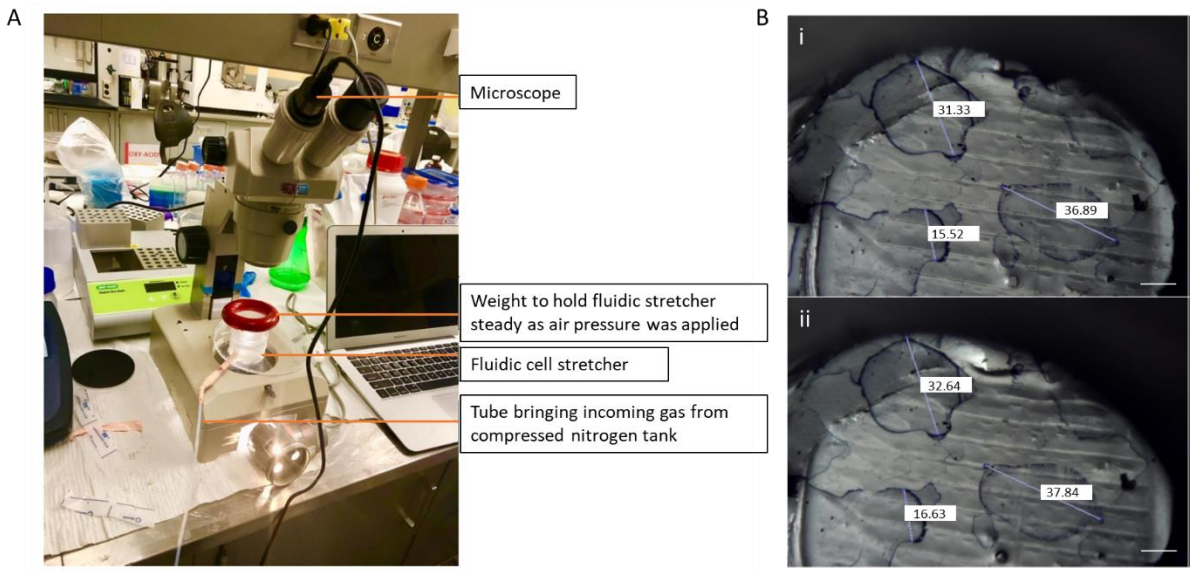

Figure. 16 Fluidic cell stretcher calibration.

A, Calibration setup. B, cell culture membrane before (i) and after (ii) stretching labelled with markers. Scale bar is 10 mm [188].

3.6 Electric cell stretcher fabrication, setup and calibration

3.6.1 Electric cell stretcher fabrication

The electric cell stretcher was 3D printed with Aluminum 6061. The linear actuator was selected as Acutonix Micro Linear Actuator L16 DC Linear Servo Motor (Actuonix motion devices Inc.) and was incorporated in the electric cell stretcher as controlling part. The cell culture membrane was made of PDMS with the same method stated above.

3.6.2 Electric cell stretcher setup

The linear actuator was connected to a computer through an Arduino uno board (Actuonix motion devices Inc.) following the manufacturer's instruction (Figure 17 A). Customized codes were written together with Jonathan Rasmussen, another master student in our group, to control the movement of the linear actuator as is listed in appendix I.

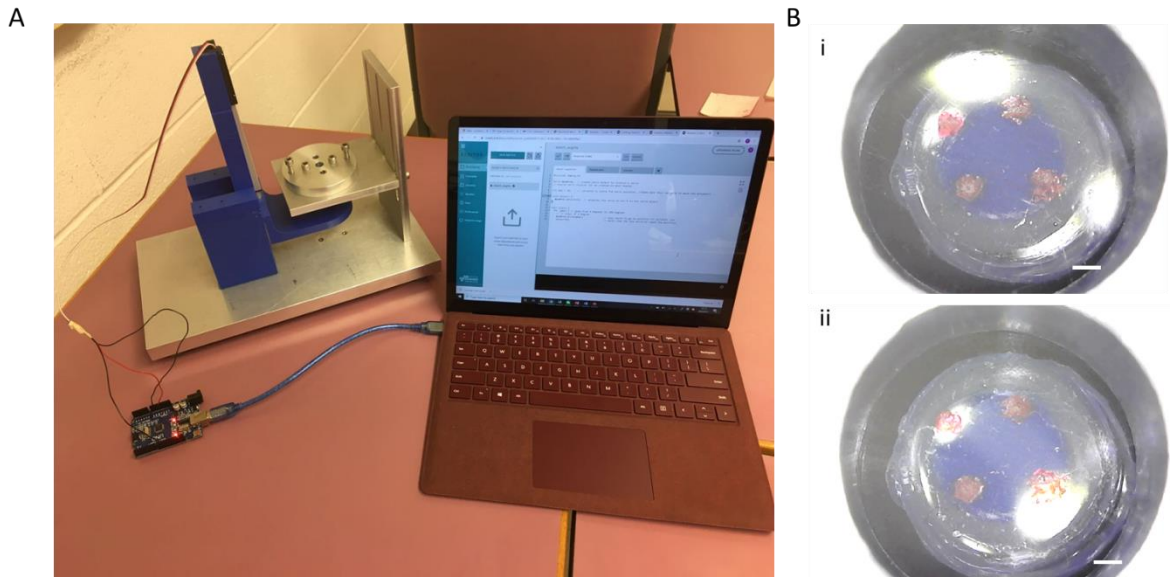

Figure. 17 Electric cell stretcher setup and calibration.

A, Electric cell stretcher assembly. B, Images of PDMS membrane before (i) and after (ii) stretching. Scale bar is 10 mm.

3.6.3 Electric cell stretcher calibration

The indenter was programmed to stay initially at the bottom of a specifically marked cell culture membrane. Then it was programmed to go up for 1-5 mm with pauses between movements of each mm. Images of the stretched membrane were taken using a digital microscope (pluggable USB2-MICRO-250X Digital Microscope, Think Up Themes Ltd.) (Figure 17 B) and analyzed by ImageJ. Fitted linear correlation of the strain - indenter displacement was calculated in Origin 8.

3.7 Compressive device design and setup

3.7.1 Fabrication of compression stamps and compression setup

Stamps for cell compression studies were made of PDMS. Pre-crosslinked PDMS solution was poured into mold wells with an area of 0.95 cm^2, which was then put in an oven at 60 °C for 24 hours. PDMS columns were then taken out from the mold and immersed in 0.1 % Pluronic solution (Pluronic F127, Sigma, diluted in DI water) for 24 hours in order to inhibit cell adhesion. Before compression, the stamps were sterilized by UV irradiation for 30 minutes (Figure 18).

HCEpCs were seeded on PDMS membrane for compression. The cell culture membrane was made with the same method stated in section 3.1. After crosslinking, the PDMS membrane was punched to small round discs to fit into 24 well plates. The well plate with PDMS membrane inside was then air-plasma-treated for 1 minute (Specialty coating systems Inc.) and then UV irradiated for 30 minutes. Prior to cell seeding, FNC coating mix (AthenaES, 0.2 ml/cm^2) was added to wells with PDMS membrane and was incubated for 30 seconds. To conduct cell compression, HCEpCs were cultured until confluence, then half of the culture medium was removed from the well. The coated PDMS stamp was then put on top of cell layer. Metal blocks of different mass (2 g, 5 g, 0 g, 50 g, and 90 g) were placed on top of the

stamp to generate various loading (0.03 N/cm^2, 0.05 N/cm^2, 0.10 N/cm^2, 0.52 N/cm^2, and 0.93 N/cm^2) (Figure 18).

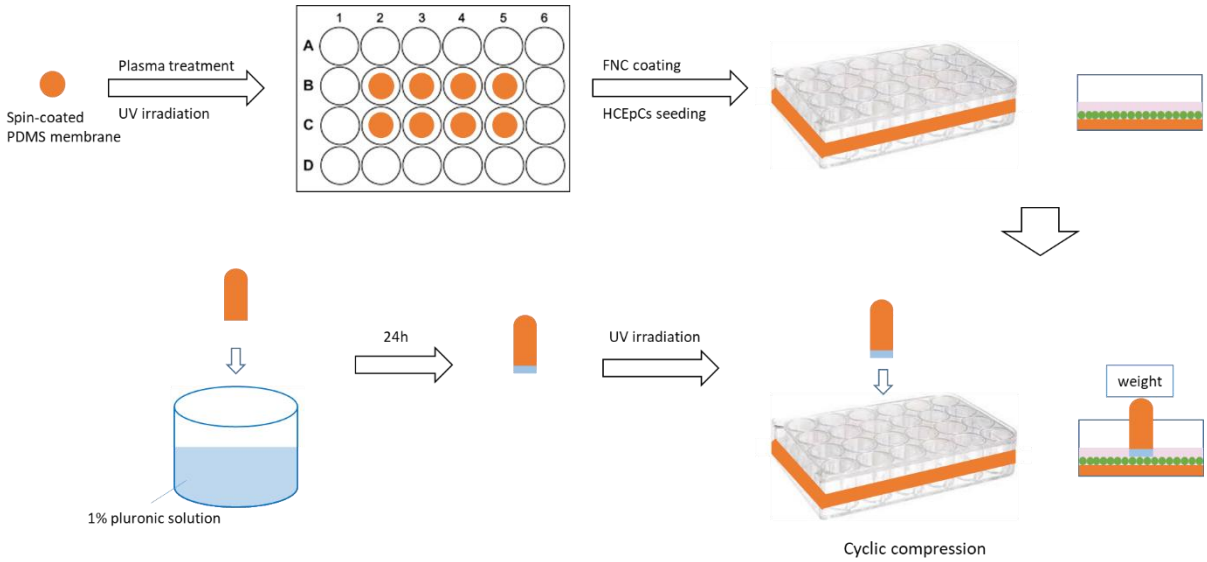

Figure. 18 Cell compression experiment setup.

3.7.2 Cyclic compression on corneal epithelial cells

Four compression episodes were conducted on HCEpCs to mimic cyclic eye rubbing pattern. Each set of compression episodes represents 3 minutes of cell compression at room temperature. Two compression episodes with an interval of 30 minutes were applied on cell monolayer followed by one-hour resting/recovery period, after which the same two compression sets were repeated. Cells were incubated in an incubator except when compressing.

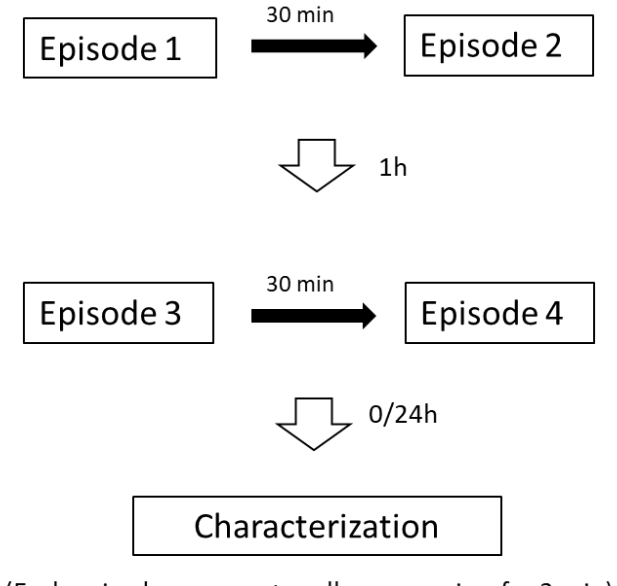

Figure. 19 Cyclic cell compression protocol.

3.8 Cell culture and characterization

3.8.1 HCEpCs culture and monolayer formation

Immortalized HPV-HCEpCs were seeded on FNC-coated PDMS at 20,000 cells/cm^2. Cell culture medium was replaced every other day till confluence (6 days) or till expressing ZO-1 (11 days) for characterization.

3.8.2 Cell characterization after stretching

HCEpCs were seeded in the middle area of the PDMS membrane and incubated for 6 days before stretching. The cell-seeded PDMS membrane was then assembled in the cell culture chamber of the electric cell stretcher. The linear actuator was connected to a computer to control the movement of the indenter. The cell culture membrane was stretched with an indenter displacement of 1 mm for 3 minutes. Cell viability was measured with LIVE/DEAD™ Cell Imaging Kit (Invitrogen) after stretching.

3.8.3 Cell characterization after compression

3.8.3.1 Viability

Cell viability was detected immediately (0 h) and 24 h after compression. Cells were incubated in the incubator before analyzing (for 24 h group). For Calcein AM uptake investigation, compressed cells were incubated for 0 min, 30 min, 60 min and 90 min before analyzing. Cell viability was conducted with the staining of LIVE/DEAD™ Cell Imaging Kit (Invitrogen). Calcein AM stains live cells and Ethidium Homodimer-1 (EthD-1) stains dead cells. Cells were washed with HEPES-BSS buffer (Lonza) twice before staining and were incubated at room temperature for 45 minutes after staining. 2 % of Hoechst (Immunochemistry technologies) was then added with medium and cells were incubated for 10 minutes for counterstaining. Fluorescence images were taken with an immunofluorescence microscope (Zeiss, X-Cite 120 LED). The microscope settings were kept the same when imaging different samples. Representative images were analyzed with Image J.

3.8.3.2 Apoptosis

Apoptosis test was conducted immediately (0 h), 1.5 h and 24 h after compression. Cells were incubated in the incubator before analyzing (for 1.5 h and 24 h groups). Cell apoptosis was conducted with Fluorochrome - Fluorochrome-Labeled Inhibitors of Caspases (FAM-FLICA) ® Poly Caspase Assay Kit (ImmunoChemistry Technologies) following the manufacturer's instruction. The FAM-FLICA kit probe general caspase enzymes including caspase 1-10. Specifically, each vial of FLICA was reconstituted with 50 µl DMSO and then diluted 1:5 with PBS. Diluted FLICA was added to cell medium at 1:20 and was incubated for one hour at 37 °C. After incubation, medium was removed and the cells were washed three times with a 1x apoptosis wash buffer. 2 % of Hoechst 33342 (Immunochemistry technologies) was then added with media and cells were incubated for 10 minutes for counterstaining. After staining, cells were washed with 1x apoptosis wash buffer and kept at 4 °C before imaging. Positive control of apoptosis cells was induced by exposing cells to 2 µM Staurosporine (Sigma) at 37 °C for 3 hours. Images were analyzed with an immunofluorescence microscope (Zeiss,

X-Cite 120 LED). Three separate experiments were conducted with two replicas included for each group. Four images were taken from each sample in the central area. Images were adjusted in ImageJ for proper brightness and exposure. Cell number was counted manually with ImageJ for the whole image. Percentage of apoptosis cells was calculated by dividing the number of apoptosis cells by the number of total cells.

3.8.3.3 Cytoskeleton rearrangement

Cytoskeleton rearrangement was detected immediately (0 h) and 24 h after compression. Cells were incubated in an incubator before analyzing (for 24 h group). Cells were washed with DPBS buffer (1x) (Gibco) before fixation with 4 % paraformaldehyde (PFA) (Sigma Aldrich) for 15 minutes. Cell permeabilization was done by incubation with 0.05 % Triton X-100 (Sigma) and 50 nM glycine (Aldrich) for 20 minutes. Cell nuclei and F-actin were stained with 4',6-diamidino-2-phenylindole (DAPI, Invitrogen, 1:5000) and Alexa Fluor™ 488 Phalloidin (Invitrogen, 1:500) respectively and were incubated for 30 minutes. After staining, cells were washed with PBS and imaged with immunofluorescence microscope (Zeiss, X-Cite 120 LED). The microscope settings including exposure time, light intensity, light path and magnification were kept the same when imaging different samples. Images were adjusted in ImageJ for proper brightness and exposure. For cell growth characterization, cell number was counted manually with ImageJ for the whole image.

3.8.3.4 Tight junction characterization

ZO-1 expression was detected before and after compression with ZO-1 antibody conjugated with Alexa Fluor 488 (Invitrogen). Post-compressive analysis of ZO-1 was done 0 h and 24 h after compression. Cells were incubated in the incubator before analyzing (for 24 h group). Cells were washed with PBS and 1 ml cold methanol (-20 °C) was added into each well for fixing. 15 minutes later, cells were washed with PBS 3 times. PBS containing 0.1 %TritonX-100, 0.2 % Bovine serum albumin (BSA) and 5 µg/ml ZO-1- Alexa Fluor 488 was added to each well and well plate was incubated for 1 hour at room temperature. After incubation, cells were washed with PBS 3 times. Then 1:5000 DAPI diluted with PBS was added to stain nuclei. After 30 minutes of staining, cells were mounted and imaged with an immunofluorescence microscope (Zeiss, X-Cite 120 LED). Twelve images from three samples were selected and analyzed with ImageJ. Specifically, three random zones of each image were selected for analysis. Cell number and number of cells expressing ZO-1 were manually counted. Cells with all edges expressing ZO-1 were characterized as ZO-1 expressing cells. Percentage of ZO-1 expressing cells was calculated by dividing ZO-1 expressing cells over total cells.

3.8.3.5 Cell image acquisition

After staining, cells were mounted and imaged using an immunofluorescence microscope (Zeiss, X-Cite 120 LED). For the same characterization, microscope setting including exposure time, light intensity, light path and magnification were kept the same when imaging different samples. Four images were taken from each sample in the central area of the PDMS membrane. Images from each sample were selected and analyzed with ImageJ.

3.9 Statistics

Each experiment was repeated three times. Duplicates were made for each characterization method except for ZO-1. Statistical differences were compared between experimental groups with T-test analysis. Statistical significance with $p<0.05$ is denoted as *.

4.0 Results and Discussion

4.1 HCEpCs monolayer formation

HCEpCs were seeded and cultured with the method stated in section 3.3. To better understand the growth properties of HCEpCs, the effects of substrate, protein coating and cell incubation time were analyzed.

4.1.1 Effect of substrate

HCEpCs were stained and counted after 3 days of culturing on uncoated tissue culture polystyrene (TCPS) and PDMS substrate (Figure 20). As a stretchable material with comparable elastic modulus to cornea [190], PDMS is a promising candidate material for HCEpCs culture. However, there was almost a 30 % decrease in cell growth on PDMS membrane compared to that on TCPS.

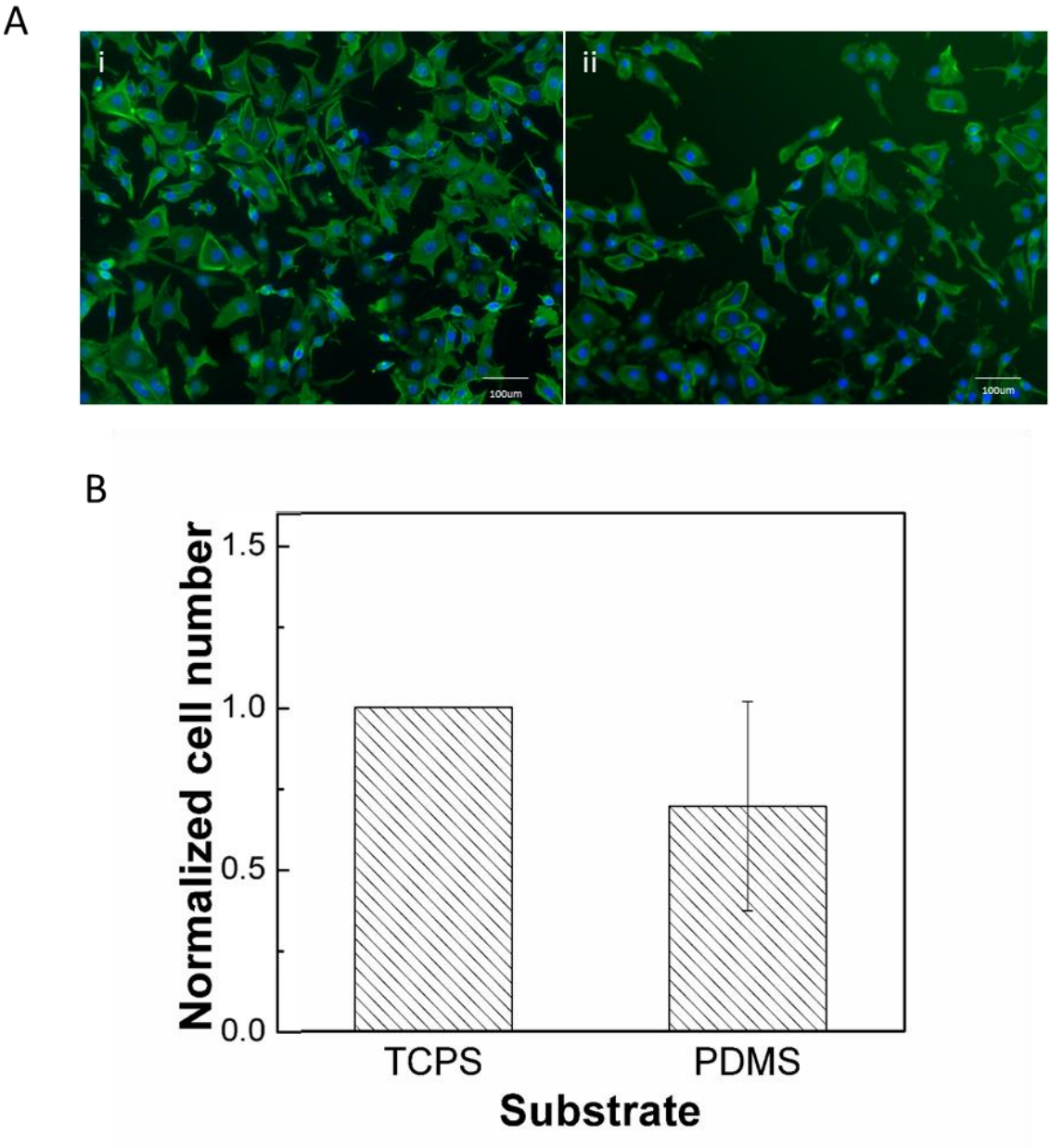

Figure. 20 HCEpCs culture on different substrates.

A, DAPI/ F-actin staining of HCEpCs monolayer at day 3 seeding on TCPS (i) and PDMS (ii). Scale bar is 100 µm. B, Cell number comparison of HCEpCs. The number of cells in 12 pictures (4 per sample) was counted using Image J. Cell number is normalized by dividing cell count seeded on different substrates with that seeded on TCPS. n=3.

4.1.2 Effect of protein coating

Various extracellular matrix (ECM) proteins were selected as a coating agent to promote cell growth and attachment on PDMS. The coating proteins chosen in this project include FNC coating mix, gelatin A and gelatin B. FNC-coated PDMS showed a significant increase in cell number at day 3; however, gelatin A and gelatin B had no significant effect on promoting cell growth (Figure 21 A). Additionally, FNC coating time was found to have no effect on cell growth or adhesion. The coating time ranging

from 30 seconds to 30 minutes all promoted cell adhesion and / or proliferation compared to non-coated PDMS; no significant difference was found among groups with different coating time (Figure 21 B).

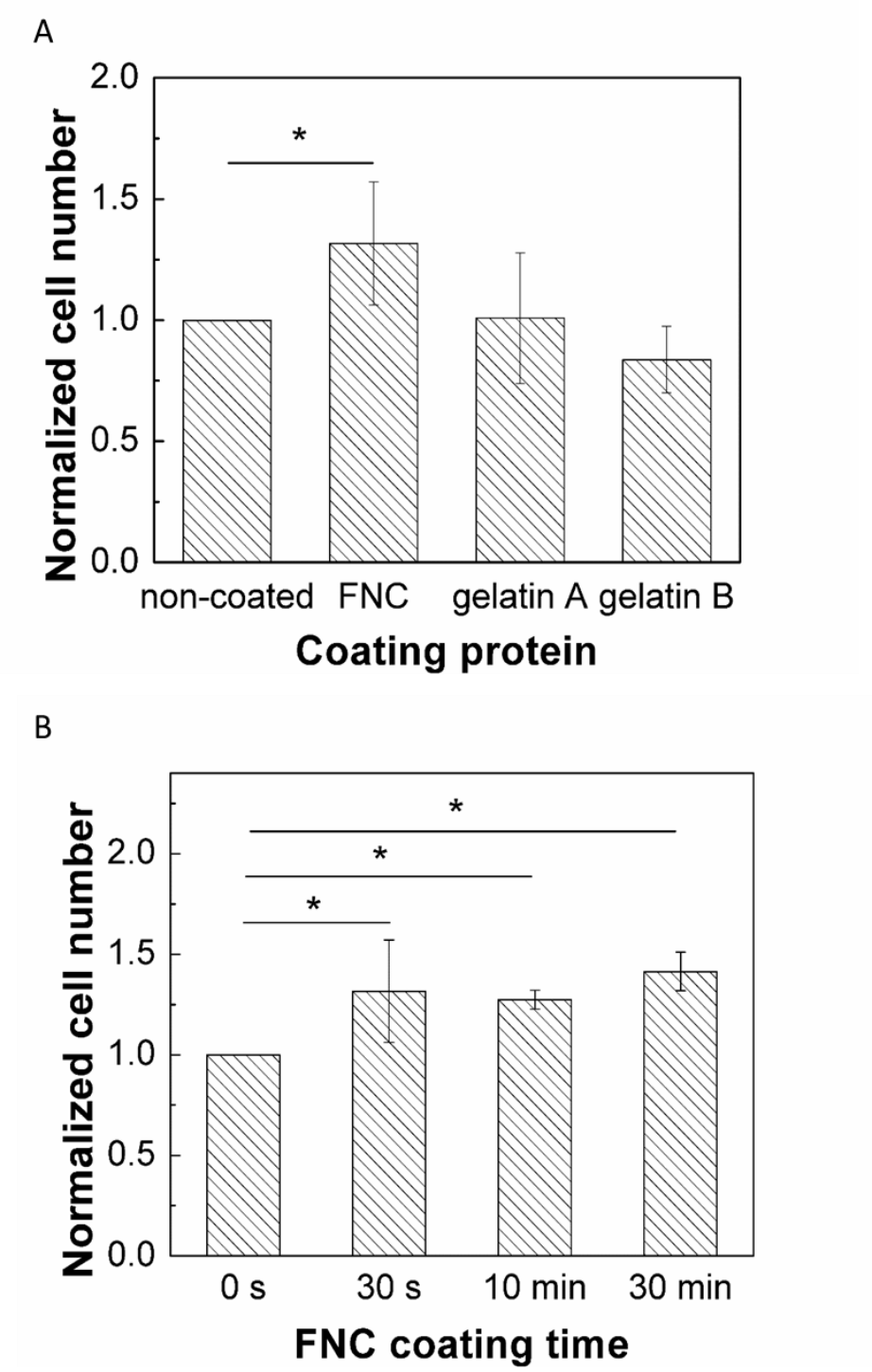

Figure. 21 Effect of coating protein.

A, HCEpCs culture on PDMS with various coating proteins. B, HCEpCs cultured on PDMS with different FNC coating time. The number of cells in 12 pictures (4 per sample) was counted using Image J. Cell number is normalized by dividing cell count under each condition with cell count on non-coated PDMS (A) and 0s (B) respectively. * $p<0.05$, n=3.

4.1.3 Effect of incubation time

We further analyzed the culture time needed to obtain confluent cell layer and tight junction protein expression. After 2 days of seeding, HCEpCs were attached to substrate with a relatively low density (Figure 22 A-i, ii). It took 4 days for HCEpCs to become confluent on FNC-coated PDMS (Figure 22 A-iii, iv). However, at this time the cells were not expressing ZO-1. As is shown in Figure 22 B-i and ii, there was signs of ZO-1 expression at day 7, which was 3 days after reaching confluence, and an increased ZO-1 expression was observed until 11 days after seeding when abundant tight junctions were then present (Figure 22 B-iii-vi).

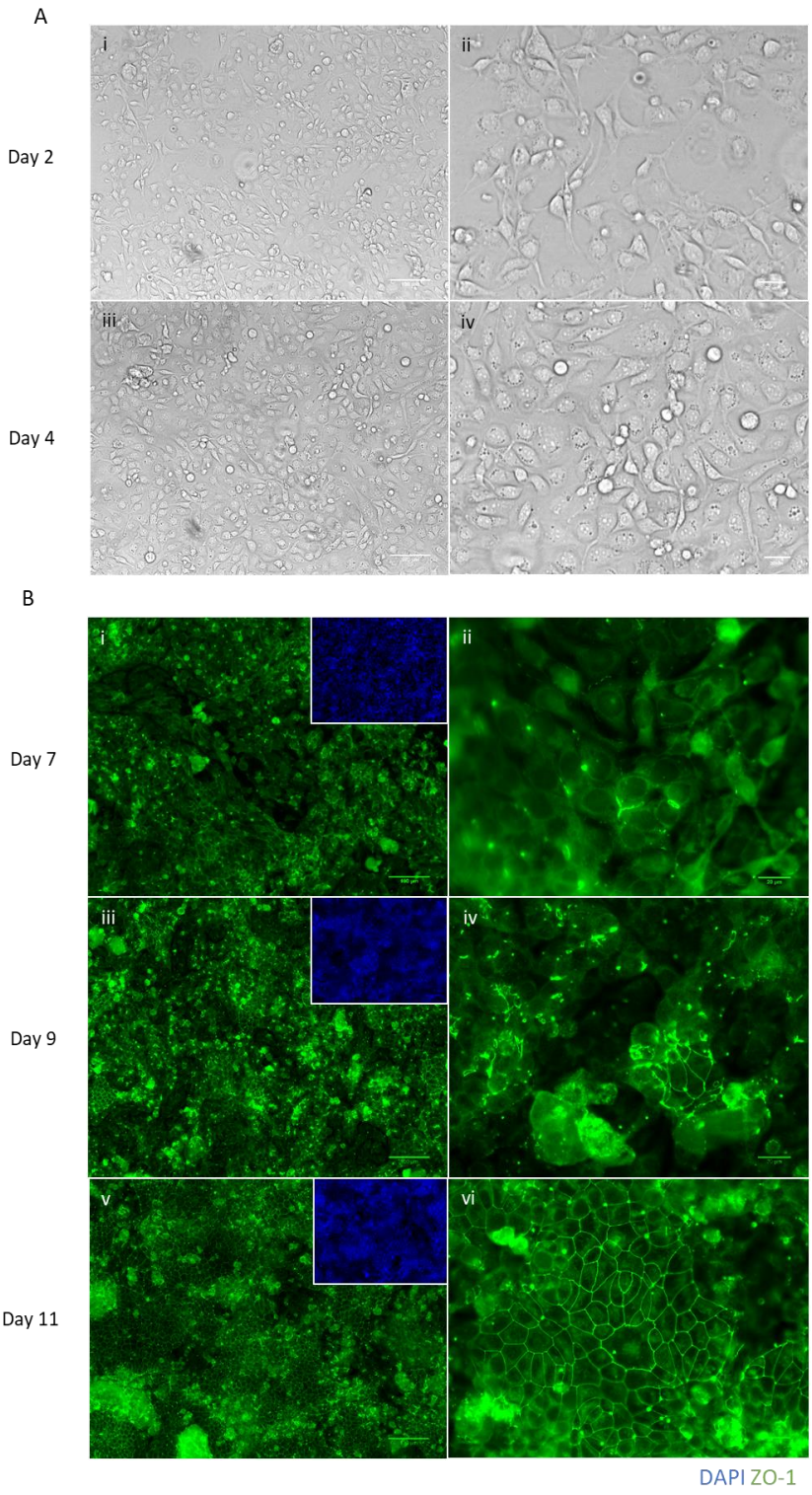

Figure. 22 Effect of incubation time on cell confluence and tight junction formation.

A, Effect of incubation time on cell confluence with different incubation time. (i), (ii), HCEpCs at day 2; (iii), (iv), HCEpCs at day 4. B, Effect of incubation time on tight junction formation of HCEpCs monolayer with different incubation time. (i), (ii), day 7; (iii), (iv), day 9; (v), (vi), day 11. Tight junction formation was characterized with ZO-1 staining (green). Representative images were selected from 3 separate experiments. Scale bar is 100 μm.

4.2 Cell stretcher calibration and cell stretching test

4.2.1 Stress-strain curve of PDMS membrane

Aiming to investigate corneal epithelial cell response under eye rubbing like tensile stress, it is essential to transfer the strain on cell culture membrane (PDMS) to tensile stress experienced by cells. To obtain a stress-strain curve, elongation of the cell culture membrane under given tensile stress was tested. Figure 23 shows that within 10 % of elongation of the PDMS membrane, the fitted linear equation is as follows:

$$Y=1.88X+1.24 \qquad eq.1$$

Where Y is the tensile stress on PDMS membrane (N/cm^2) and X is strain (%) of the PDMS membrane.

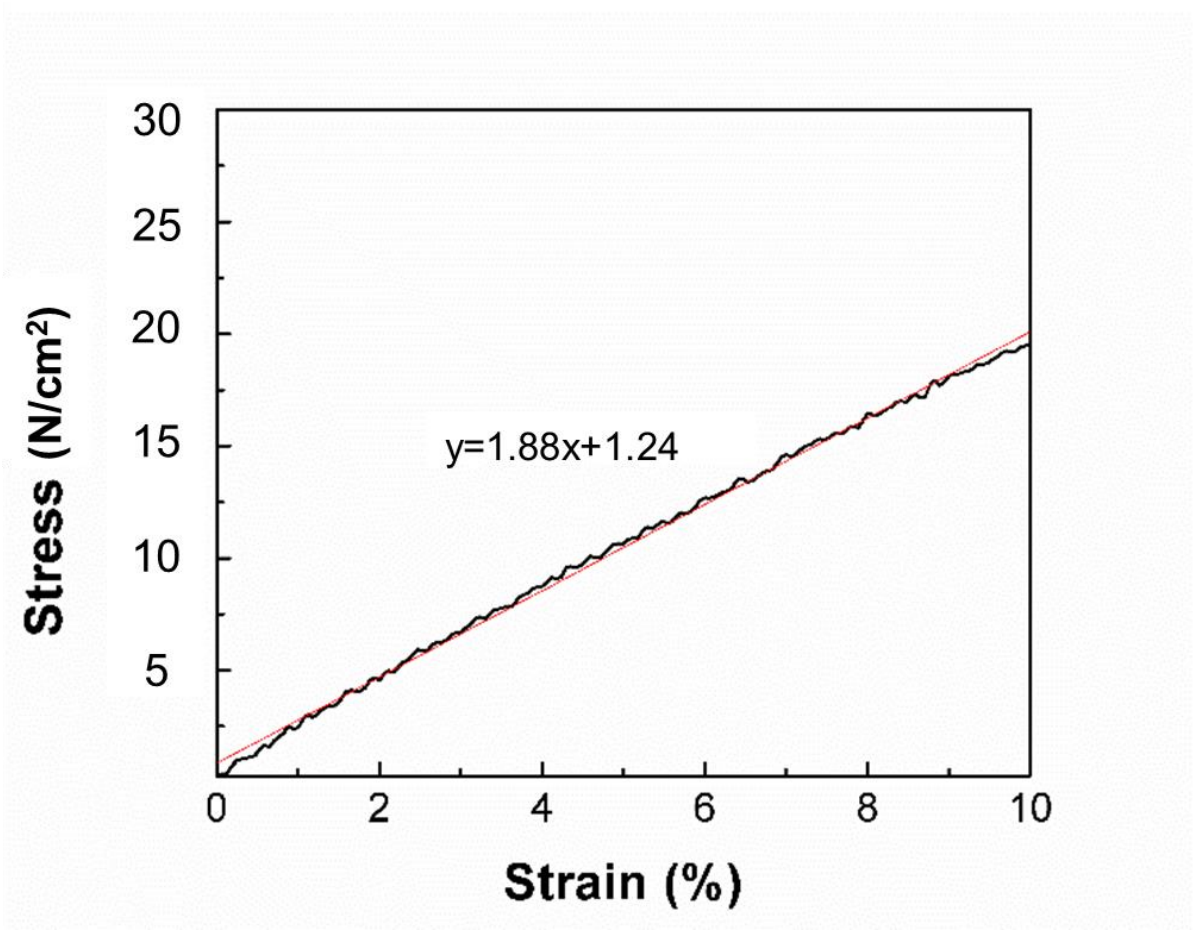

Figure. 23 PDMS stress-strain curve. n=3.

The severe eye rubbing stress has been reported as 17 N/cm^2 [149], which corresponds to 8.7 % strain of the PDMS membrane. Thus, it is critical to maintain the cell culture membrane deformation at or less than 8.7 % in order to investigate cell behavior affected by eye rubbing stress.

4.2.2 Fluidic cell stretcher characterization

Fluidic cell stretcher calibration was conducted with the method stated in section 3.3. The effect of inlet air pressure and time were investigated.

Effect of pressure

Air inlet was controlled at 7 N/cm^2, 10 N/cm^2 and 13 N/cm^2 and the cell culture membrane deformation was measured separately. Our results showed that the average strain increased with an elevated inlet pressure. The mean obtained strain for each pressure was 2.5 %, 3.6 % and 4.2 % respectively. The fitted strain-air pressure curve is shown in equation 1, which enabled us to predict and adjust the deformation of cell culture membrane by controlling inlet air pressure.

$$Y=0.26X+0.74 \qquad eq.2$$

Where Y is the obtained strain (%) on cell culture membrane and X is the inlet air pressure (N/cm^2).

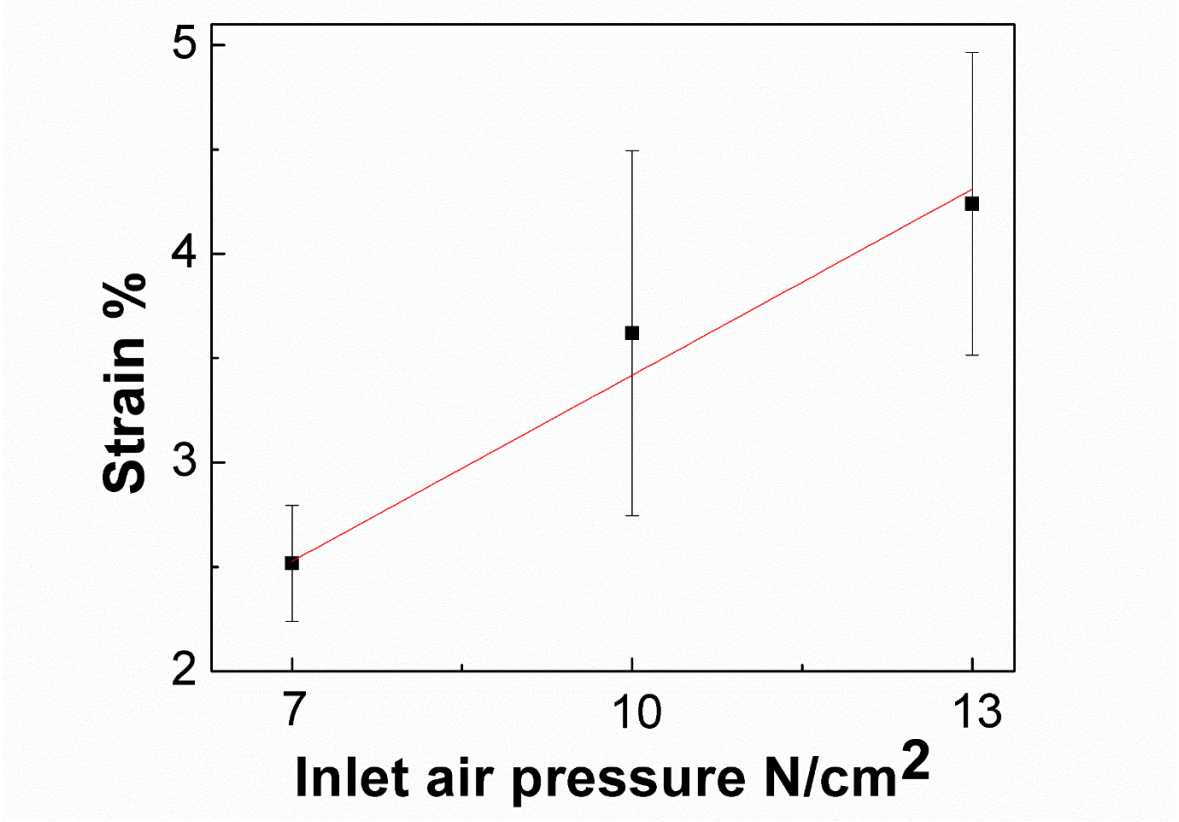

Figure. 24 Fluidic cell stretcher calibration curve.

PDMS strain under various inlet pressure. n=3.

Effect of time

The change of PDMS membrane deformation over time is shown in Figure 25. As is shown, the strain was obtained within one minute of air inflation. Although the strain was kept stable for five minutes with negligible disturbance, a relatively high standard error was observed under 13 N/cm^2 of inlet air

pressure compared with that at 7 N/cm^2 and 10 N/cm^2, indicating the intolerance of such high pressure of the built stretching system.

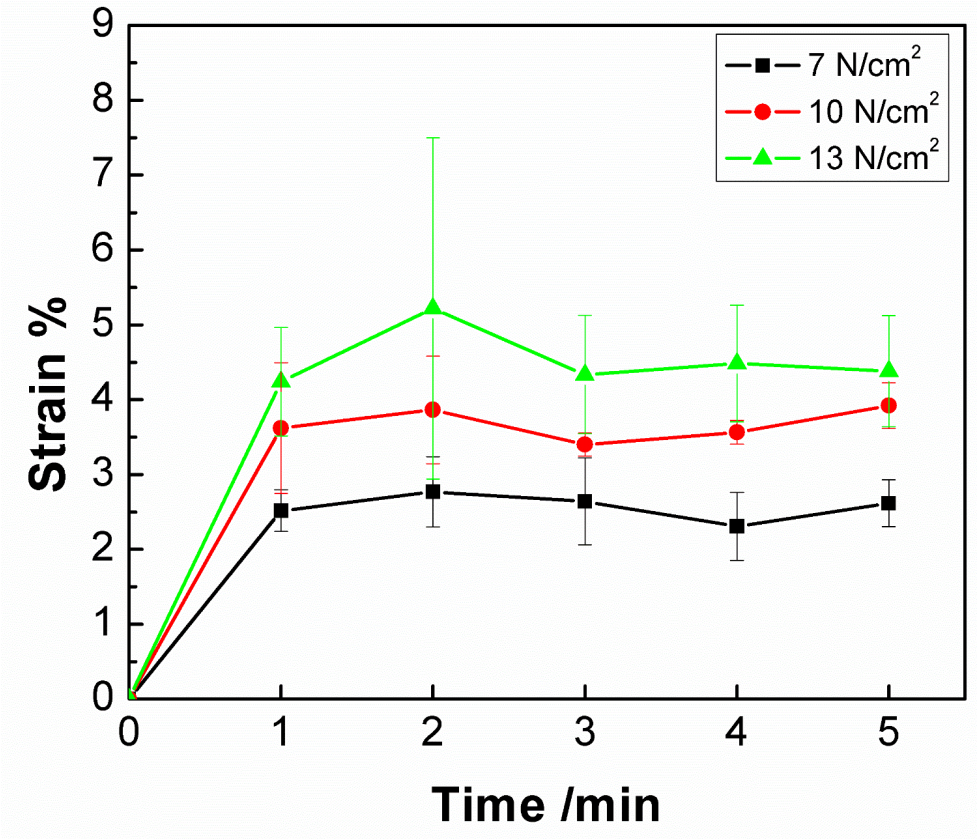

Figure. 25 PDMS strain obtained on fluidic cell stretcher over time with different inlet air pressure. n=3.

Our calibration results demonstrated a linear fit of the strain on the cell culture membrane and the inflated air pressure. Moreover, the strain variance was relatively low under a pressure at and lower than 10 N/cm^2 over the first four minutes of stretching. These results indicate that our customized stretching system was controllable and stable at certain conditions, thus capable of cell stretching investigation.

Based on equation 1 and equation 2, the relation between tensile stress sensed by cells and the inlet air pressure is shown below:

$$Y=0.49X+1.39 \qquad eq.3$$

Where Y is the tensile stress sensed by cells (N/cm^2) and X is inlet air pressure (N/cm^2).

The calculated relation of inlet air pressure, membrane strain and tensile stress sensed by cells are listed in Table 4. The highest stress listed was noted as severe eye rubbing stress. As is shown in this table, the three set of tested inlet air pressure all induced tensile stress on the cell culture membrane within the range of severe eye rubbing stress.

Table. 4 Relation of inlet air pressure, PDMS membrane strain and tensile stress sensed by cells.

Inlet air pressure N/cm^2	Strain on PDMS membrane %	Stress sensed by cells N/cm^2
7	2.5	5
10	3.6	8
13	4.2	9
29	8.8	17

4.2.3 Electric cell stretcher calibration curve

Effect of indenter displacement

Due to the limitation of the linear actuator, the minimum displacement of the indenter was 1 mm. Thus, the cell culture membrane could not be deformed continuously. As is shown in Figure 26, the strain of cell culture membrane increased with increased displacement of the indenter, which were 2.6 %, 6.5 %, 13.3 %, 23.0 %, 32.0 % at the indenter displacement of 1 mm, 2 mm, 3 mm, 4 mm, 5 mm, respectively.

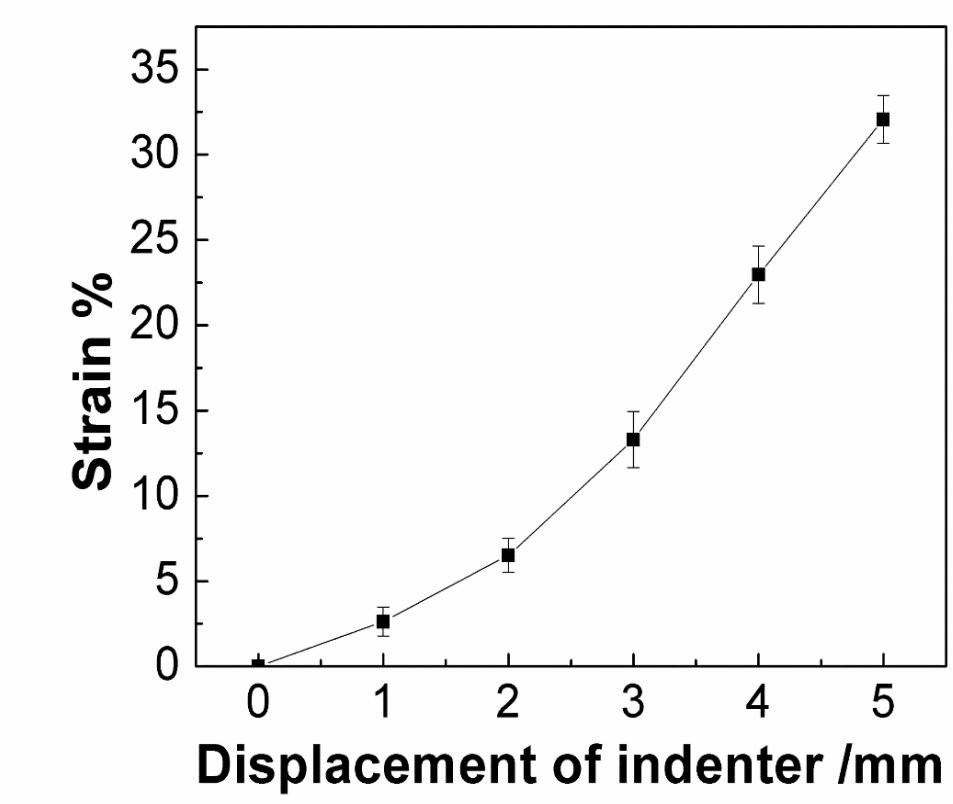

Figure. 26 Electric cell stretcher calibration curve with PDMS strain under various indenter displacement. n=4.

Effect of time

The strain of the cell culture membrane was measured within 5 minutes of stretching with an indenter

displacement of 1-2 mm. It is shown in Figure 27 that no significant difference was detected on the strain of the cell culture membrane, indicating the stability of the electric stretching system.

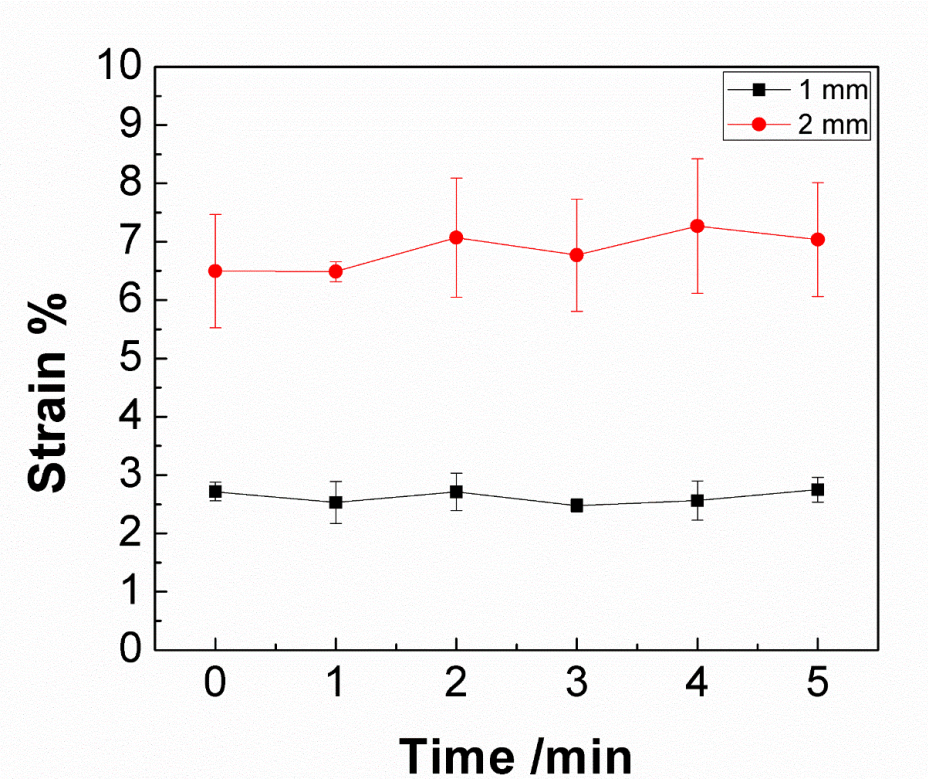

Figure. 27 PDMS strain on the electric cell stretcher under indenter displacement of 1 mm and 2 mm. n=3.

4.2.4 Cell viability upon stretching

HCEpCs were seeded on the PDMS membrane of the electric cell stretcher and were stretched with the indenter displacement of 1 mm. HCEpCs viability was assessed with Live/Dead assay (Calcein AM stains live cells, EthD-1 stains dead cells). As shown in Figure 28, increased cell detachment was observed after stretching. This may result from either mechanically-induced detachment of the cells from the substrate or cell death induced detachment. The result was consistent with the previous reported observation where human alveolar basal epithelial cells (A 549 cells) presented significant cell detachment after stretching at 20 % strain for 8 hours [191]. Another study observed increased A549 cell death and cell detachment when cells were exposed to a combination of tensile stress (from 50 % strain stretch) and shear stress for 2 minutes, indicating short-period induced cell damage upon high mechanical stress gradient [192]. Calculated from equation 1, the selected cell culture membrane deformation exposed the cells to a tensile stress of 6 N/cm^2, which would be considered a severe rubbing stress (see Table 4). If one may compare the difference between cell monolayer and the corneal epithelium (stratified layer), the stress used in the cell stretching study may be considered at a high level for monolayer, which may result in cell death immediately after stretching. Our results presented here indicate a direct damage on HCEpCs by tensile stress, highlighting potential of epithelium wounding caused by eye rubbing.

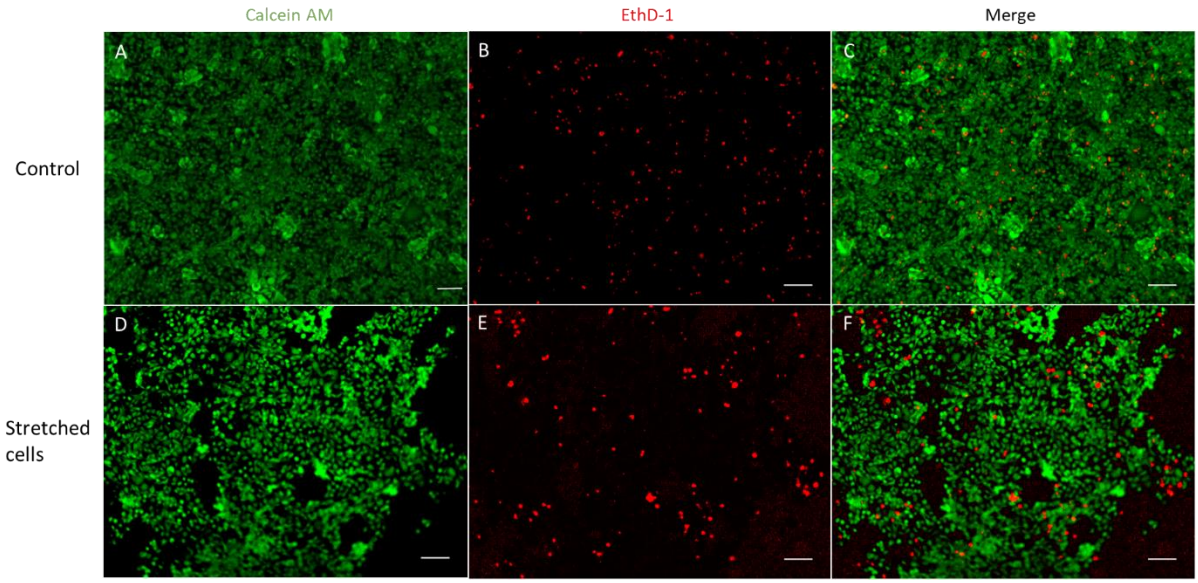

Figure. 28 Effect of tensile stress on cell viability. Immortalized HCEpCs were stretched for 3 minutes and then stained with Calcein AM / EthD-1. Calcein AM stains live cells in green and EthD-1 stains dead cells in red. Representative images were selected from 2 separate experiments. Scale bar is 100 µm.

4.3 Cell behavior upon compression

4.3.1 Cell viability upon compression

HCEpCs viability was assessed with Live/Dead assay (Calcein AM stains live cells, EthD-1 stains dead cells) immediately and 24 hours after compression. At 0h, no change was observed under 0.03 N/cm^2 compressive stress (Figure 29 A-i, ii). However, HCEpCs stained with EthD-1 after being exposed to compressive stress at or higher than 0.05 N/cm^2 (Figure 29 A-iii, iv), suggesting that cells had died. When the compressed cells were allowed to recover for 24 hours, no difference in live/dead staining was seen on the HCEpCs exposed to 0.03 N/cm^2 and 0.05 N/cm^2 compressive stress compared to control group (Figure 29 A-v,vii), suggesting that the compression induced cellular damage and the uptake of EthD-1 was reversible within 24 hours. In contrary, cellular uptake of EthD-1 at 0.10 N/cm^2 compressive stress did not change after 24 hours, indicating exposing cells to such a compressive stress resulted in killing the majority of the cells (Figure 29 A-viii). Primary HCEpCs showed similar fluorescence uptake upon 0.05 N/cm^2 compression where most cells were permeable to EthD-1 after compression but recovered and stained with Calcein AM after 24 h of incubation (Figure 29 B).

Unlike the higher compressive stress (0.10 N/cm^2), which resulted in cell death in immortalized HCECs, the medium compressive stress (0.05 N/cm^2) seemed to only induce damage to cells transiently, which was overcome within 24 h. Cell damage and cell death induced by compression has been reported extensively in various cell types [193]–[195], which is consistent with our result upon the highest compressive stress (Figure 29 A). However, the “reversible cell damage” observed on HCEpCs under a compressive stress of 0.05 N/cm^2 may likely be explained by the cellular uptake of EthD-1 immediately after compression resulting from a transient damage in cell membrane permeability.

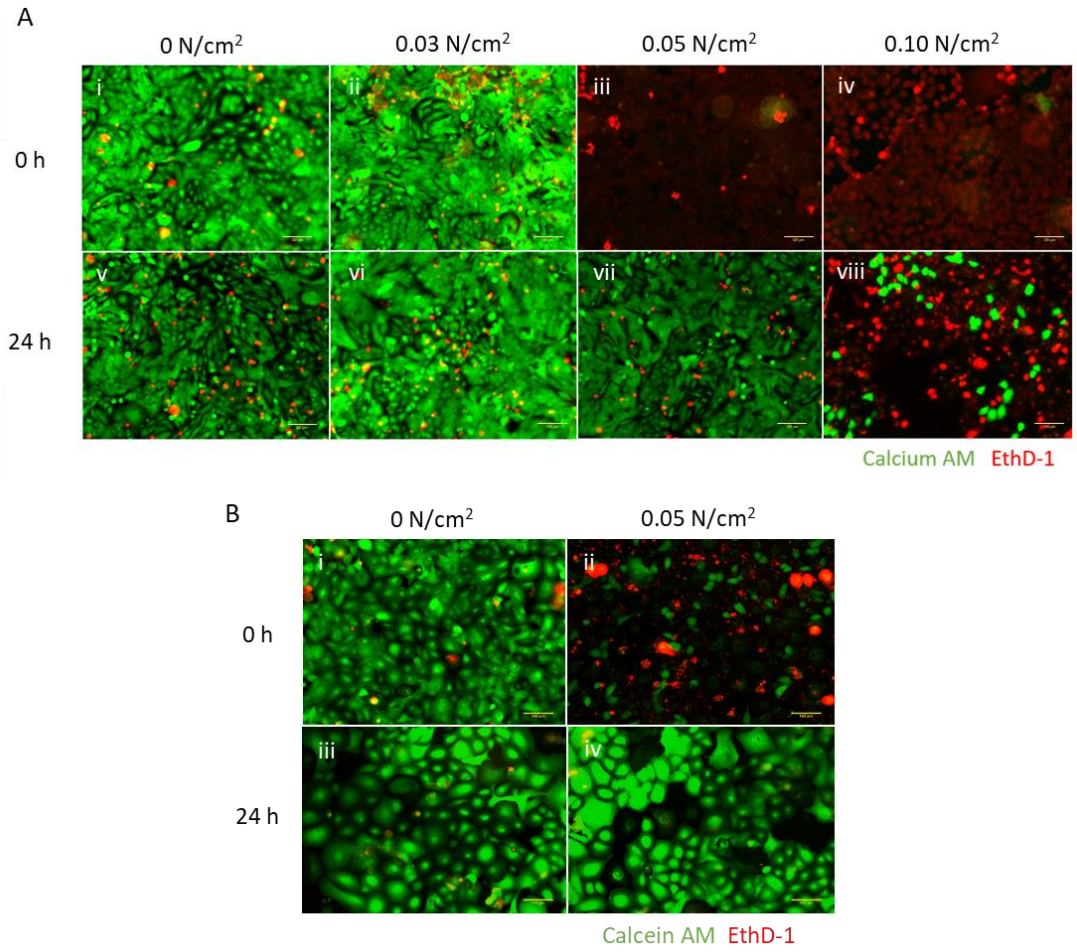

Figure. 29 Effect of compressive stress on cell viability.

A, Immortalized HCEpCs viability under different compressive stress. B, Effect of medium load stress (0.05 N/cm^2) on primary HCEpCs. Calcein AM (stains live cells in green) / EthD-1 (stains dead cells in red) staining was conducted immediately after compression (0 h) and after cells were incubated for 24 h after compression (24 h). Representative images were selected from 3 separate experiments. Scale bar is 100 µm.

Cell viability was further characterized for the HCEpC monolayer with developed tight junctions. After forming tight junctions, HCEpC monolayer could hold a compressive stress of 0.93 N/cm^2, 9 times more than the highest load tested earlier. At 0h, no change was seen on cells under 0.52 N/cm^2 (Figure 30 A, B). At higher compressive stress (0.93 N/cm^2), cell detachment was observed after compression (Figure 30 C) and the detachment increased with increasing compressive stress (data not shown). Increased cell death and cell detachment were also present 24 hours after compression (Figure 30 D, E, F). Different from the HCEpCs without ZO-1, which were still attached on the substrate after compression even when they stained dead (Figure 29 A-G), cells with ZO-1 detached immediately from the substrate once they died from compression. Moreover, unlike HCEpCs without ZO-1 formation/expression, there was no change in EthD-1 uptake within 24 hours after compression. These differences may indicate the protective role of ZO-1 on HCEpCs upon compression in that cells with ZO-1 could tolerate higher loading of compression and that cell membrane permeability could maintain

stable after compression.

The protective role of ZO-1 upon compression has been reported with the finding that Salvianolic Acid B [196] and curcumin [197] could protect rat spinal cord against compressive injury, both of which work through upregulating the expression of ZO-1.

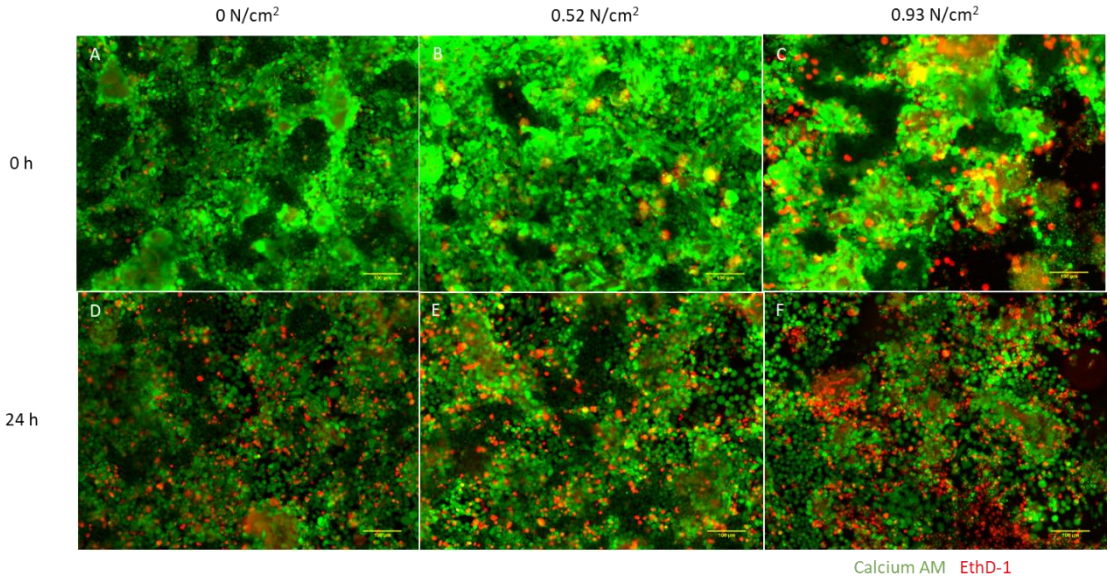

Figure. 30 Effect of high compressive stress on cell viability.

Viability test of ZO-1 expressing immortalized HCEpCs 0 h (A-C) and 24 h (D-F) after compression. Calcein AM (stains live cells in green) / EthD-1 (stains dead cells in red) staining was conducted immediately after compression (0 h) and after cells were incubated for 24 h after compression (24 h). Representative images were selected from 3 separate experiments.

Scale bar is 100 μm.

4.3.2 Calcein AM uptake upon compression

The previous section indicated cell permeability change after compression with a compressive stress of 0.05 N/cm^2. Although no change in Calcein AM /EthD-1 uptake was seen at 0.03 N/cm^2 immediately after compression, we decided to detect whether cell permeability was also affected by compression at this loading weight. Calcein AM/EthD-1 staining was conducted within 90 minutes after compression of 0.03 N/cm^2. No change in HCEpCs was seen immediately after compression (Figure 31 A, i-iv); however, dramatically increased Calcein AM uptake was observed when cells were incubated for 30-90 min after compression at low compressive stress (0.03 N/cm^2) (Figure 31 A, v-xii). Excessive Calcein AM was washed with PBS after staining, indicating that the observed increased Calcein AM intensity was a result of cellular uptake. Thus, we speculate a change in cell permeability caused by compression. However, this phenomenon was not observed on primary HCEpCs, which showed no change of Calcein AM uptake within 30 min after compression (Figure 31 B). The increased Calcein AM uptake observed here correlates with the finding that increased fluorescein permeability was shown in the cornea after penetrating keratoplasty as a result of mechanical stimuli [198].

A

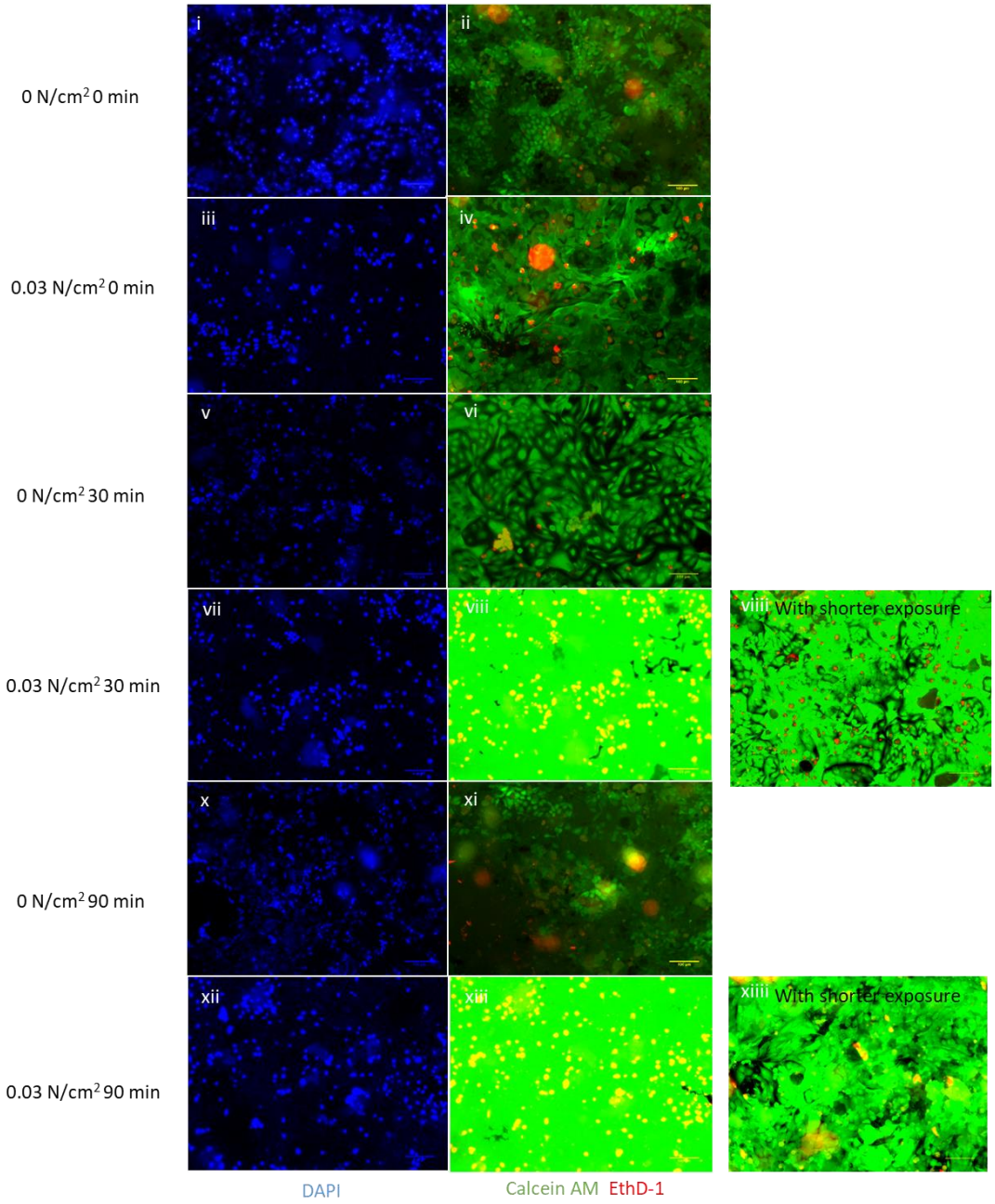
0 N/cm² 0 min
0.03 N/cm² 0 min
0 N/cm² 30 min
0.03 N/cm² 30 min
0 N/cm² 90 min
0.03 N/cm² 90 min
i
ii
iii
iv
v
vi
vii
viii
viiii With shorter exposure
x
xi
xii
xiii
xiiii With shorter exposure
DAPI
Calcein AM EthD-1

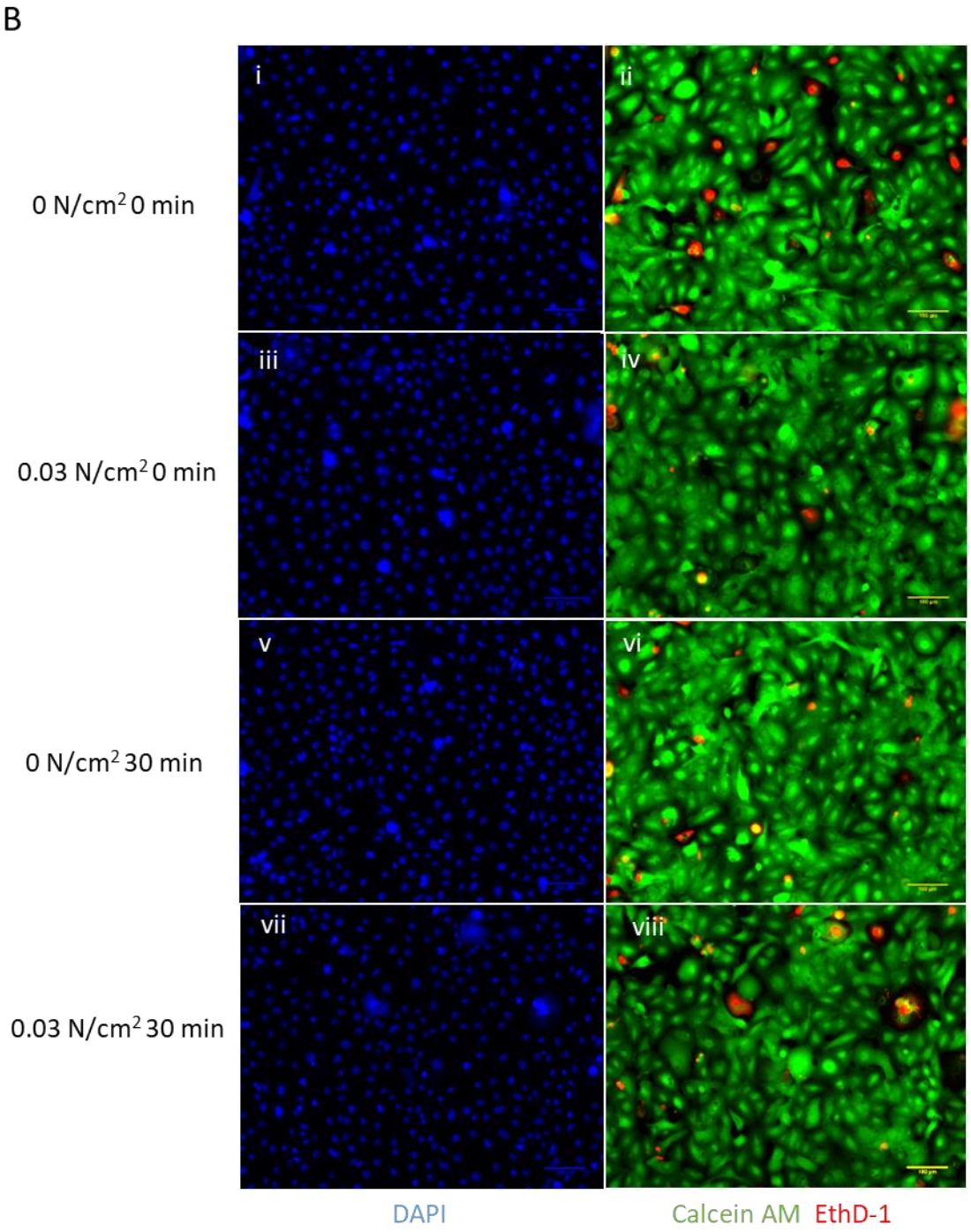

Figure. 31 Effect of compressive stress on Calcein AM uptake.

Calcein AM uptake of immortalized HCEpCs (A) and primary HCEpCs (B) under compressive stress. Calcein AM (stains live cells in green) / EthD-1 (stains dead cells in red) staining was conducted immediately after compression (0 min) and after cells were incubated for 30 min and 90 min after compression. Representative images were selected from 3 separate experiments. Scale bar is 100 μm.

The Calcein AM uptake was also assessed on HCEpC monolayer with ZO-1 formation. Unlike the HCEpCs without tight junction, ZO-1 expressing cell monolayer displayed no minimal change in

Calcein AM uptake at any loading weight (Figure 32) when incubated for up to 60 minutes after compression.

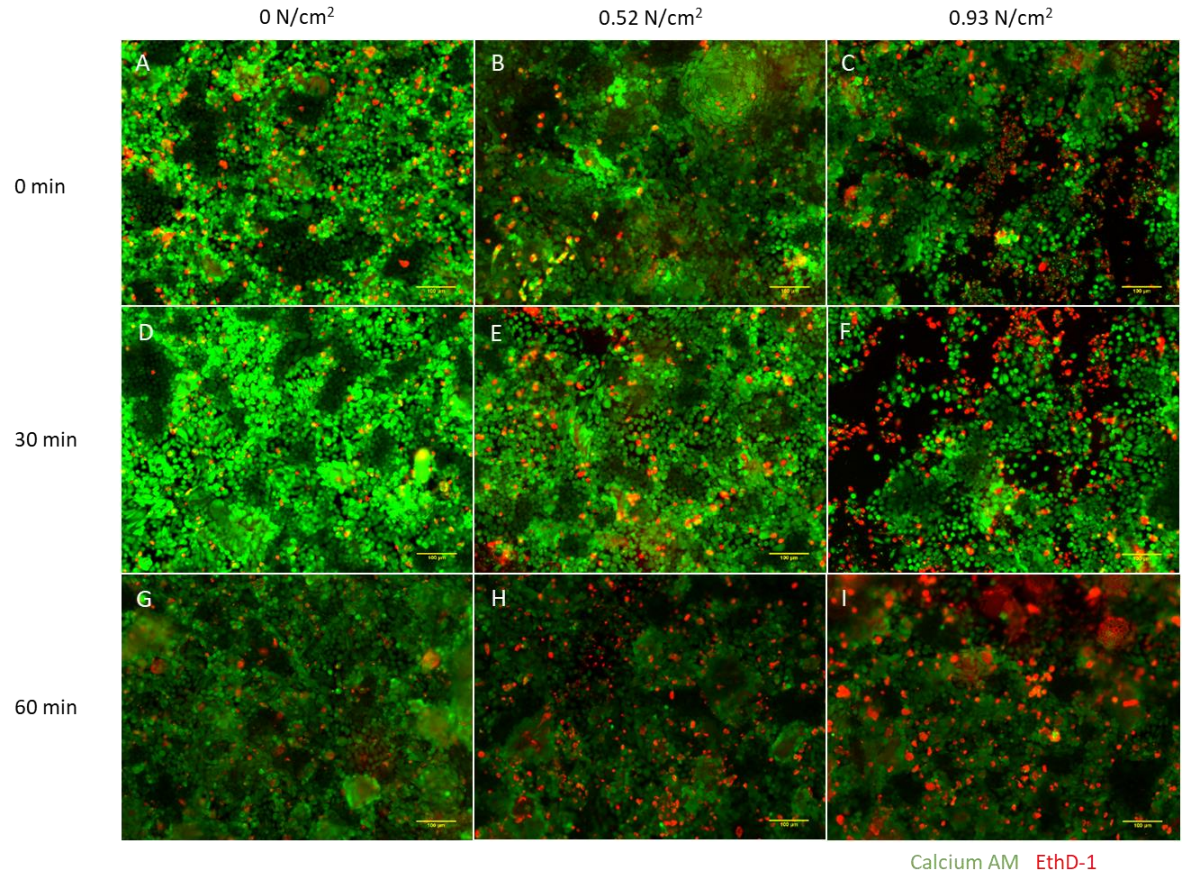

Figure. 32 Effect of high compressive stress on Calcein AM uptake.

Calcein AM uptake of immortalized HCEpCs under compressive stress. Calcein AM (stains live cells in green) / EthD-1 (stains dead cells in red) staining was conducted immediately after compression (0 min) and after cells were incubated for 30 min and 60 min after compression. Representative images were selected from 3 separate experiments. Scale bar is 100 μm.

4.3.3 Cell apoptosis upon compression

Caspases, members of cysteine proteases which are activated in apoptotic cells, were characterized in HCEpCs 0 h, 1.5 h and 24 h after compression. As is shown in Figure 33, Figure 34 and Figure 35, no difference was seen in cellular expression of caspase for cells 0 h and 1.5 h after compression. However, 24 hours after compression, a significantly increased apoptosis rate was observed in cells which had been exposed to a compressive stress of 0.05 N/cm^2 (Figure 35, Figure 36). Similar results were observed on ZO-1 expressing cells. No difference in caspase expression was detected 0 h (Figure 37) and 1.5 h (Figure 38) after compression. However, when HCEpCs were incubated for 24 h after compression, an increase in caspase expression was observed on the cells compressed with 0.52 N/cm^2 compressive stress (Figure 39, Figure 40).

Apoptosis is a form of programmed cell death that exists in normal cells under physiological condition in order to eliminate damaged cells. Aberrant cellular apoptosis upon external mechanical compression

has been reported in various cell types [199]–[202]. Although no research has been published on compression-induced apoptosis on HCEpCs, the findings of increased apoptosis observed in HCEpCs under shear stress [136] and substrate stiffness [122] highlight the potential of apoptosis activation as a mechanoresponse of HCEpCs.

It has been found that corneal keratocytes could undergo increased apoptosis as a result of wounded epithelium [203]. In this process, IL-1 [204] has been suggested as a potential mediator in regulating apoptosis. The potential role of IL-1 on HCEpCs apoptosis has also been proven with the finding that IL-1 Receptor Antagonist could inhibit cell apoptosis in human corneal limbal epithelial cells [205]. Thus, the increased apoptosis observed at 24 hours after compression in our results may be related to IL-1 released by HCEpCs.

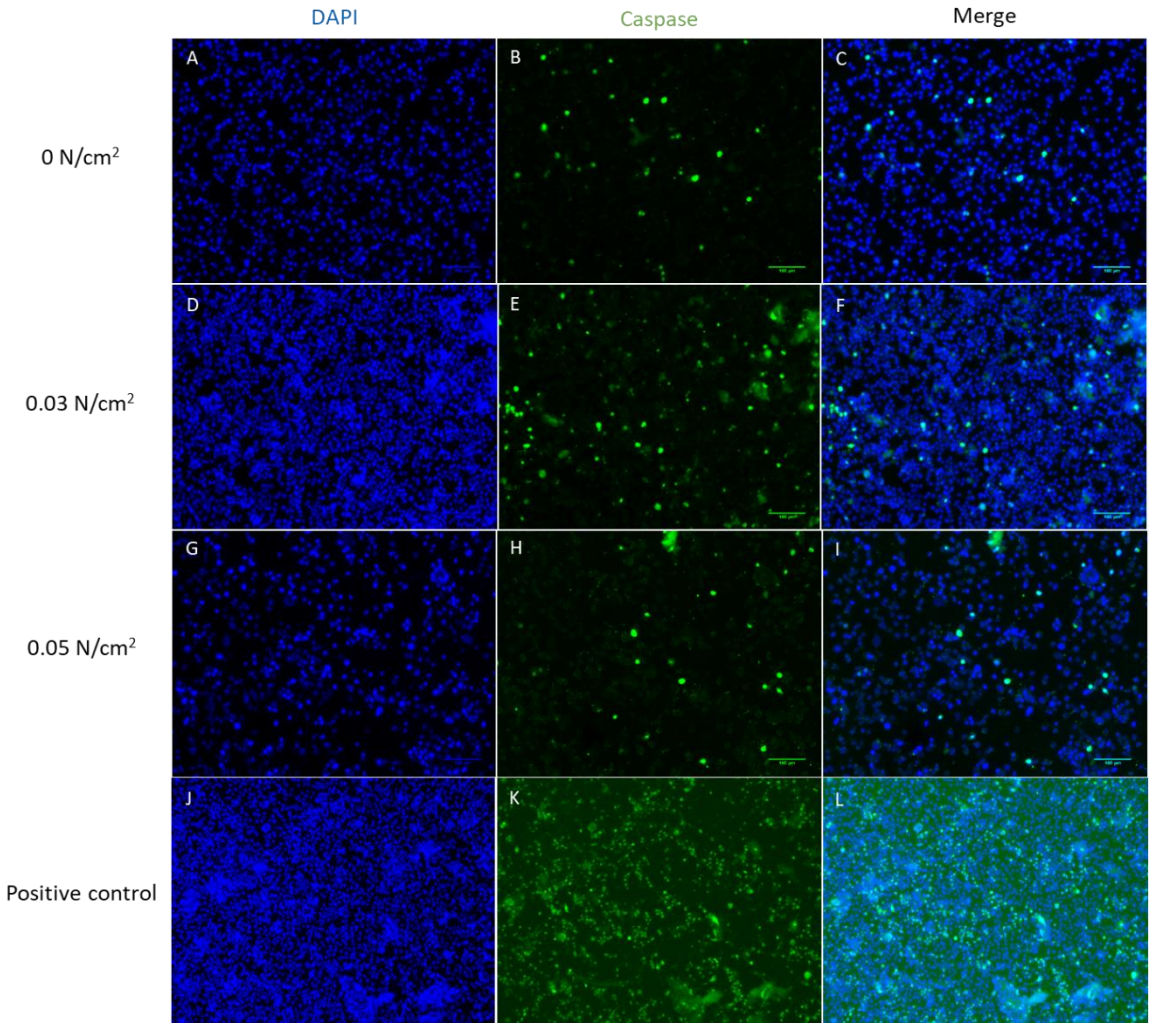

Figure. 33 Effect of compressive stress on apoptosis of immortalized HCEpCs (0 h).

Cell apoptosis was detected by poly caspase staining (FAM-FLICA, green) immediately after compression. In the positive control, apoptosis was induced by staurosporine. Representative images were selected from 3 separate experiments. Scale bar is 100 μm.

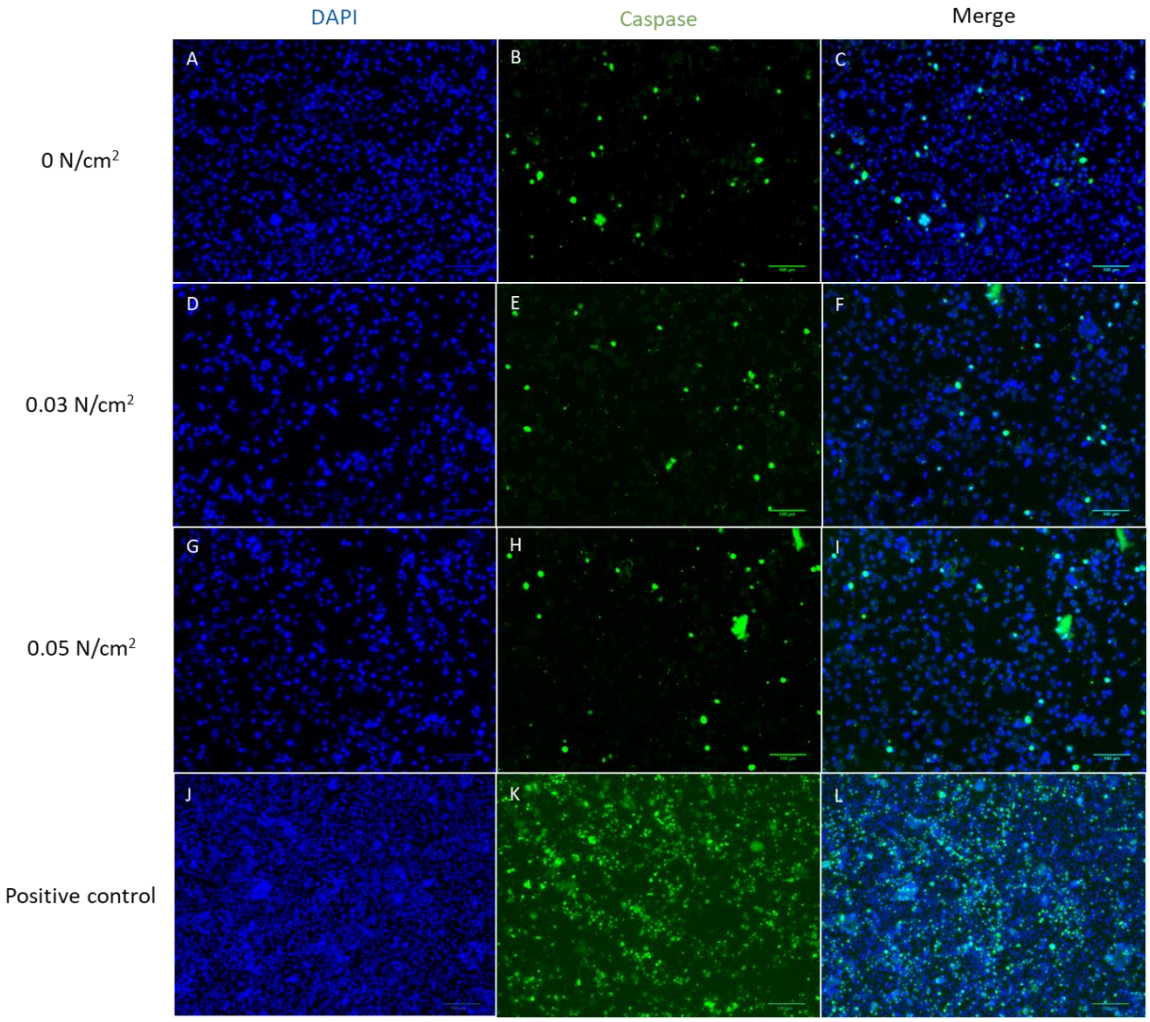

Figure. 34 Effect of compressive stress on apoptosis of immortalized HCEpCs (1.5 h).

Cell apoptosis was detected by poly caspase staining (FAM-FLICA, green) after incubating cells for 1.5 h post-compression. In the positive control, apoptosis was induced by staurosporine. Representative images were selected from 3 separate experiments. Scale bar is 100 μm.

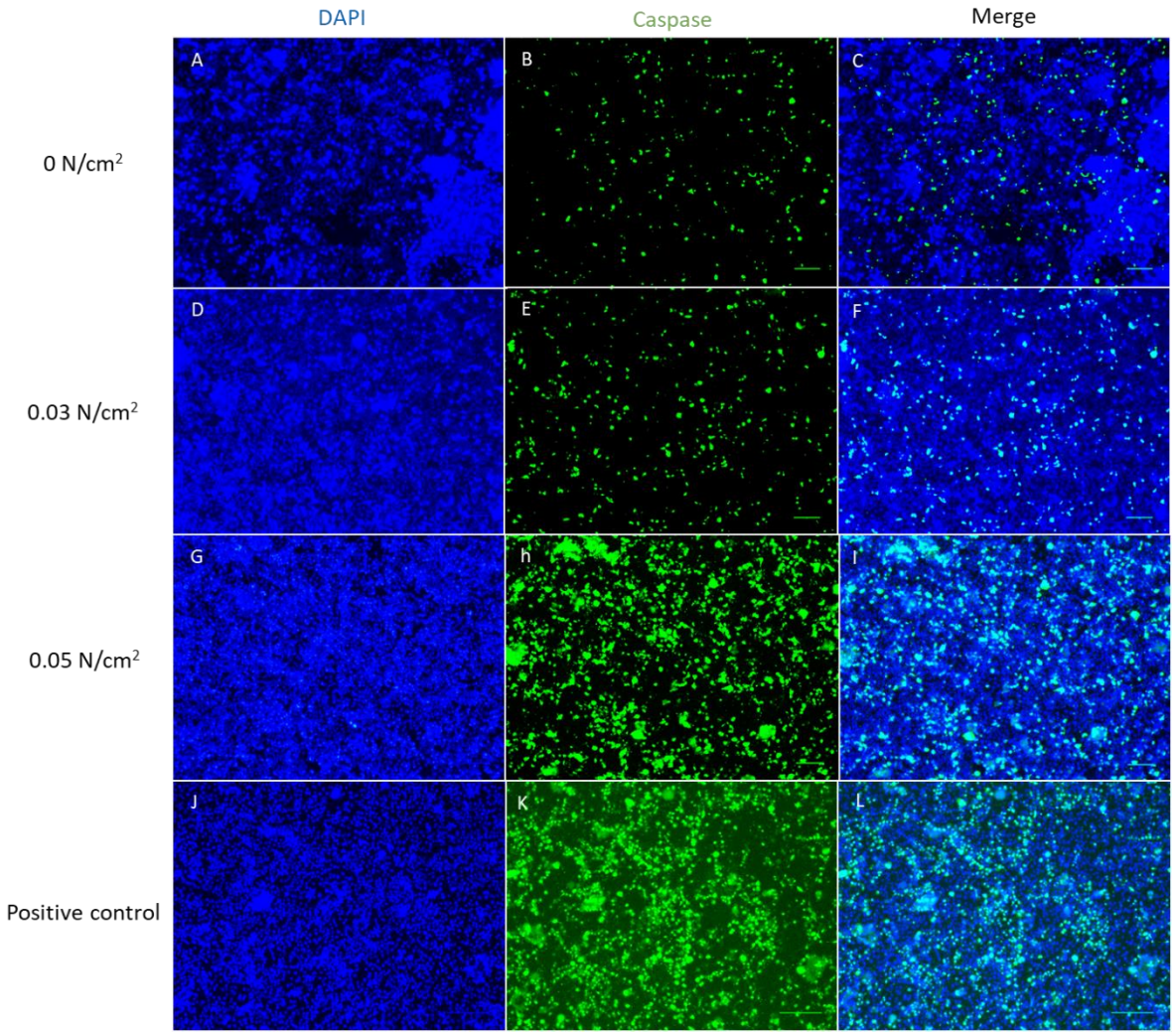

Figure. 35 Effect of compressive stress on apoptosis of immortalized HCEpCs (24 h).

Cell apoptosis was detected by poly caspase staining (FAM-FLICA, green) after incubating cells for 24 h post-compression. In the positive control, apoptosis was induced by staurosporine. Representative images were selected from 3 separate experiments. Scale bar is 100 μm.

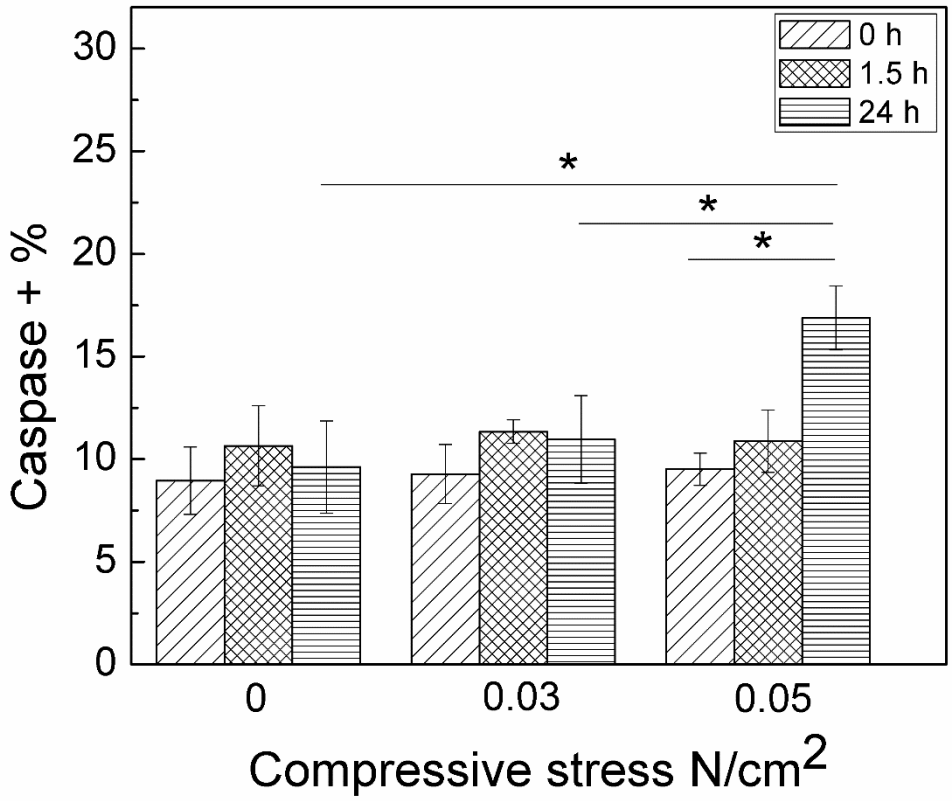

Figure. 36 Percentage of apoptosis cells after compression. Cell apoptosis was characterized with poly caspase staining (FAM-FLICA). Caspase positive cells were counted using Image J. Percentage was determined by dividing caspase expressing cell number with total cell number. *p<0.05. n=3.

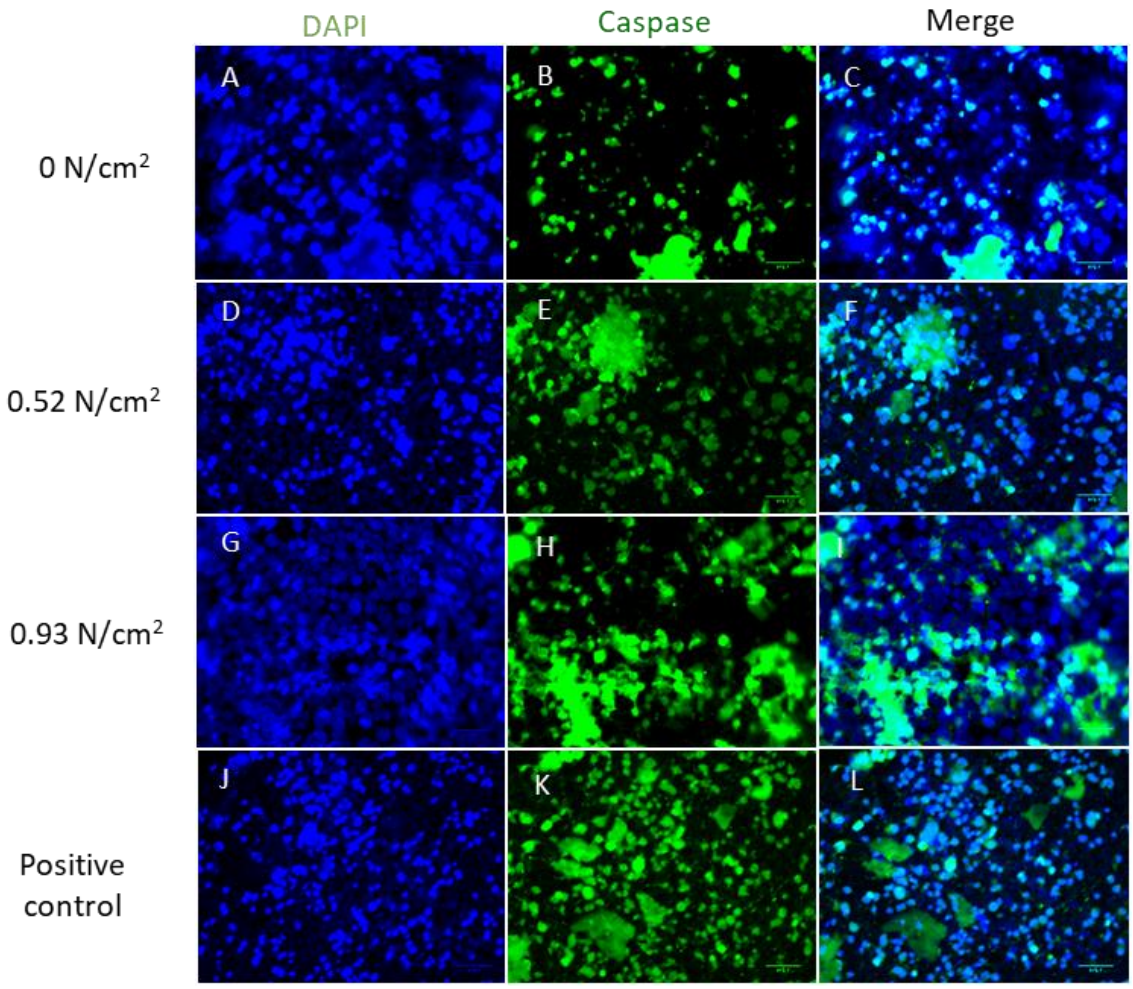

Figure. 37 Effect of compressive stress on apoptosis (0 h, ZO-1 expressing cells).

Cell apoptosis of ZO-1 expressing immortalized HCEpCs upon different compressive stress. Cell apoptosis was detected by poly caspase staining (FAM-FLICA, green) immediately after compression. In the positive control, apoptosis was induced by staurosporine. Representative images were selected from 3 separate experiments. Scale bar is 100 µm.

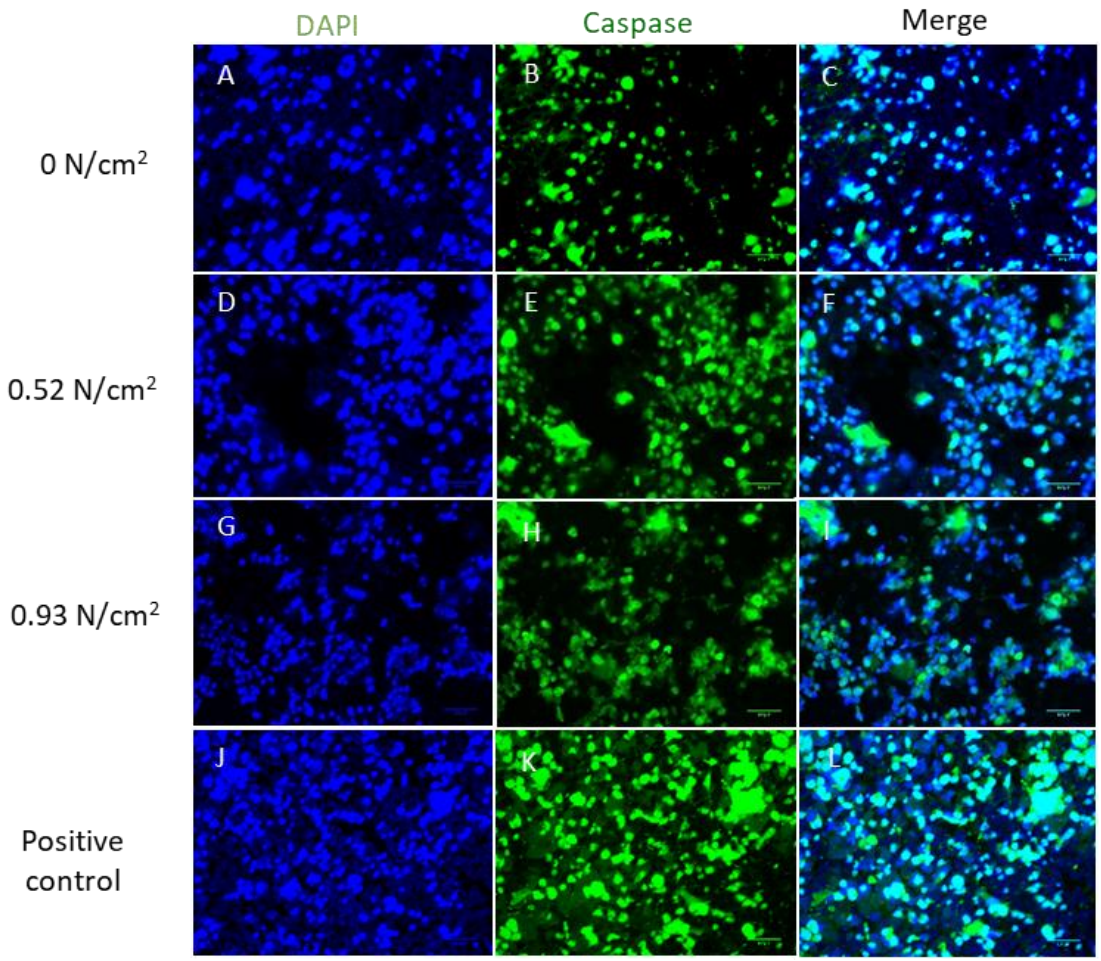

Figure. 38 Effect of compressive stress on apoptosis (1.5 h, ZO-1 expressing cells).

Cell apoptosis of ZO-1 expressing immortalized HCEpCs upon different compressive stress. Cell apoptosis was detected by poly caspase staining (FAM-FLICA, green) after incubating cells for 1.5 h post-compression. In the positive control, apoptosis was induced by staurosporine. Representative images were selected from 3 separate experiments. Scale bar is 100 µm.

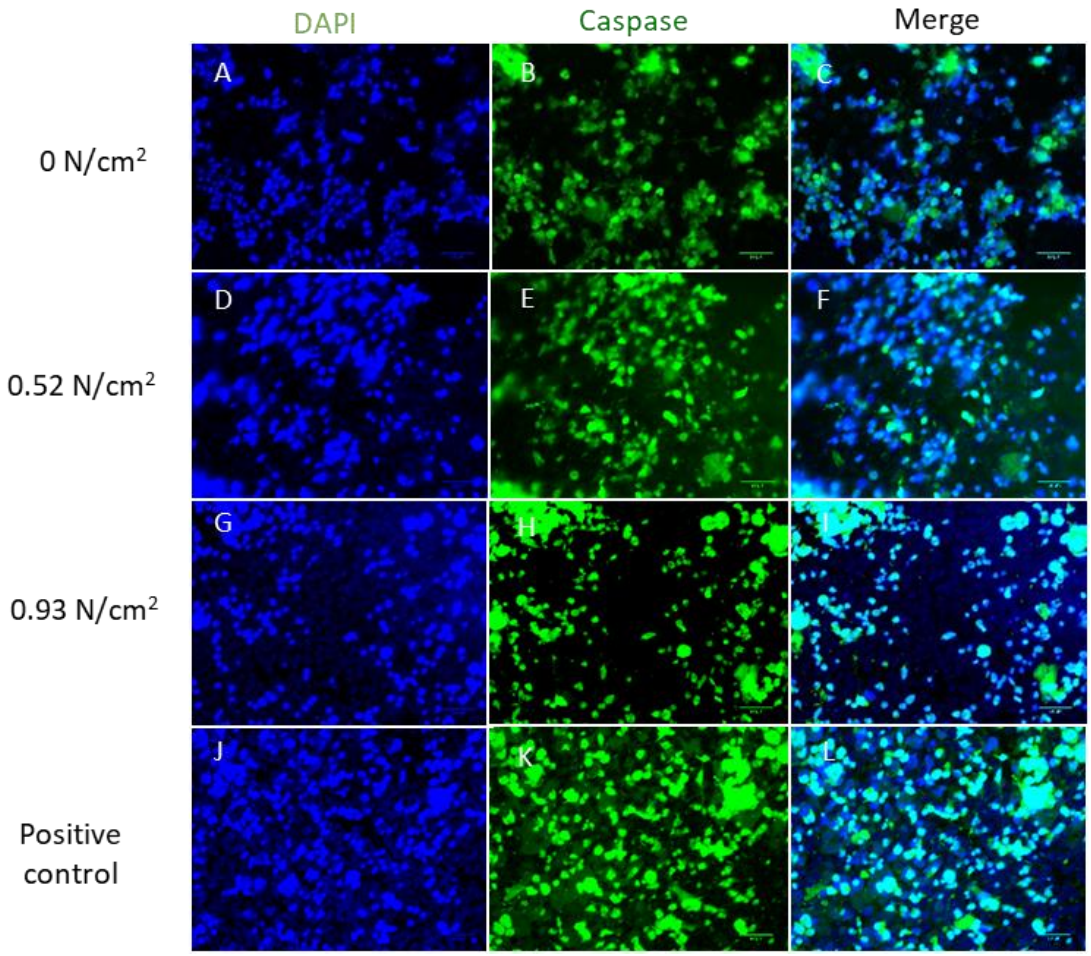

Figure. 39 Effect of compressive stress on apoptosis (24 h, ZO-1 expressing cells).

Cell apoptosis of ZO-1 expressing immortalized HCEpCs upon different compressive stress. Cell apoptosis was detected by poly caspase staining (FAM-FLICA, green) after incubating cells for 24 h post-compression. In the positive control, apoptosis was induced by staurosporine. Representative images were selected from 3 separate experiments. Scale bar is 100 µm.

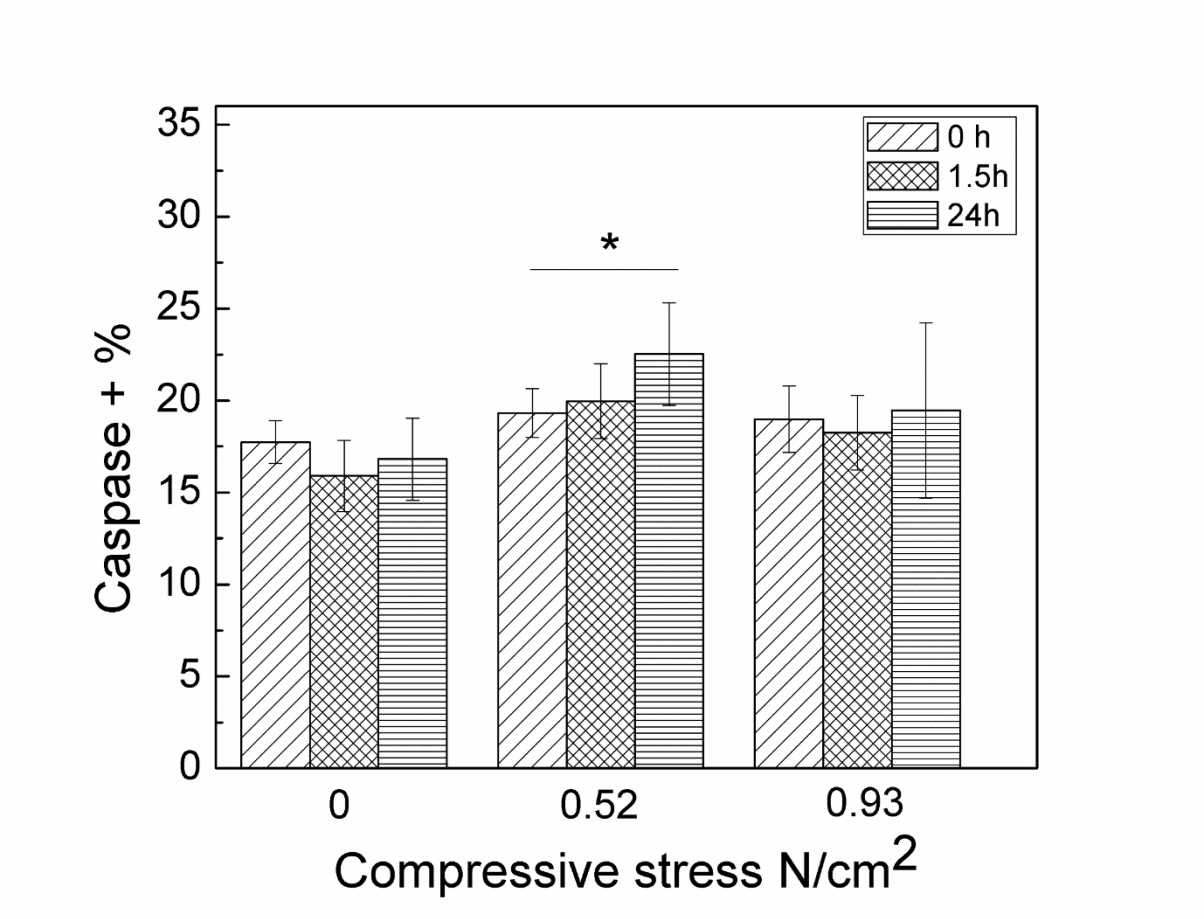

Figure. 40 Percentage of apoptosis cells after compression (ZO-1 expressing cells). Cell apoptosis were characterized with poly caspase staining (FAM-FLICA). Cells were counted using Image J. Percentage was determined by dividing caspase expressing cell number with total number. *p<0.05. n=3.

4.3.4 Cytoskeleton rearrangement upon compression

Cytoskeleton rearrangement was observed after compression as characterized with Alexa-Fluor488 - phalloidin staining. HCEpCs displayed F-actin network with peripheral stress fiber before compression (Figure 41 A-C). However, increased and thickened stress-fibers tended to accumulate in the periphery around the cells under compression, especially when the compressive stress was at or higher than 0.05 N/cm^2 (see arrows in Figure 41 H, K), indicating a responsively arranged cytoskeleton under compression.

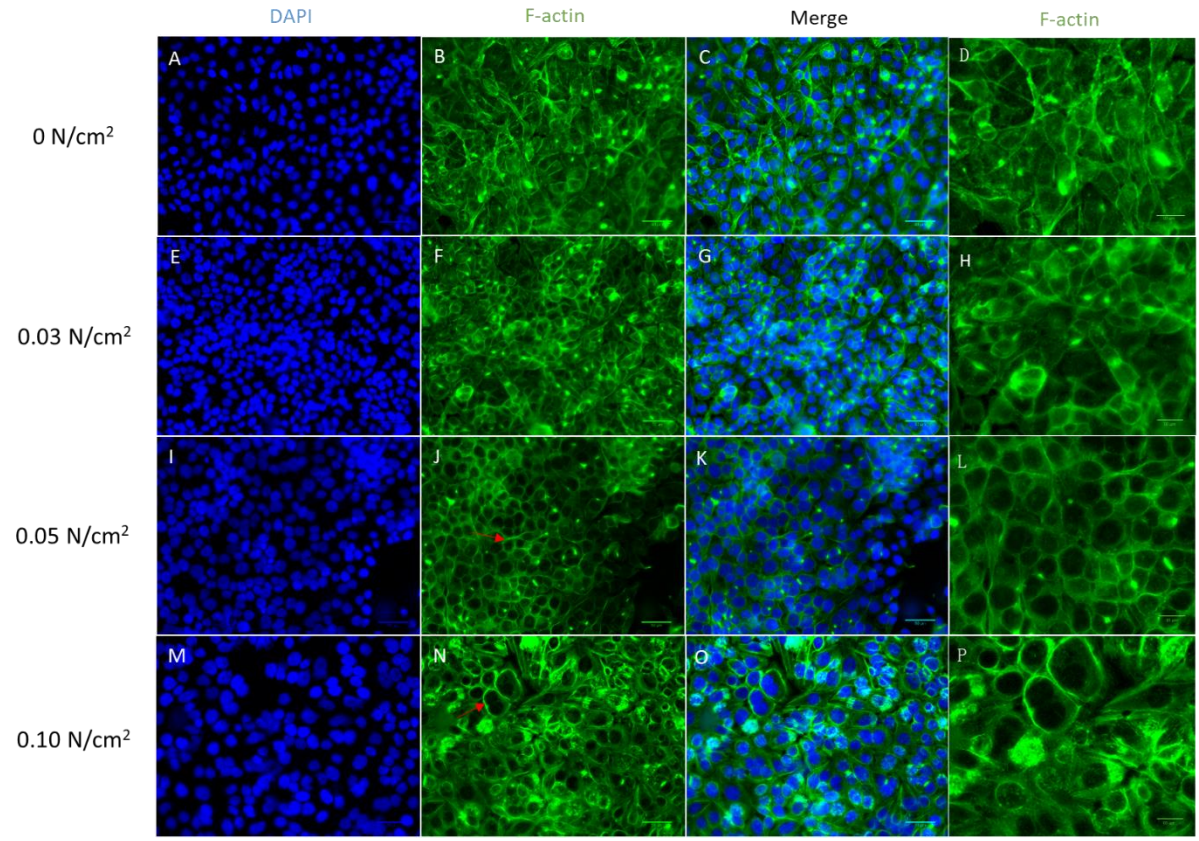

Figure. 41 Effect of compressive stress on the cytoskeleton (0 h).

F-actin arrangement of ZO-1 expressing immortalized HCEpCs before (A-C) and after (E-O) compression. Scale bar is 50 μm. D, H, I, P, Magnified view of F-actin arrangement. Scale bar is 10 μm. F-actin was stained with phalloidin (green) immediately after compression. Representative images were selected from 3 separate experiments.

The rearranged F-actin organization triggered by compression was recovered when HCEpCs were incubated for 24 hours after compression. As shown in Figure 42, F-actin network and stress fiber organization did not significantly vary among the cells both with and without compression. However, a lower intensity of the phalloidin staining was observed under the high loading (Figure 42K), showing the potential destructive effect of mechanical stimuli on F-actin polymerization. Except for changes in F-actin distribution, cell detachment and increased space between cells were also observed after compression.

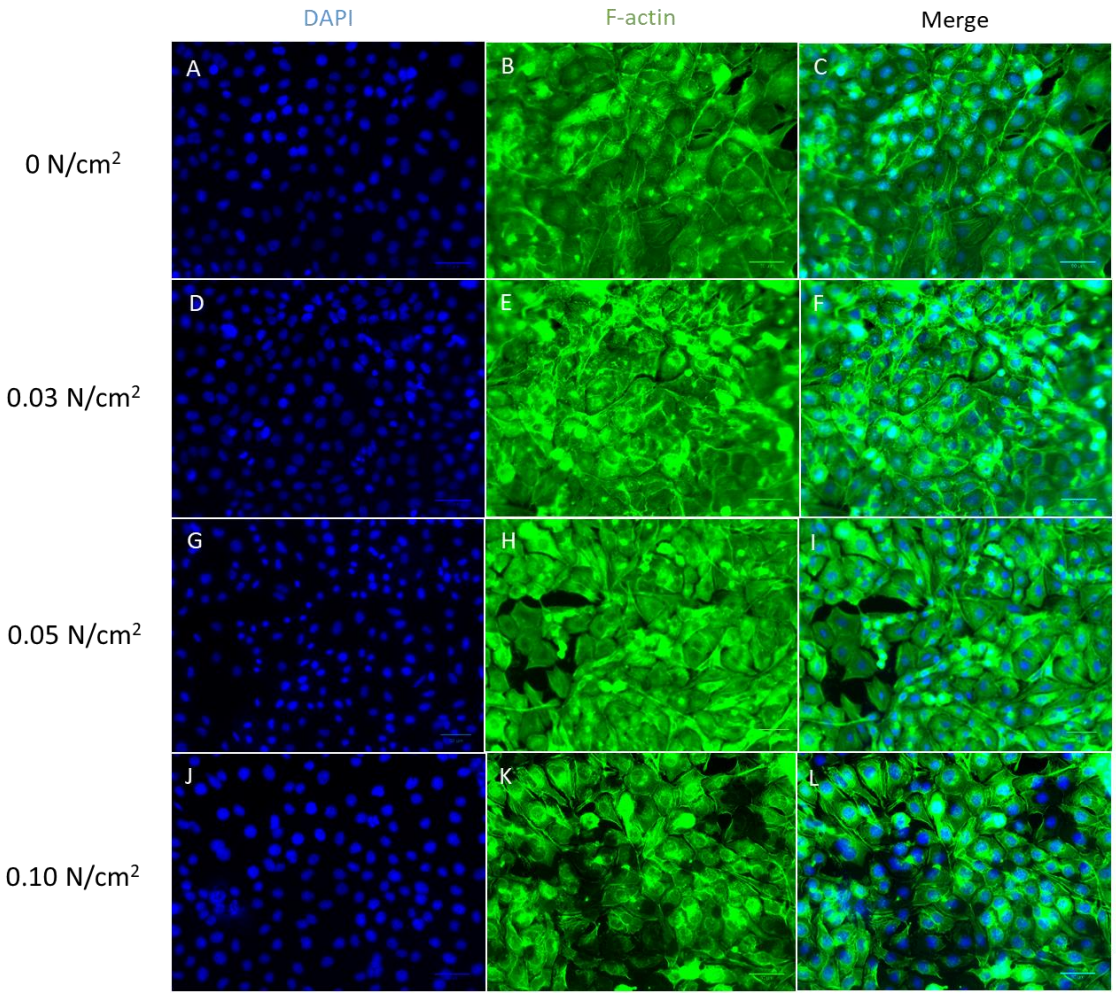

Figure. 42 Effect of compressive stress on the cytoskeleton (24 h).

F-actin arrangement of ZO-1 expressing immortalized HCEpCs before (A-C) and after (D-L) compression. F-actin was stained with phalloidin (green) after incubating cells for 24 h post-compression. Representative images were selected from 3 separate experiments.

Scale bar is 50 μm.

Medium loading was selected for a compression test on primary HCEpCs. Under compression, the accumulation of F-actin stress fiber around the primary HCEpCs was more obvious, which was shown as a dramatically increased phalloidin-staining intensity (Figure 43 A). However, this phenomenon was not seen 24 h after compression, when there was no difference on F-actin arrangement between non-compressed and compressed samples (Figure 43 B).

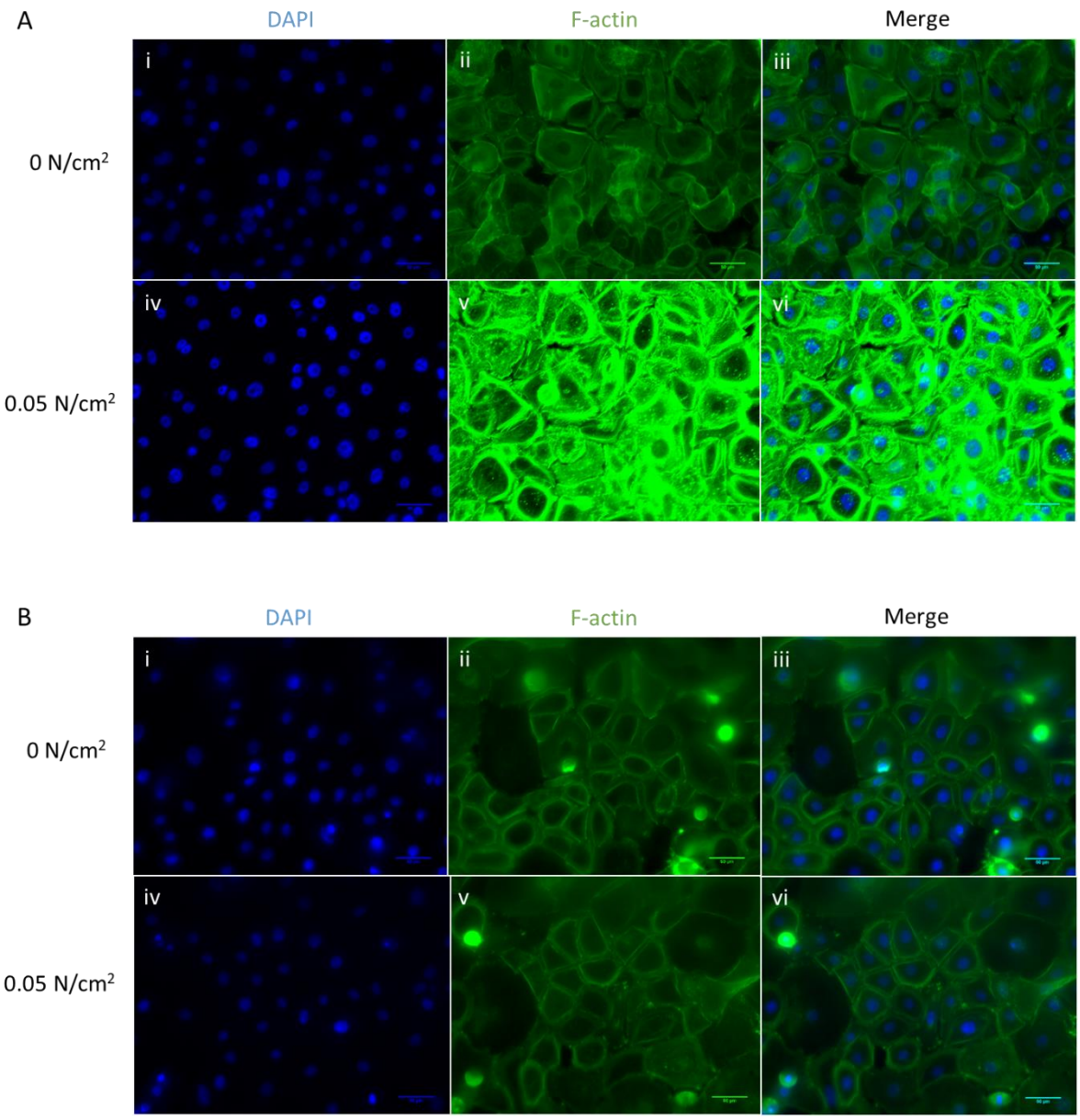

Figure. 43 Effect of compressive stress on cytoskeleton (primary cells).

F-actin arrangement of primary HCEpCs upon compressive stress of 0.05 N/cm^2. F-actin was stained with phalloidin (green) immediately (A) and after incubating cells for 24 h (B) post-compression. Representative images were selected from 3 separate experiments.

Scale bar is 50 µm.

The results presented in this section corroborate results from a previous study. It was demonstrated that the cyclic compression of 2 hour on chondrocytes resulted in punctate distribution of actin filaments and increased stress fiber intensity [206]. Stress fiber, which are F-actin bundles, are produced with the aid of cross-linking proteins including fimbrin, fascin and α–actinin [207], [208]. They act as prominent cytoskeletal structures. The mechanoresponse of stress fibers were investigated in an *in vitro* study using optical tweezers to compress individual stress fiber axially [209]. It was shown that F-actin bundles tend to buckle closer in response to mechanical stress, which may explain the increased stress

fiber in HCEpCs after compression in this thesis. When the stress fibers were allowed to relax after compression, the closely bond F-actin bundle was not recovered to initial state, indicating a deformative memory adaptive to mechanical stimuli [209]. The recovery of rearranged stress fibers has been studied at various timescale. Compression-induced rearrangement of cytoskeleton was shown to recover 1 hour after unloading of compression in chondrocytes [206]. Another *in vitro* study reported reversible and elastic response of stress fibers after 10 s of optical-tweezers-driven deformation [210]. It was also shown that long-term deformation (1000 s) of stress fibers would result in its irreversible response, indicating time-scaled mechanoresponse of stress fibers [210].

Alexa-Fluor488-phalloidin staining was also conducted on HCEpC monolayer with abundant expression of ZO-1 to assess the role of tight junctions on cellular compressive response. Our results showed no significant difference on F-actin arrangement of HCEpCs with and without compression either at 0 h or 24 h (Figure 44). Our results are consistent with a recent report that no change in F-actin recruitment was seen after compression in ZO-1-expressing S180 murine sarcoma cells [211]. The unchanged F-actin arrangement may indicate that cellular tight junction protects cytoskeleton from mechanical stimuli, which is consistent with the finding that presence of ZO-1 is essential in maintaining unified actin filaments in mouse intestinal epithelial cells both *in vivo* and *in vitro* [212]. This may result from the close interaction between F-actin and ZO-1 through their binding sites or molecules including C-terminal of ZO-1 [213], occludin [214] and myosin [215]. Additionally, ZO-1 also binds to other cytoskeleton components, such as α-catenin, vinculin and cortactin [216]. The strong network of ZO-1 and cytoskeleton provides mechanical support for cells, which is believed to stabilize the assembly and function of F-actin upon mechanical stimuli [217].

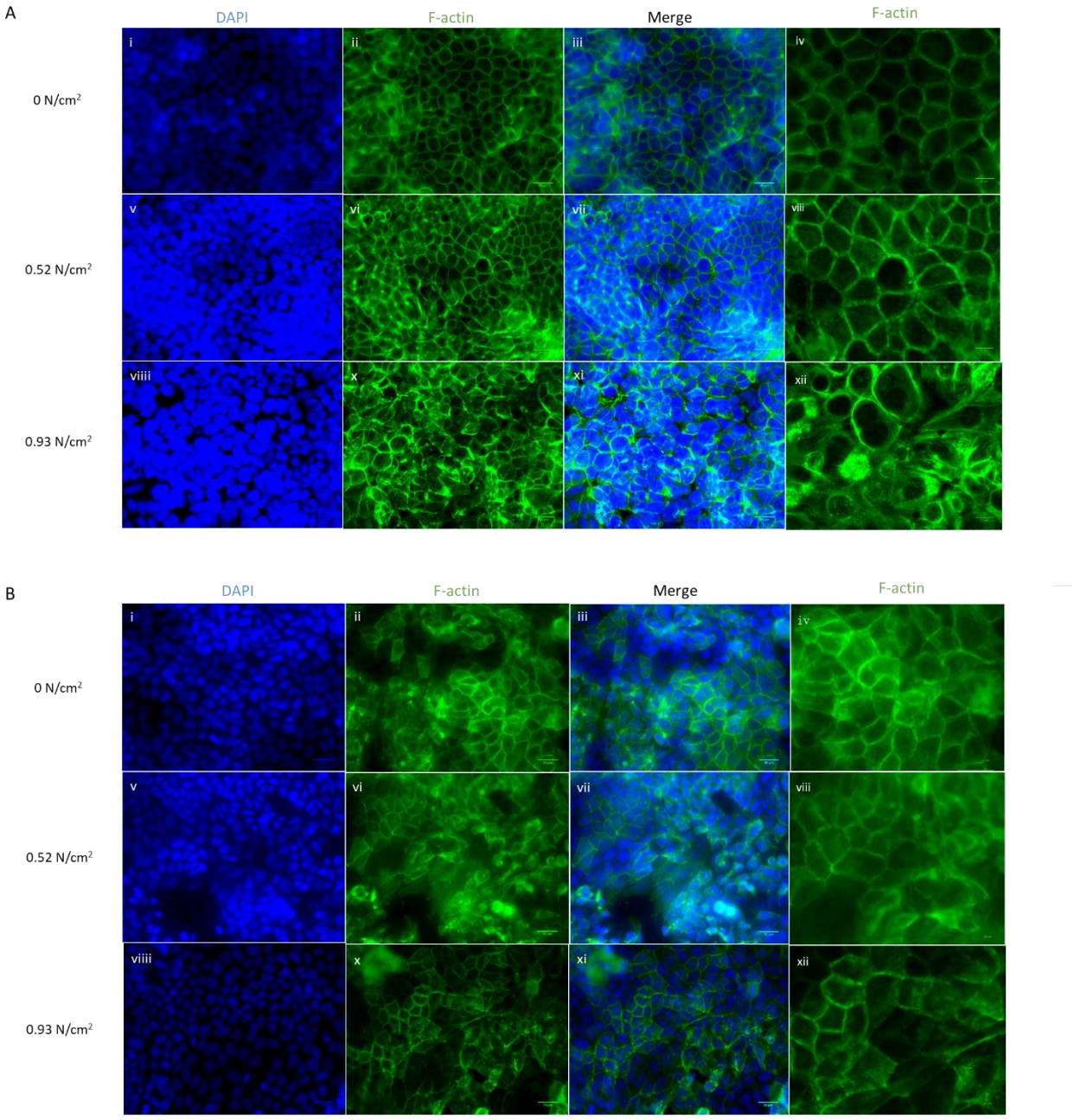

Figure. 44 Effect of compressive stress on cytoskeleton arrangement (ZO-1 expressing cells).

F-actin arrangement of ZO-1 expressing immortalized HCEpCs upon different compressive stress. F-actin was stained with phalloidin (green) immediately (A) and after incubating cells for 24 h (B) post-compression. Representative images were selected from 3 separate experiments. Images except iv, vii, xii, Scale bar is 50 µm. iv, vii, xii, Magnified view of F-actin arrangement. Representative images were selected. Scale bar is 10 µm.

Collectively, our results revealed a mechano-response of F-actin upon compression. Before the formation of ZO-1, increased peripheral stress fiber formation was observed with increased F-actin intensity. In contrast, when cells were expressing ZO-1, compression could not significantly affect the distribution and recruitment of F-actin. We postulate that ZO-1 may act as a protector to maintain stable equilibrium of the cytoskeleton under compressive stimuli.

4.3.5 ZO-1 expression upon compression

ZO-1 expression was detected at 0 h and 24 h after compression to determine the effect of compressive stimuli on cellular tight junctions. From our results, the percentage of HCEpCs expressing ZO-1 was 61 ± 8 % before compression and it was found to be decreased immediately after compression under both compressive stress (Figure 45 C). Statistical significance was shown under the load of 0.93 N/cm^2, showing a 30 % decrease of ZO-1 expressing cells (Table 5).

When cells were incubated for another 24 hour after compression, there was a further decrease on ZO-1 expressing cells. Significant difference was observed under the load of 0.93 N/cm^2 (Figure 46) compared to both the control group and the lower compressive stress group. As shown in table 4, the decrease of ZO-1 expressing cells under the compressive stress of 0.52 N/cm^2 and 0.93 N/cm^2 was 17 % and 30 %, respectively, indicating extensive damage on cellular tight junctions.

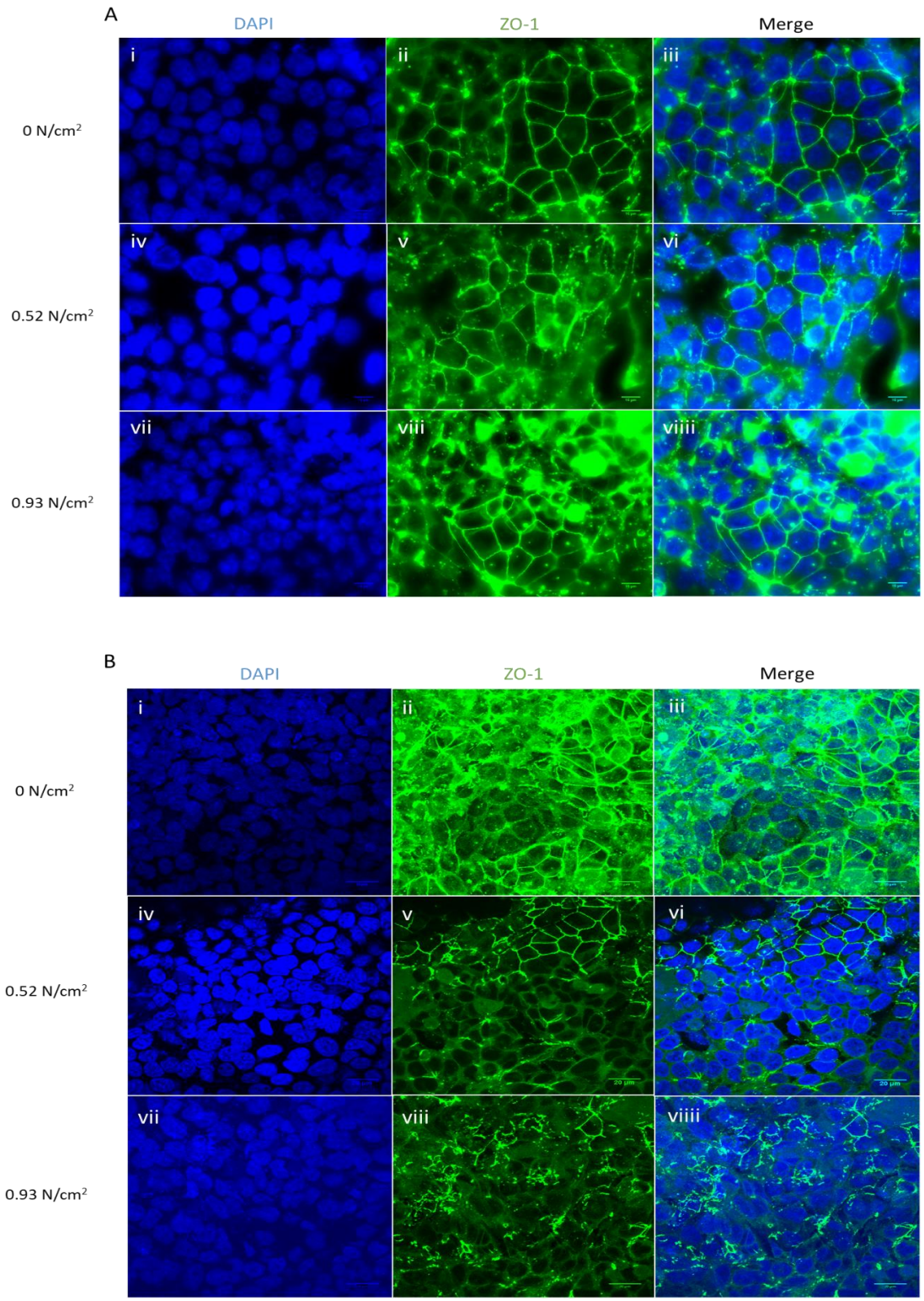

Figure. 45 Effect of compressive stress on ZO-1 formation.

ZO-1 expression of immortalized HCEpCs upon different compressive stress. ZO-1 was stained with ZO-1 antibody (green) immediately (A) and after incubating cells for 24 h (B) post-compression. Representative images were selected from 3 separate experiments. Scale bar is 10 μ m in A and 20 μ m in B.

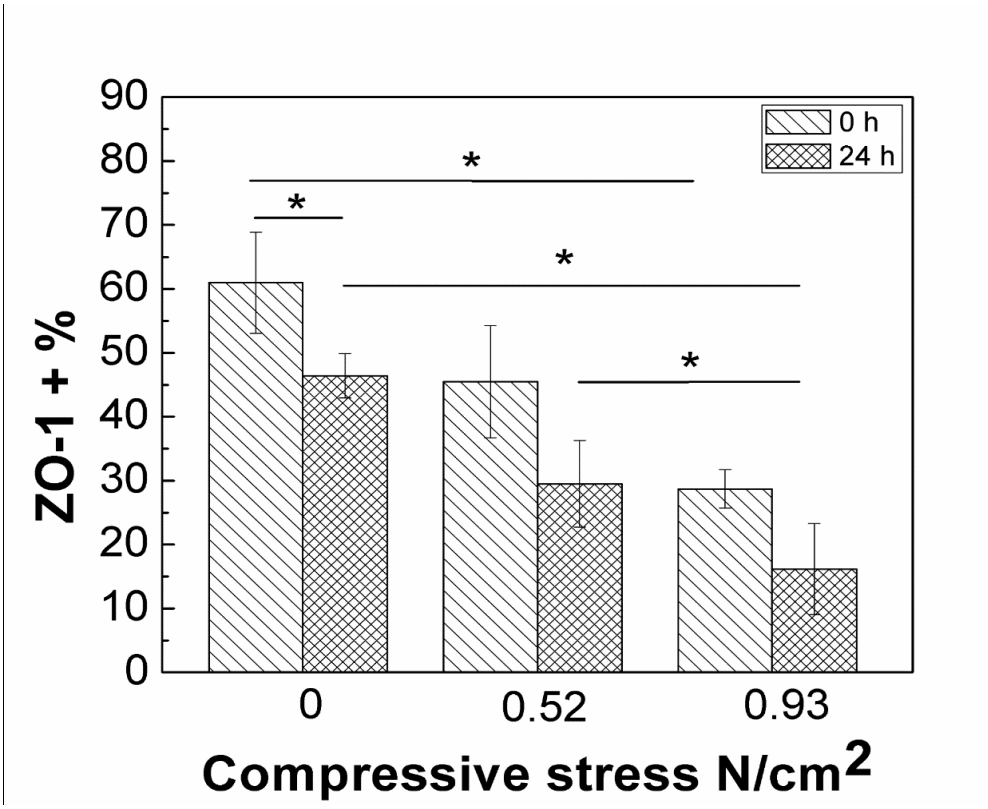

Figure. 46 Percentage of ZO-1 expressing HCEpCs comparison 0 h and 24 h after compression. Percentage of ZO-1 expressing cells were characterized by dividing ZO-1 expressing cell number with total cell number. * p<0.05 n=3.

Table. 5 Decrease of ZO-1 expressing cells under compression. n=3.

Compressive stress	Decrease of ZO-1 % induced by compression	
	0h	24h
0.52 N/cm^2	13%±3%	17%±9%
0.93N/cm^2	30%±10%	30%±10%

Tight junction, as an intercellular adhesion complex, is closely associated between adjacent cells. The responsive modulation of tight junction induced by external mechanical stress or wound has been extensively reported. The compressed rat spinal cord was shown to present dramatically decreased expression of ZO-1 24 hours after injury [196]. Decreased ZO-1 expression was also detected in rat cerebral cortex upon electromagnetic compressive stress [218]. In the contrary, two studies reported increased ZO-1 expression in response to cyclic stretching in both vascular endothelial cells [219] and ZO-1-transfected S180 murine sarcoma cells [211]. These findings demonstrate the responsive nature

of ZO-1 expression upon mechanical stimuli. ZO-1 expression has also been detected in various rat cells after exposure to electromagnetic cyclic compression [220]. Either increased or decreased ZO-1expression was detected in the investigated organ cells, indicating dual-directional mechanical-responsive expression of ZO-1 [220].

A study reported that the decreased ZO-1 expression detected in compressively triggered rat cerebral cortex [218] was a result of gelatinase-mediated degradation. It was found that the ZO-1 mRNA expression was unchanged, however, increased expression of gelatinases including MMP-2 and MMP-9 were detected [221]. This may explain the decreased ZO-1 expressing cells in our results. It is hypothesized that HCEpCs could release MMP-2 and MMP-9 upon exposure to mechanical stress based on the fact that increased MMP-2 [222] and MMP-9 [223], [224] expression has been detected in the tears of keratoconus patients. As a result, ZO-1 could be degraded by the secreted MMP-2 and MMP-9. Different from the conventional analysis of ZO-1 expression in the reported literature, the percentage of ZO-1 expressing cells was characterized in this thesis. Cells were regarded ZO-1 expressing only when all edges of the cells are fluorescently stained with ZO-1. In this case, cells with free cell boundary (i.e. cells not being surrounded by other cells when the cell layer confluence was interrupted) would be neglected, yielding an underestimation of ZO-1 expressing cells. It is recommended to quantify ZO-1 expression with the commonly adopted ZO-1 quantification method, the analysis of ZO-1 fluorescence intensity, which could be further compared to previous literature in characterizing the change of ZO-1.

5.0 Conclusion and Recommendations

This project put forward two different kinds of mechanical models to investigate HCEpCs behavior under in-plane tensile stress and out-of-plane compressive stress. The mechanoresponse of HCEpCs showed signs observed in KC epithelium, highlighting the potential impact of eye rubbing on the formation of KC.

5.1 Design of cell stretching system and characterization of cell response to in-plane tensile stress

Two stretching models were designed and fabricated to investigate HCEpCs response to in-plane tensile stress: a fluidic cell stretcher and an electric cell stretcher that could stretch the substrate on which HCEpCs were seeded or a real cornea. The fluidic cell stretcher was built with air pressure controlled stretching system, and the electric cell stretcher was built with electrically controlling system. As a proof-of-concept, a nitrogen gas tank was used as the source of air pressure. Calibration and cell test were conducted on the fluidic cell stretcher and the electric cell stretcher.

Our calibration results showed that the lab-built fluidic cell stretcher could achieve designated stretching strain, which could be kept stable within five minutes under low inlet pressure. However, variation in strains was observed under high inlet air pressure. This may limit our investigation of HCEpC response to tensile stress at high range. The variations observed in the data may result from the deformation or air leak of the PDMS cell stretcher at high pressure. Upgrades, such as strengthening the binding of different layers, need to be made to prevent these problems. The variability in the data may also be due to the limitation of the gas tank. Unlike a pump that could automatically and precisely control the air pressure, a gas tank can only be handled manually by the switch to achieve a certain pressure. A lag time exists after switching on to achieve a steady pressure as well as after switching off to remove the pressure. In this way, the air pressure injected into the fluidic cell stretcher was not steady during the lag time, resulting in the disturbance observed during calibration. It is recommended that a pump should be incorporated as a more precise air pressure controlling system. Calibration of the electric cell stretcher displayed precise and stable deformation of the cell culture membrane at certain indenter displacement within five minutes.

With a precise controlling system and the availability to mount an animal cornea, the electric cell stretcher is regarded as a more promising in current research. A cell experiment on the electric cell stretcher showed an increased cell detachment upon stretching, revealing that HCEpCs reacted to external tensile stimuli. As part of preliminary study, only static stretch was conducted on HCEpCs. However, multiple eye rubbing occurs in KC patients. In order to better mimic eye rubbing induced mechanical stimuli, it is recommended to apply cyclic stretch on HCEpCs.

5.2 Design of cell compressing system and characterization of cell response to out-of-plane compressive stress

A compressing model was also built to investigate the effect of out-of-plane compressive stress on HCEpCs. Cyclic compressive stress was applied on HCEpCs monolayer to investigate how compressive stress could contribute to the development and progression of KC. Cellular

characterization including cell viability, apoptosis, cytoskeleton rearrangement, and ZO-1 expression were analyzed 0 and 24 hours after compression. Our findings indicated that HCEpCs were vulnerable to mechanical stimuli with increased cell death rate and apoptosis, formation of peripheral stress fiber, abnormal cell membrane Calcein AM uptake and decreased ZO-1 formation. Compared with severe eye rubbing stress of 17 N/cm^2, the compressive stress adopted during compression study was very low (0.10 N/cm^2 for cell monolayer without ZO-1 expression and 0.93 N/cm^2 for ZO-1 expressing monolayer). Cellular change upon compressive stress revealed the responsive nature of HCEpCs to mechanical stimuli, shedding light on the potential pathological path of mechanically triggered KC.

The mechanical stress-induced changes in cell viability and F-actin network rearrangement were both recovered after 24-hour incubation. However, the number of apoptotic cells was dramatically increased 24 hours after compression, indicating that cells were not fully recovered from compression. Moreover, the loss of cellular tight junctions under mechanical compression would last longer than 24 hours. As HCEpCs without tight junctions are more vulnerable to compressive stress, the compression-induced loss of ZO-1 may impose higher risk of damage on corneal epithelium without its protection. The stress-induced cell death and decreased cell-cell junction expression are in accordance with the increased epithelial cell loss found in KC cornea [66], [96], [97]. The cytoskeleton rearrangement observed under compressive stress showed a similar pattern as corneal epithelial cellular response to other mechanical stimuli including shear stress and substrate stiffness change reported recently [122], [123].

As investigation of cellular behavior under out-of-plane compressive stress was only pursued on HCEpCs monolayers instead of corneal epithelium, the results presented in this thesis may be limited regarding the pathological path of KC. Thus, it is recommended to continue these studies to include stratified corneal epithelial cells and an animal cornea.

5.3 Recommendations for future work

As a pilot study, this thesis successfully designed and fabricated *in vitro* mechanical models that could apply in-plane tensile stress and out-of-plane compressive stress on corneal cells. It was put in evidence that corneal epithelial cells react to mechanical stimuli, which can contribute to a better understanding of the pathological path of KC. Recommendation is proposed to strengthen the fluidic cell stretcher and to remedy for the imprecise controlling system of the cell stretcher for further investigation. It is also recommended to perform experiments with in-plane tensile stress and out-of-plane compressive stress on stratified corneal epithelial cells or animal corneas in order to better understand corneal response to mechanical stimuli.

Copyright permission license

Figure 2 A: 1071319-1

Figure 2 B: 1071318-1

Figure 2 C: 4932670918191

Figure 3 A: 4932730304184

Figure 3 B, D; Figure 4 C-F: 4932660576289

Figure 3 C: 4932660160127

Figure 4 B: 1071324-1

Figure 5: 4932680412917

Figure 8 A: 4932681344620

Figure 10 C: 4932690424459

Figure 12, 13, 14, 16 have been used with authors' permission

References

[1] J. T. Holladay, “Standardizing constants for ultrasonic biometry, keratometry, and intraocular lens power calculations,” *J. Cataract Refract. Surg.*, vol. 23, no. 9, pp. 1356–1370, 1997.

[2] C. W. Mcmonnies, “Abnormal Rubbing and Keratectasia,” *Eye Contact Lens*, vol. 33, no. 6, pp. 265–271, 2007.

[3] J. T. Barr *et al.*, “Estimation of the Incidence and Factors Predictive of Corneal Scarring in the Collaborative Longitudinal Evaluation of Keratoconus (CLEK) Study,” *Clin. Sci.*, vol. 25, no. 1, pp. 16–25, 2006.

[4] J. A. Cameron, “Corneal abnormalities in Ehlers-Danlos syndrome type VI.” *Cornea*, vol. 12, no. 1, pp. 54–59, 1993.

[5] A. M. Bawazeer, W. G. Hodge, and B. Lorimer, “Atopy and keratoconus : a multivariate analysis,” *Br J Ophthalmol*, vol. 84, pp. 834–836, 2000.

[6] N. Publishing and G. All, “The Dundee University Scottish Keratoconus study : demographics, corneal signs, associated diseases, and eye rubbing,” *Eye*, vol. 22, pp. 534–541, 2008.

[7] C. W. Mcmonnies, “Management of chronic habits of abnormal eye rubbing,” *Contact Lens Anterior Eye*, vol. 31, pp. 95–102, 2008.

[8] R. Ambekar, K. C. Toussaint, and A. Wagoner Johnson, “The effect of keratoconus on the structural, mechanical, and optical properties of the cornea,” *J. Mech. Behav. Biomed. Mater.*, vol. 4, no. 3, pp. 223–236, 2011.

[9] C. W. Mcmonnies, A. Alharbi, and G. C. Boneham, “Epithelial Responses to Rubbing-Related Mechanical Forces,” *Clin. Sci.*, vol. 29, no. 11, pp. 1223–1231, 2010.

[10] S. A. Balasubramanian, D. C. Pye, and M. D. P. Willcox, “Effects of eye rubbing on the levels of protease, protease activity and cytokines in tears: Relevance in keratoconus,” *Clin. Exp. Optom.*, vol. 96, no. 2, pp. 214–218, 2013.

[11] P. Shih, I. Wang, W. Cai, and J. Yen, “Biomechanical Simulation of Stress Concentration and Intraocular Pressure in Corneas Subjected to Myopic Refractive Surgical Procedures,” *Sci. Rep.*, vol. 7, no. 13906, pp. 1–15, 2017.

[12] A. A. Khodadoust, A. M. Silverstein, K. R. Kenyon, and J. E. Dowling, “Adhesion of regenerating corneal epithelium: The role of basement membrane,” *Am. J. Ophthalmol.*, vol. 65, no. 3, pp. 339–348, Mar. 1968.

[13] M. Davanger and A. Evensen, “Role of the Pericorneal Papillary Structure in Renewal of Corneal Epithelium,” *Nature*, vol. 229, p. 560, Feb. 1971.

[14] Y. J. Son, J. W. Tse, Y. Zhou, and W. Mao, “Biomaterials Science Biomaterials and controlled release strategy for epithelial wound healing,” *Biomater. Sceince*, vol. 7, pp. 4444–4471, 2019.

[15] S. Masterton and M. Ahearne, “Mechanobiology of the corneal epithelium,” *Exp. Eye Res.*, vol. 177, no. August, pp. 122–129, 2018.

[16] I. K. Gipson, S. M. Grill, S. J. Spurr, and S. J. Brennan, “Hemidesmosome formation in vitro,” *J. Cell Biol.*, vol. 97, no. 3, pp. 849 LP – 857, Sep. 1983.

[17] D. R. Garrod, “Desmosomes and hemidesmosomes,” *Curr. Opin. Cell Biol.*, vol. 5, no. 1, pp. 30–40, 1993.

[18] M. Pavelka and J. Roth, “Cellular Interdigitations,” in *Functional Ultrastructure*, Springer, 2010, pp. 176–177.

[19] W. H. Evans and P. E. M. Martin, “Gap junctions: structure and function (Review),” *Mol. Membr. Biol.*, vol. 19, no. 2, pp. 121–136, Jan. 2002.

[20] C. M. Niessen, “Tight junctions/adherens junctions: basic structure and function,” *J. Invest. Dermatol.*, vol. 127, no. 11, pp. 2525–2532, 2007.

[21] K. M. Meek and C. Boote, “The use of X-ray scattering techniques to quantify the orientation and distribution of collagen in the corneal stroma,” *Prog. Retin. Eye Res.*, vol. 28, no. 5, pp. 369–392, 2009.

[22] L. J. Müller, E. Pels, and G. F. J. M. Vrensen, “The specific architecture of the anterior stroma accounts for maintenance of corneal curvature,” *Br. J. Ophthalmol.*, vol. 85, no. 4, pp. 437–443, Apr. 2001.

[23] T. Møller-Pedersen, M. Vogel, H. F. Li, W. M. Petroll, H. D. Cavanagh, and J. V Jester, “Quantification of Stromal Thinning, Epithelial Thickness, and Corneal Haze after Photorefractive Keratectomy Using In Vivo Confocal Microscopy,” *Ophthalmology*, vol. 104, no. 3, pp. 360–368, 1997.

[24] Y. Komai and T. Ushikif, “The Three-Dimensional Organization of Collagen Fibrils in the Human Cornea and Sclera,” *Invest. Ophthalmol. Vis. Sci.*, vol. 32, no. 8, pp. 2244–2258, 1991.

[25] M. Winkler *et al.*, “Nonlinear Optical Macroscopic Assessment of 3-D Corneal Collagen Organization and Axial Biomechanics,” *IOVS*, vol. 52, no. 12, pp. 8818–8827, 2011.

[26] A. Montanino, A. Pandolfi, M. Vasta, and M. Angelillo, “Modeling the biomechanics of the human cornea accounting for local variations of the collagen fibril architecture,” *Z Angew Math Mech*, vol. 98, pp. 2122–2134, 2018.
[27] D. A. Newsome, J. Gross, and J. R. Hassell, “Human corneal stroma contains three distinct collagens.” *Invest. Ophthalmol. Vis. Sci.*, vol. 22, no. 3, pp. 376–381, 1982.
[28] A. J. Quantock and R. D. Young, “Development of the corneal stroma, and the collagen–proteoglycan associations that help define its structure and function,” *Dev. Dyn.*, vol. 237, no. 10, pp. 2607–2621, Oct. 2008.
[29] D. W. DelMonte and T. Kim, “Anatomy and physiology of the cornea,” *J. Cataract Refract. Surg.*, vol. 37, no. 3, pp. 588–598, 2011.
[30] T. Nishida, “Commanding Roles of Keratocytes in Health and Disease,” *Cornea*, vol. 29, no. 11, 2010.
[31] J. V Jester *et al.*, “The cellular basis of corneal transparency: evidence for ‘corneal crystallins,’” *J. Cell Sci.*, vol. 112, no. 5, pp. 613–622, 1999.
[32] A. Bukowiecki, D. Hos, C. Cursiefen, and S. A. Eming, “Wound-healing studies in cornea and skin: parallels, differences and opportunities,” *Int. J. Mol. Sci.*, vol. 18, no. 6, p. 1257, Jun. 2017.
[33] K. E. Kadler, D. F. Holmes, J. A. Trotter, and J. A. Chapman, “Collagen fibril formation,” *Biochem. J.*, vol. 316, pp. 1–11, 1996.
[34] X. Cheng, S. J. Petsche, and P. M. Pinsky, “A structural model for the in vivo human cornea including collagen-swelling interaction,” *J. R. Soc. Interface.*, vol. 12, p. 20150241, 2015.
[35] N. C. Joyce, “Prog Retinal Eye Res. 2003; 22: 359. [PubMed] b) Zhu C, Joyce NC,” *Invest Ophthalmol Vis Sci*, vol. 45, p. 1743, 2004.
[36] S. Hodson, “The regulation of corneal hydration to maintain high transparency in fluctuating ambient temperatures,” *Exp. Eye Res.*, vol. 20, no. 4, pp. 375–381, 1975.
[37] S. E. Wilson and H. E. R. E. Kaufman, “Graft failure after penetrating keratoplasty,” *Survey of Ophthalmology*, vol. 34, no. 5. Elsevier Inc, pp. 325–356, 1990.
[38] H. Obata and T. Tsuru, “Corneal wound healing from the Perspective of keratoplasty specimens with special reference to the function of the Bowman layer and Descemet Membrane,” *Cornea*, vol. 26, pp. 82–89, 2007.
[39] C. E. M. Clinic, “Keratoconus,” *Surv Ophthalmol*, vol. 42, no. 4, pp. 297–319, 1998.
[40] T. Ardan, “The imbalance between matrix metalloproteinases and their tissue inhibitors in corneal epithelium upon UV irradiation,” *Invest. Ophthalmol. Vis. Sci.*, vol. 53, no. 14, p. 1831, Mar. 2012.
[41] J. Yamada, M. R. Dana, C. Sotozono, and S. Kinoshita, “Local suppression of IL-1 by receptor antagonist in the rat model of corneal alkali injury,” *Exp. Eye Res.*, vol. 76, no. 2, pp. 161–167, 2003.
[42] N. Ebihara, A. Matsuda, S. Nakamura, H. Matsuda, and A. Murakami, “Role of the IL-6 classic-and trans-signaling pathways in corneal sterile inflammation and wound healing,” *Invest. Ophthalmol. Vis. Sci.*, vol. 52, no. 12, pp. 8549–8557, 2011.
[43] C. Sunderkötter, J. Roth, and C. Sorg, “Immunohistochemical detection of bFGF and TNF-alpha in the course of inflammatory angiogenesis in the mouse cornea.,” *Am. J. Pathol.*, vol. 137, no. 3, p. 511, 1990.
[44] C. L. Cubitt, R. N. Lausch, and J. E. Oakes, “Differences in Interleukin-6 Gene Expression Between Cultured Human Corneal Epithelial Cells and Keratocytes,” *Invest. Ophthalmol. Vis. Sci.*, vol. 36, no. 2, pp. 330–336, 1995.
[45] S. Sugaya, T. Sakimoto, J. Shoji, and M. Sawa, “Regulation of soluble interleukin-6 (IL-6) receptor release from corneal epithelial cells and its role in the ocular surface,” *Jpn. J. Ophthalmol.*, vol. 55, no. 3, pp. 277–282, 2011.
[46] R. R. Mohan, R. R. Mohan, W.-J. Kim, and S. E. Wilson, “Modulation of TNF-α–Induced Apoptosis in Corneal Fibroblasts by Transcription Factor NF-κB,” *Invest. Ophthalmol. Vis. Sci.*, vol. 41, no. 6, pp. 1327–1336, May 2000.
[47] S. Kling and F. Hafezi, “Corneal biomechanics – a review,” *Ophthalmic Physiol. Opt.*, vol. 37, pp. 240–252, 2017.
[48] W. J. Dupps and S. E. Wilson, “Biomechanics and wound healing in the cornea,” *Exp. Eye Res.*, vol. 83, no. 4, pp. 709–720, 2006.
[49] A. Kotecha, “What Biomechanical Properties of the Cornea Are Relevant for the Clinician?,” *Surv. Ophthalmol.*, vol. 52, no. 6 SUPPL., pp. 109–114, 2007.
[50] B. L. Boyce, J. M. Grazier, R. E. Jones, and T. D. Nguyen, “Full-field deformation of bovine cornea under constrained inflation conditions,” *Biomaterials*, vol. 29, no. 28, pp. 3896–3904, 2008.
[51] J. A. Last, S. M. Thomasy, C. R. Croasdale, P. Russell, and C. J. Murphy, “Compliance profile of the human cornea as measured by atomic force microscopy,” *Micron*, vol. 43, no. 12, pp. 1293–1298, 2012.
[52] G. Lombardo, S. Serrao, M. Rosati, and M. Lombardo, “Analysis of the Viscoelastic Properties of the

Human Cornea Using Scheimpflug Imaging in Inflation Experiment of Eye Globes," vol. 9, no. 11, 2014.
[53] S. M. Thomasy *et al.*, "Elastic modulus and collagen organization of the rabbit cornea: epithelium to endothelium," *Acta Biomater.*, vol. 10, no. 2, pp. 785–791, 2014.
[54] D. A. Luce, "Determining in vivo biomechanical properties of the cornea with an ocular response analyzer," *J. Cataract Refract. Surg.*, vol. 31, no. 1, pp. 156–162, 2005.
[55] M. Winkler *et al.*, "Nonlinear optical macroscopic assessment of 3-D corneal collagen organization and axial biomechanics," *Investig. Ophthalmol. Vis. Sci.*, vol. 52, no. 12, pp. 8818–8827, 2011.
[56] T. Georgiou, C. L. Funnell, A. Cassels-Brown, and R. O'Conor, "Influence of ethnic origin on the incidence of keratoconus and associated atopic disease in Asians and white patients.," *Eye (Lond).*, vol. 18, no. 4, pp. 379–383, Apr. 2004.
[57] A. R. Pearson, B. Soneji, N. Sarvananthan, and J. H. Sandford-Smith, "Does ethnic origin influence the incidence or severity of keratoconus?," *Eye (Lond).*, vol. 14 (Pt 4), pp. 625–628, Aug. 2000.
[58] D. A. Godefrooij, G. A. de Wit, C. S. Uiterwaal, S. M. Imhof, and R. P. L. Wisse, "Age-specific Incidence and Prevalence of Keratoconus: A Nationwide Registration Study," *Am. J. Ophthalmol.*, vol. 175, pp. 169–172, 2017.
[59] R. H. Kennedy, W. M. Bourne, and J. A. Dyer, "A 48-Year Clinical and Epidemiologic Study of Keratoconus," *Am. J. Ophthalmol.*, vol. 101, no. 3, pp. 267–273, Mar. 1986.
[60] W. Hammerstein, "Zur Genetik des Keratoconus," *Exp. Ophthalmol.*, vol. 190, no. 4, pp. 293–308, 1974.
[61] S. Etzine, "Conical cornea in identical twins.," *South African Med. J.*, vol. 28, no. 8, pp. 154–155, Feb. 1954.
[62] M. C. Kenney and D. J. Brown, "The Cascade Hypothesis of Keratoconus," *Contact Lens Anterior Eye*, vol. 26, pp. 139–146, 2003.
[63] F. Aslani, M. Khorrami-Nejad, M. Aghazadeh Amiri, H. Hashemian, F. Askarizadeh, and B. Khosravi, "Characteristics of posterior corneal astigmatism in different stages of keratoconus," *J. Ophthalmic Vis. Res.*, vol. 13, no. 1, pp. 3–9, 2018.
[64] A. J. Munsamy *et al.*, "A frequency analysis of cone characteristics for the different stages of keratoconus," *African Vis. Eye Heal. Vol 74, No 1*, vol. 74, no. 1, p. a302, 2015.
[65] M.-S. H. El-Agha, Y. M. El Sayed, R. M. Harhara, and H. M. Essam, "Correlation of Corneal Endothelial Changes with Different Stages of Keratoconus," *Cornea*, vol. 33, no. 7, 2014.
[66] Y. Shen, J. Son, and X. Zhou, "One-Year Follow-Up of Changes in Corneal Densitometry Collagen Cross-Linking for Keratoconus," *Cornea*, vol. 35, no. 11, pp. 1434–1440, 2016.
[67] Y. S. Rabinowitz, "Keratoconus," *Surv. Ophthalmol.*, vol. 42, no. 4, pp. 297–319, 1998.
[68] E. Barraquer-Somers, C. C. Chan, and W. R. Green, "Corneal epithelial iron deposition," *Ophthalmology*, vol. 90, no. 6, pp. 729–734, 1983.
[69] L. J. Davis, J. T. Barr, and D. Vanotteren, "Transient rigid lens-induced striae in keratoconus," *Optom. Vis. Sci.*, vol. 70, no. 3, pp. 216–219, 1993.
[70] L. Dienes *et al.*, "Corneal Sensitivity and Dry Eye Symptoms in Patients with Keratoconus," *PLoS One*, vol. 10, no. 10, p. e0141621, Oct. 2015.
[71] N. H. Brookes, I.-P. Loh, G. M. Clover, C. A. Poole, and T. Sherwin, "Involvement of corneal nerves in the progression of keratoconus," *Exp. Eye Res.*, vol. 77, no. 4, pp. 515–524, 2003.
[72] G. A. Stern, A. Knapp, and C. I. Hood, "Corneal amyloidosis associated with keratoconus," *Ophthalmology*, vol. 95, no. 1, pp. 52–55, 1988.
[73] A. J. Bron, D. J. Lobascher, W. S. Dixon, S. N. Das, and M. Ruben, "Fibrillary lines of the cornea. A clinical sign in keratoconus.," *Br. J. Ophthalmol.*, vol. 59, no. 3, pp. 136–140, 1975.
[74] X. Li, Y. S. Rabinowitz, K. Rasheed, and H. Yang, "Longitudinal study of the normal eyes in unilateral keratoconus patients," *Ophthalmology*, vol. 111, no. 3, pp. 440–446, 2004.
[75] S. Thota, W. L. Miller, and J. P. G. Bergmanson, "Acute corneal hydrops: A case report including confocal and histopathological considerations," *Contact Lens Anterior Eye*, vol. 29, no. 2, pp. 69–73, 2006.
[76] D. G. Brodland and G. B. Bartley, "Kayser-Fleischer Rings in a Patient with Basal Cell Carcinoma: Fo~tuitous Diagnosis ofPresymptomatic Wilson's Disease," *Mayo Clin. Proc.*, vol. 67, no. 2, pp. 142–143, 1992.
[77] M. Romero-Jiménez, J. Santodomingo-Rubido, and J. S. Wolffsohn, "Keratoconus: A review," *Contact Lens Anterior Eye*, vol. 33, no. 4, pp. 157–166, 2010.
[78] J. Colin, B. Cochener, G. Savary, and F. Malet, "Correcting keratoconus with intracorneal rings," *J. Cataract Refract. Surg.*, vol. 26, no. 8, pp. 1117–1122, 2000.
[79] J. L. Alió, M. H. Shabayek, and A. Artola, "Intracorneal ring segments for keratoconus correction:

Long-term follow-up," *J. Cataract Refract. Surg.*, vol. 32, no. 6, pp. 978–985, 2006.
[80] K. M. Wang, A. S. Jun, J. G. Ladas, A. A. Siddiqui, F. Woreta, and D. Srikumaran, "Accuracy of intraocular lens formulas in eyes with keratoconus," *Am. J. Ophthalmol.*, vol. 212, pp. 26–33, 2020.
[81] R. R. Krueger and A. J. Kanellopoulos, "Stability of simultaneous topography-guided photorefractive keratectomy and riboflavin/UVA cross-linking for progressive keratoconus: case reports," *J. Refract. Surg.*, vol. 26, no. 10, p. S827, 2010.
[82] G. Wollensak, E. Spoerl, and T. Seiler, "Riboflavin/ultraviolet-a–induced collagen crosslinking for the treatment of keratoconus," *Am. J. Ophthalmol.*, vol. 135, no. 5, pp. 620–627, 2003.
[83] R. Shetty *et al.*, "Characterization of Corneal Epithelial Cells in Keratoconus," *TVST*, vol. 8, no. 1, p. Article 2, 2019.
[84] Y. Yang, F. Wang, Z. Wu, and Y. Xing, "TNF-α Stimulates MMP-2 and MMP-9 Activities in Human Corneal Epithelial Cells via the Activation of FAK / ERK Signaling," *Ophthalmic Res*, vol. 48, pp. 165–170, 2012.
[85] M. Wolf, S. M. Clay, C. E. Oldenburg, J. Rose-nussbaumer, G. David, and M. F. Chan, "Overexpression of MMPs in corneas requiring penetrating and deep anterior lamellar keratoplasty," *IVOS*, vol. 60, no. 5, pp. 1734–1747, 2019.
[86] R. A. Laing, M. M. Sandstrom, A. R. Berrospi, and H. M. Leibowitz, "The Human Corneal Endothelium in Keratoconus: A Specular Microscopic Study," *Arch. Ophthalmol.*, vol. 97, no. 10, pp. 1867–1869, Oct. 1979.
[87] E. Sykakis, F. Carley, L. Irion, J. Denton, and M. C. Hillarby, "An in depth analysis of histopathological characteristics found in keratoconus," *Pathology*, vol. 44, no. 3, p. 234, 2012.
[88] T. T. Andreassen, J. Simonsen, H. Oxlund, A. Kommunehospital, and D.-A. C, "Biomeehanieal Properties of Keratoeonus and Normal Corneas Institute of Anatomy C, University of Aarhus, and Department of Ophthalmology," *Exp. Eye Res.*, vol. 31, pp. 435–441, 1980.
[89] G. Scarcelli, S. Besner, R. Pineda, and S. H. Yun, "Biomechanical Characterization of Keratoconus Corneas Ex Vivo with Brillouin Microscopy," *IOVS*, vol. 55, no. 7, pp. 4490–4495, 2014.
[90] R. D. Johnson, M. T. Nguyen, N. Lee, and D. R. Hamilton, "Corneal Biomechanical Properties in Normal Cornea, Forme Fruste Keratoconus , and Manifest Keratoconus After Statistical Correction for Potentially Confounding Factors," *Cornea*, vol. 30, no. 5, pp. 516–523, 2011.
[91] J. Cui, X. Zhang, Q. Hu, W. Zhou, and F. Yang, "Evaluation of Corneal Thickness and Volume Parameters of Subclinical Keratoconus Using a Pentacam Scheimflug System Evaluation of Corneal Thickness and Volume Parameters of Subclinical Keratoconus Using a Pentacam Scheimflug System," *Curr. Eye Res.*, vol. 41, no. 7, pp. 923–926, 2016.
[92] N. Morishige, K. Magome, A. Ueno, T. Matsui, and T. Nishida, "Relations Among Corneal Curvature , Thickness , and Volume in Keratoconus as Evaluated by Anterior Segment – Optical Coherence Tomography," *IOVS*, vol. 60, no. 12, pp. 3794–3802, 2019.
[93] K. Hashemi, "Topographic changes simulating keratoconus in patients with irregular inferior epithelial thickening documented by anterior segment optical coherence tomography," *Clin. Ophthalmol.*, vol. 13, pp. 2103–2110, 2019.
[94] O. Sandali *et al.*, "Fourier-Domain Optical Coherence Tomography Imaging in Keratoconus: A Corneal Structural Classification," *Ophthalmology*, vol. 120, no. 12, pp. 2403–2412, 2013.
[95] S. Somodi, C. Hahnel, C. Slowik, A. Richter, D. G. Weiss, and R. Guthoff, "Confocal in vivo microscopy and confocal laser-scanning fluorescence microscopy in keratoconus," *Ger. J. Ophthalmol.*, vol. 5, no. 6, pp. 518–525, 1996.
[96] C. Amit, P. Padmanabhan, J. Narayanan, T. Nadu, T. Nadu, and T. Nadu, "Deciphering the mechanoresponsive role of β-catenin in Keratoconus epithelium," *Biorix*, 2019.
[97] K. Nielsen and K. Birkenkamp-demtro, "Identification of Differentially Expressed Genes in Keratoconus Epithelium Analyzed on Microarrays," *IOVS*, vol. 44, no. 6, pp. 2466–2476, 2003.
[98] N. Erbakan, "corneal confocal microscopic analysis in patients with keratoconus," *Int J Ophthalmol*, vol. 8, no. 3, pp. 534–539, 2014.
[99] H. Kaya, A. Çavuşoğlu, H. B. Çakmak, B. Şen, and E. Çalık, "Chapter 31 - Keratoconus Disease and Three-Dimensional Simulation of the Cornea throughout the Process of Cross-Linking Treatment," in *Emerging Trends in Computer Science and Applied Computing*, Q. N. Tran and H. B. T.-E. T. in C. B. Arabnia Bioinformatics, and Systems Biology, Eds. Boston: Morgan Kaufmann, 2015, pp. 561–575.
[100] S. Pantanelli, S. MacRae, T. M. Jeong, and G. Yoon, "Characterizing the wave aberration in eyes with keratoconus or penetrating keratoplasty using a high–dynamic range wavefront sensor," *Ophthalmology*, vol. 114, no. 11, pp. 2013–2021, 2007.
[101] H. Oxlund and A. H. Simonsen, "Biochemical studies of normal and keratoconus corneas," *Acta Ophthalmol.*, vol. 63, pp. 666–669, 1985.

[102] M. Matsuda, T. Suda, and R. Manabe, “Quantitative Analysis of Endothelial Mosaic Pattern Changes in Anterior Keratoconus,” *Am. J. Ophthalmol.*, vol. 98, no. 1, pp. 43–49, 1984.
[103] C. W. Sturbaum and J. Peiffer R.L., “Pathology of Corneal Endothelium in Keratoconus,” *Ophthalmologica*, vol. 206, no. 4, pp. 192–208, 1993.
[104] D. Press, “Association of fluorescein anterior corneal mosaic and corneal K-structures by in vivo laser confocal microscopy in patients with keratoconus,” *Clin. Ophthalmol.*, vol. 11, pp. 1359–1363, 2017.
[105] T. Fukuchi, B. Y. J. T. Yue, J. Sugar, and S. Lam, “Lysosomal enzyme activities in conjunctival tissues of patients with keratoconus,” *Arch. Ophthalmol.*, vol. 112, no. 10, pp. 1368–1374, 1994.
[106] S. C. Pflugfelder *et al.*, “Matrix Metalloproteinase-9 Knockout Confers Resistance to Corneal Epithelial Barrier Disruption in Experimental Dry Eye,” *Am. J. Pathol.*, vol. 166, no. 1, pp. 61–71, 2005.
[107] S. Sawaguchi, B. Y. J. T. Yue, J. Sugar, and J. E. Gilboy, “Lysosomal enzyme abnormalities in keratoconus,” *Arch. Ophthalmol.*, vol. 107, no. 10, pp. 1507–1510, 1989.
[108] K. Kimura, S. Teranishi, K. Fukuda, K. Kawamoto, and T. Nishida, “Delayed Disruption of Barrier Function in Cultured Human Corneal Epithelial Cells Induced by Tumor Necrosis Factor-α in a Manner Dependent on NF-κB,” *Invest. Ophthalmol. Vis. Sci.*, vol. 49, no. 2, pp. 565–571, Feb. 2008.
[109] A. J. Bron and Y. S. Rabinowitz, “Corneal dystrophies and keratoconus.,” *Curr. Opin. Ophthalmol.*, vol. 7, no. 4, pp. 71–82, 1996.
[110] S. E. Wilson *et al.*, “Epithelial injury induces keratocyte apoptosis: hypothesized role for the interleukin-1 system in the modulation of corneal tissue organization and wound healing,” *Exp. Eye Res.*, vol. 62, no. 4, pp. 325–338, 1996.
[111] Z. Gatzioufas and B. Seitz, “Determination of corneal biomechanical properties in vivo : a review Determination of corneal biomechanical properties in vivo : a review,” *Mater. Sci. Technol.*, vol. 31, no. 2, pp. 188–196, 2015.
[112] E. R. Mikula, J. V Jester, and T. Juhasz, “Measurement of an Elasticity Map in the Human Cornea,” *IOVS*, vol. 57, no. 7, pp. 3282–3286, 2016.
[113] D. A. Luce, “Determining in vivo biomechanical properties of the cornea with an ocular response analyzer,” *J Cataract Refract SURG*, vol. 31, pp. 156–162, 2004.
[114] A. Gefen, R. Shalom, D. Elad, and Y. Mandel, “Biomechanical analysis of the keratoconic cornea,” *J. Mech. Behav. Biomed. Mater.*, vol. 2, no. 3, pp. 224–236, 2009.
[115] A. Saad, Y. Lteif, E. Azan, D. Gatinel, and P. U. Measuring, “Biomechanical Properties of Keratoconus Suspect Eyes AND,” *IOVS*, vol. 51, no. 6, pp. 2912–2916, 2009.
[116] E. Mikula *et al.*, “Axial mechanical and structural characterization of keratoconus corneas,” *Exp. Eye Res.*, vol. 175, pp. 14–19, 2018.
[117] K. Kamiya, M. Hagishima, F. Fujimura, and K. Shimizu, “Factors affecting corneal hysteresis in normal eyes,” *Graefe’s Arch. Clin. Exp. Ophthalmol.*, vol. 246, no. 10, p. 1491, 2008.
[118] J. L. Alio, R. I. Barraquer, and R. Michael, “Aberrometry in Keratoconus : An Integrated Study,” *IOVS*, vol. 51, no. 4, pp. 1948–1955, 2010.
[119] C. Edmund, “Corneal elasticity and ocular rigidity in normal and keratoconic eyes,” *Acta Ophthamologica*, vol. 66, pp. 134–140, 1988.
[120] C. Kirwan, O. Malley, and M. O. Keefe, “Corneal Hysteresis and Corneal Resistance Factor in Keratoectasia : Findings Using the Reichert Ocular Response Analyzer,” *Ophthalmologica*, vol. 222, pp. 334–337, 2008.
[121] J. W. Foster, R. R. Jones, C. A. Bippes, R. M. Gouveia, and C. J. Connon, “Differential nuclear expression of Yap in basal epithelial cells across the cornea and substrates of differing stiffness,” *Exp. Eye Res.*, vol. 127, pp. 37–41, 2014.
[122] S. Molladavoodi, H. J. Kwon, J. Medley, and M. Gorbet, “Human corneal epithelial cell response to substrate stiffness,” *Acta Biomater.*, vol. 11, no. 1, pp. 324–332, 2015.
[123] S. Molladavoodi, M. Robichaud, D. Wulff, and M. Gorbet, “Corneal epithelial cells exposed to shear stress show altered cytoskeleton and migratory behaviour,” *PLoS One*, vol. 12, no. 6, pp. 1–16, 2017.
[124] F. Ridley, “Eye-rubbing contact,” *Brit. J. Ophthal.*, vol. 45, p. 631, 1961.
[125] C. W. Mcmonnies, “The Evidentiary Significance of Case Reports : Eye Rubbing and Keratoconus,” *Optom. Vis. Sci.*, vol. 85, no. 4, pp. 262–269, 2008.
[126] C. W. Mcmonnies, “Contact Lens & Anterior Eye Behaviour modification in the management of chronic habits of abnormal eye rubbing,” *Contact Lens Anterior Eye*, vol. 32, pp. 55–63, 2009.
[127] Y. L. Dorland and S. Huveneers, “Cell–cell junctional mechanotransduction in endothelial remodeling,” *Cell. Mol. Life Sci.*, vol. 74, no. 2, pp. 279–292, 2017.
[128] J.-C. Röper *et al.*, “The major β-catenin/E-cadherin junctional binding site is a primary molecular mechano-transductor of differentiation in vivo,” *Elife*, vol. 7, p. e33381, 2018.
[129] A. Totaro, T. Panciera, and S. Piccolo, “YAP/TAZ upstream signals and downstream responses,” *Nat.*

Cell Biol., vol. 20, no. 8, pp. 888–899, 2018.
[130] W. M. Petroll, M. Vishwanath, and L. Ma, "Corneal Fibroblasts Respond Rapidly to Changes in Local Mechanical Stress," *Invest. Ophthalmol. Vis. Sci.*, vol. 45, no. 10, pp. 3466–3474, Oct. 2004.
[131] I. Epithelial, M. Weliky, and G. Oster, "The mechanical basis of cell rearrangement. I. Epithelial morphogenesis during Fundulus epiboly," *Development*, vol. 109, no. 2, pp. 373–386, 1990.
[132] U. Hampel, F. Garreis, F. Burgemeister, N. Eßel, and F. Paulsen, "The Ocular Surface E ff ect of intermittent shear stress on corneal epithelial cells using an in vitro fl ow culture model ☆," *Ocul. Surf.*, vol. 16, no. 3, pp. 341–351, 2018.
[133] J. R. Mackley, J. Ando, P. Herzyk, and S. J. Winder, "Phenotypic responses to mechanical stress in fibroblasts from tendon, cornea and skin," *Biochem. J.*, vol. 396, no. 2, pp. 307–316, May 2006.
[134] T. Utsunomiya *et al.*, "Transforming Growth Factor-β Signaling Cascade Induced by Mechanical Stimulation of Fluid Shear Stress in Cultured Corneal Epithelial Cells," *Invest. Ophthalmol. Vis. Sci.*, vol. 57, no. 14, pp. 6382–6388, Nov. 2016.
[135] S. M. Hart, G. D. Degen, J. Manuel, U. Padraic, P. L. W. Gregory, and A. A. Pitenis, "Friction - Induced Apoptosis," *Tribol. Lett.*, vol. 67, no. 3, pp. 1–12, 2019.
[136] H. Ren and G. Wilsonf, "Apoptosis in the Corneal Epithelium," *Invest. Ophthalmol. Vis. Sci.*, vol. 37, no. 6, pp. 1017–1025, 1996.
[137] R. J. Pelham and Y. Wang, "Cell locomotion and focal adhesions are regulated by substrate flexibility," *Proc. Natl. Acad. Sci.*, vol. 94, no. 25, pp. 13661–13665, 1997.
[138] X. Y. Wu, K. K. H. Svoboda, and V. Trinkaus-Randall, "Distribution of F-actin, vinculin and integrin subunits (alpha6 and beta4) in response to corneal substrata," *Exp. Eye Res.*, vol. 60, no. 4, pp. 445–458, 1995.
[139] R. R. Jones, I. W. Hamley, and C. J. Connon, "Ex vivo expansion of limbal stem cells is affected by substrate properties," *Stem Cell Res.*, vol. 8, no. 3, pp. 403–409, 2012.
[140] E. Optom, "Keratoconus, allergy, itch, eye-ru bbing and hand-dominance," *Clin Exp Optom*, vol. 86, no. 6, pp. 376–384, 2003.
[141] C. W. Mcmonnies, "Mechanisms of Rubbing-Related Corneal Trauma in Keratoconus," *Cornea*, vol. 28, no. 6, pp. 607–615, 2009.
[142] Y. S. Rabinowitz, A. B. Nesburn, and P. J. McDonnell, "Videokeratography of the fellow eye in unilateral keratoconus," *Ophthalmology*, vol. 100, no. 2, pp. 181–186, 1993.
[143] R. J. Harrison, P. T. Klouda, D. L. Easty, M. Manku, J. Charles, and C. M. Stewart, "Association between keratoconus and atopy.," *Br. J. Ophthalmol.*, vol. 73, no. 10, pp. 816–822, 1989.
[144] A. J. Bron, *Wolff's Anatomy of the Eye and Orbit*, vol. 223. London: Chapman & Hall Medical, 1997, 1997.
[145] J. C. Fan Gaskin, W. R. Good, C. A. Jordan, D. V Patel, and C. N. J. McGhee, "The Auckland keratoconus study: identifying predictors of acute corneal hydrops in keratoconus," *Clin. Exp. Optom.*, vol. 96, no. 2, pp. 208–213, 2013.
[146] Charlaas, "Eye rubbing and Keratoconus," *Charlaas Optometry*, 2013. [Online]. Available: https://www.charllaas.com/eye-rubbing-keratoconus/. [Accessed: 14-Sep-2020].
[147] C. W. Mcmonnies, "OPTOMETRY," *Clin. Exp. Optom. 99.4*, vol. 99, no. July, pp. 366–372, 2016.
[148] D. R. Korb, C. D. Leahy, and J. V Greiner, "Prevalence and characteristics of eye-rubbing for keratoconic and non-keratoconic subjects," in *Investigative Ophthalmology & Visual Science*, 1991, vol. 32, no. 4, p. 884.
[149] A. Mazharian *et al.*, "Incorrect sleeping position and eye rubbing in patients with unilateral or highly asymmetric keratoconus: a case-control study," *Graefe's Arch. Clin. Exp. Ophthalmol.*, pp. 1–9, 2020.
[150] F. Hafezi *et al.*, "Assessment of the mechanical forces applied during eye rubbing," *BMC Ophthalmol.*, vol. 20, no. 301, pp. 1–5, 2020.
[151] C. W. McMonnies and G. C. Boneham, "Corneal responses to intraocular pressure spikes in keratoconus," *Cornea*, vol. 29, no. 7, pp. 764–770, 2010.
[152] J. T. Ernest, T. K. Goldstick, M. A. Stein, and J. D. Zheutlin, "Ocular massage before cataract surgery." *Trans. Am. Ophthalmol. Soc.*, vol. 83, p. 205, 1985.
[153] T. Bettahar, C. Rahmoune, and D. Benazzouz, "Keratoconus prognosis study for patients with corneal external mechanical stress mode," *Int. Ophthalmol.*, vol. 2, no. 72, 2020.
[154] C. D. Leahy, J. V Greiner, E. Hebert, L. Hanninen, K. R. Kenyon, and D. R. Korb, "The effects of eye rubbing on the ocular surface," *Invest Ophthalmol Vis Sci*, vol. 31, pp. 208–231, 1990.
[155] A. H. E. Lsheikh, D. E. F. U. W. Ang, A. A. K. Otecha, M. I. B. Rown, and D. A. G. A. Eath, "Evaluation of Goldmann Applanation Tonometry Using a Nonlinear Finite Element Ocular Model," *Ann. Biomed. Eng.*, vol. 34, no. 10, pp. 1628–1640, 2006.

[156] A. Elsheikh, D. Wang, A. Elsheikh, and D. Wang, "Computer Methods in Biomechanics and Biomedical Engineering Numerical modelling of corneal biomechanical behaviour Numerical modelling of corneal biomechanical behaviour †," *Comput. Methods Biomech. Biomed. Engin.*, vol. 10, no. 2, pp. 85–95, 2011.
[157] H. D. Conway and M. W. Richman, "The effects of contact lens deformation on tear film pressure and thickness during motion of the lens towards the eye," *J. Biomech. Eng.*, vol. 105, no. 1, p. 47, 1983.
[158] C. Liu, P. Feng, X. Li, J. Song, and W. Chen, "Expression of MMP-2 , MT1-MMP , and TIMP-2 by cultured rabbit corneal fibroblasts under mechanical stretch," *Exp. Biol. Med.*, vol. 239, pp. 907–912, 2014.
[159] P. Feng *et al.*, "Combined effects of interleukin - 1β and cyclic stretching on metalloproteinase expression in corneal fibroblasts in vitro," *Biomed. Eng. Online*, vol. 15, no. 63, pp. 1–10, 2016.
[160] O. Chaudhuri, S. H. Parekh, W. A. Lam, and D. A. Fletcher, "Combined atomic force microscopy and side-view optical imaging for mechanical studies of cells," *Nat. Methods*, vol. 6, no. 5, pp. 383–387, 2009.
[161] Y. Tan, D. Sun, S. Member, J. Wang, and W. Huang, "Mechanical Characterization of Human Red Blood Cells under Different Osmotic Conditions by Robotic Manipulation With Optical Tweezers," vol. 57, no. 7, pp. 1816–1825, 2010.
[162] N. J. Sniadecki, C. M. Lamb, Y. Liu, C. S. Chen, D. H. Reich, and D. H. Reich, "Magnetic microposts for mechanical stimulation of biological cells : Fabrication , characterization , and analysis Fabrication , characterization , and analysis," vol. 044302, no. April, 2008.
[163] J. P. Vande Geest, E. S. Di Martino, and D. A. Vorp, "An analysis of the complete strain field within FlexercellTM membranes," *J. Biomech.*, vol. 37, no. 12, pp. 1923–1928, 2004.
[164] S. Higgins, J. S. Lee, L. Ha, and J. Y. Lim, "Inducing neurite outgrowth by mechanical cell stretch," *Biores. Open Access*, vol. 2, no. 3, pp. 212–216, 2013.
[165] S. Dhein *et al.*, "Mechanical control of cell biology. Effects of cyclic mechanical stretch on cardiomyocyte cellular organization," *Prog. Biophys. Mol. Biol.*, vol. 115, no. 2, pp. 93–102, 2014.
[166] H. Kamble, M. J. Barton, M. Jun, S. Park, and N.-T. Nguyen, "Cell stretching devices as research tools: engineering and biological considerations," *Lab Chip*, vol. 16, no. 17, pp. 3193–3203, 2016.
[167] Y. Cui *et al.*, "Cyclic stretching of soft substrates induces spreading and growth," *Nat. Commun.*, vol. 6, pp. 1–8, 2015.
[168] Y. J. Heo, T. Kan, E. Iwase, K. Matsumoto, and I. Shimoyama, "Stretchable cell culture platforms using micropneumatic actuators," *Micro Nano Lett.*, vol. 8, no. 12, pp. 865–868, 2013.
[169] K. Sato, S. Kamada, and K. Minami, "Development of microstretching device to evaluate cell membrane strain field around sensing point of mechanical stimuli," *Int. J. Mech. Sci.*, vol. 52, no. 2, pp. 251–256, 2010.
[170] C. P. Ursekar, S. K. Teo, H. Hirata, I. Harada, K. H. Chiam, and Y. Sawada, "Design and construction of an equibiaxial cell stretching system that is improved for biochemical analysis," *PLoS One*, vol. 9, no. 3, 2014.
[171] G. Nava *et al.*, "All-silica microfluidic optical stretcher with acoustophoretic prefocusing," *Microfluid. Nanofluidics*, vol. 19, no. 4, pp. 837–844, 2015.
[172] L. Wang, Y. Wang, and S. Ran, "Yang G," *J. Electron Spectrosc. Relat. Phenom.*, vol. 2009, p. 173, 2009.
[173] "Induction of MMP-1 and -3 by cyclical mechanical stretch is mediated by IL-6 in cultured fibroblasts of keratoconus," *Mol. Med. Rep.*, vol. 15, pp. 3885–3892, 2017.
[174] A. Medina, "Method of altering the shape of the cornea," 5,690,123, 1997.
[175] A. M. T. Quinlan, L. N. Sierad, A. K. Capulli, L. E. Firstenberg, and L. Kristen, "Combining Dynamic Stretch and Tunable Stiffness to Probe Cell Mechanobiology In Vitro," *PlosOne*, vol. 6, no. 8, p. e23272, 2011.
[176] "FlexCell Compression Systems," *Corporation, Flexcell® International*. [Online]. Available: https://www.flexcellint.com/category/compression%0A.
[177] J. Shi, M. Folwaczny, and A. Wichelhaus, "Differences in RUNX2 and P2RX7 gene expression between mono - and coculture of human periodontal ligament cells and human osteoblasts under compressive force application," vol. 2, no. February, pp. 168–176, 2019.
[178] S. Grimm *et al.*, "Influence of clodronate and compressive force on IL-1ß-stimulated human periodontal ligament fibroblasts," pp. 343–350, 2020.
[179] G. Hossain *et al.*, "Compressive force inhibits adipogenesis through COX-2-mediated down-regulation of PPAR γ 2 and C / EBP α," vol. 109, no. 3, pp. 297–303, 2010.
[180] Y. Iwawaki *et al.*, "MiR-494-3p induced by compressive force inhibits cell proliferation in," *J. Biosci. Bioeng.*, vol. 120, no. 4, pp. 456–462, 2015.

[181] L. Chen, “Compressive force-induced autophagy in periodontal ligament cells downregulates osteoclastogenesis during tooth movement,” no. January, pp. 1170–1181, 2019.
[182] K. Damodaran, S. Venkatachalapathy, F. Alisafaei, A. V Radhakrishnan, and V. M. Weaver, “Compressive force induces reversible chromatin condensation and cell geometry – dependent transcriptional response,” vol. 29, pp. 3039–3051, 2018.
[183] B. G. Kim *et al.*, “Mechanical compression induces VEGFA overexpression in breast cancer via DNMT3A-dependent miR-9 downregulation,” pp. 1–12, 2017.
[184] H. Hatami-marbini and E. Etebu, “An experimental and theoretical analysis of uncon fi ned compression of corneal stroma,” *J. Biomech.*, vol. 46, no. 10, pp. 1752–1758, 2013.
[185] H. Hatami-marbini and E. Etebu, “Rate dependent biomechanical properties of corneal stroma in unconfined compression,” vol. 50, pp. 133–147, 2013.
[186] Y. Klymenko *et al.*, “Modeling the effect of ascites-induced compression on ovarian cancer multicellular aggregates,” *Dis. Model. Mech.*, vol. 11, no. 9, p. dmm034199, Sep. 2018.
[187] R. A. Blanton, N. Perez-reyes, D. T. Merrick, and J. K. Mcdougall, “Epithelial Cells Immortalized by Human Papillomaviruses Have Premalignant Characteristics in Organotypic Culture,” vol. 138, no. 3, pp. 673–685, 1991.
[188] M. Akinbola, S. Esmail, U. Mbanefo, and T. Sebastiampillai, “In-Vitro Mechanical Model for Keratoconus,” *FYDP report, Univ. Waterloo*, 2019.
[189] S. Seriani *et al.*, “The cell-stretcher: A novel device for the mechanical stimulation of cell populations,” *Rev. Sci. Instrum.*, vol. 87, no. 8, 2016.
[190] H. J. Kim, Y. H. Seo, and B. H. Kim, “New intraocular pressure measurement method using reflected pneumatic pressure from cornea deformed by air puff of ring-type nozzle,” *PLoS One*, vol. 12, no. 12, p. e0186738, 2017.
[191] E. Roan, C. M. Waters, B. Teng, M. Ghosh, and A. Schwingshackl, “The 2-pore domain potassium channel TREK-1 regulates stretch-induced detachment of alveolar epithelial cells,” *PLoS One*, vol. 9, no. 2, p. e89429, 2014.
[192] N. J. Douville *et al.*, “Combination of fluid and solid mechanical stresses contribute to cell death and detachment in a microfluidic alveolar model,” *Lab Chip*, vol. 11, no. 4, pp. 609–619, 2011.
[193] S. Chen *et al.*, “RIPK1/RIPK3/MLKL-mediated necroptosis contributes to compression-induced rat nucleus pulposus cells death,” *Apoptosis*, vol. 22, no. 5, pp. 626–638, 2017.
[194] R. G. M. B. Reuls, C. V. C. B. Outen, C. W. J. O. Omens, D. L. B. Ader, and F. P. T. B. Aaijens, “Compression Induced Cell Damage in Engineered Muscle Tissue : An In Vitro Model to Study Pressure Ulcer Aetiology,” *Annu. Biomed. Eng.*, vol. 31, pp. 1357–1364, 2003.
[195] W. Xu *et al.*, “Increased production of reactive oxygen species contributes to motor neuron death in a compression mouse model of spinal cord injury,” *Spinal Cord*, vol. 43, no. 4, pp. 204–213, 2005.
[196] Z. Fan *et al.*, “The Protective Effect of Salvianolic Acid B on Blood – Spinal Cord Barrier After Compression Spinal Cord Injury in Rats,” *J Mol Neurosci*, vol. 51, pp. 986–993, 2013.
[197] D. Yu *et al.*, “Curcumin improves the integrity of blood–spinal cord barrier after compressive spinal cord injury in rats,” *J. Neurol. Sci.*, vol. 346, no. 1, pp. 51–59, 2014.
[198] J. Shimazaki, S. Shimmura, K. Mochizuki, and K. Tsubota, “Morphology and barrier function of the corneal epithelium after penetrating keratoplasty: association with original diseases, tear function, and suture removal,” *Cornea*, vol. 18, no. 5, pp. 559–564, 1999.
[199] L. Gui, D. M, and B. GREGER, “Apoptosis and Expression of Bcl-2 after Compression Trauma to Rat Spinal Cord,” *J. Neuropathol. Exp. Neurol.*, vol. 55, no. 3, pp. 280–289, 1996.
[200] R. Gupta and O. Steward, “Chronic Nerve Compression Induces Concurrent Apoptosis and Proliferation of Schwann Cells,” *J. Comp. Neurol.*, vol. 186, no. 461, pp. 174–186, 2003.
[201] A. M. Loening *et al.*, “Injurious mechanical compression of bovine articular cartilage induces chondrocyte apoptosis,” *Arch. Biochem. Biophys.*, vol. 381, no. 2, pp. 205–212, 2000.
[202] F. Ding and Z. S. S. Yang, “Role of mitochondrial pathway in compression-induced apoptosis of nucleus pulposus cells,” *Apoptosis*, vol. 17, pp. 579–590, 2012.
[203] S. E. Wilson, “Role of Apoptosis in Wound Healing in the Cornea,” *Cornea*, vol. 19, no. 3, 2000.
[204] C. Biology, “Epithelial Injury Induces Keratocyte Apoptosis : Hypothesized Role for the Interleukin-1 System in the Modulation of Corneal Tissue Organization and Wound Healing,” pp. 325–337, 1996.
[205] C. Gung, M. Hospital, M. Sciences, and G. Medicine, “Interleukin-1 Receptor Antagonist (IL-1RA) Prevents Apoptosis in Ex Vivo Expansion of Human Limbal Epithelial Cells Cultivated on Human Amniotic Membrane,” *StemCells*, vol. 2118800, pp. 2130–2139, 2006.
[206] M. M. Knight, T. Toyoda, D. A. Lee, and D. L. Bader, “Mechanical compression and hydrostatic pressure induce reversible changes in actin cytoskeletal organisation in chondrocytes in agarose,” *J. Biomech.*, vol. 39, pp. 1547–1551, 2006.

[207] Y.-B. Li, R. Xu, C. Liu, N. Shen, L.-B. Han, and D. Tang, “Magnaporthe oryzae fimbrin organizes actin networks in the hyphal tip during polar growth and pathogenesis,” *PLoS Pathog.*, vol. 16, no. 3, p. e1008437, 2020.
[208] J. D. Winkelman *et al.*, “Fascin-and α-actinin-bundled networks contain intrinsic structural features that drive protein sorting,” *Curr. Biol.*, vol. 26, no. 20, pp. 2697–2706, 2016.
[209] M. Lenz, T. Betz, J. Manzi, J. Martiel, M. Safouane, and R. Florian, “Adaptive Response of Actin Bundles under Mechanical Stress,” *Biophys. J.*, vol. 113, pp. 1072–1079, 2017.
[210] C. Heussinger and B. Gentry, “Transiently crosslinked F-actin bundles,” *Eur Biophys J*, vol. 40, pp. 93–101, 2011.
[211] X. Gao *et al.*, “Probing compression versus stretch activated recruitment of cortical actin and apical junction proteins using mechanical stimulations of suspended doublets,” *APL Bioeng.*, vol. 2, no. 2, p. 26111, 2018.
[212] M. A. Odenwald *et al.*, “EDITORS ’ PICK cro The scaffolding protein ZO-1 coordinates actomyosin and epithelial apical specializations in vitro and in vivo,” *J. Biol. Chem*, vol. 293, no. 45, pp. 17317–17335, 2018.
[213] A. S. Fanning, T. Y. Ma, and J. M. Anderson, “Isolation and functional characterization of the actin binding region in the tight junction protein ZO-1,” no. 1, 2002.
[214] M. Itoh, A. Nagafuchi, S. Moroi, and S. Tsukita, “Involvement of ZO-1 in cadherin-based cell adhesion through its direct binding to α catenin and actin filaments,” *J. Cell Biol.*, vol. 138, no. 1, pp. 181–192, 1997.
[215] R. Etournay, I. Zwaenepoel, I. Perfettini, P. Legrain, C. Petit, and A. El-amraoui, “directly interacts with ZO-1 at tight junctions,” pp. 2838–2850, 2007.
[216] S. Citi, “The mechanobiology of tight junctions,” pp. 783–793, 2019.
[217] A. S. Fanning, B. J. Jameson, L. A. Jesaitis, and J. Melvin, “The Tight Junction Protein ZO-1 Establishes a Link between the Transmembrane Protein Occludin and the Actin Cytoskeleton *,” vol. 273, no. 45, pp. 29745–29753, 1998.
[218] G.-R. Ding *et al.*, “EMP-induced alterations of tight junction protein expression and disruption of the blood–brain barrier,” *Toxicol. Lett.*, vol. 196, no. 3, pp. 154–160, 2010.
[219] C. N. T. *et al.*, “Cyclic Strain–Mediated Regulation of Vascular Endothelial Occludin and ZO-1,” *Arterioscler. Thromb. Vasc. Biol.*, vol. 26, no. 1, pp. 62–68, Jan. 2006.
[220] C. Chen, “The Effects of Electromagnetic Pulse on the Protein Levels of Tight Junction Associated-Proteins in the Cerebral Cortex, Hippocampus, Heart, Lung, and Testis of Rats,” *Biomed. Environ. Sci.*, vol. 24, no. 4, pp. 438–444, 2011.
[221] L.-B. Qiu *et al.*, “Synthetic gelatinases inhibitor attenuates electromagnetic pulse-induced blood–brain barrier disruption by inhibiting gelatinases-mediated ZO-1 degradation in rats,” *Toxicology*, vol. 285, no. 1, pp. 31–38, 2011.
[222] V. A. Smith, F. J. Matthews, M. A. Majid, and S. D. Cook, “Keratoconus : Matrix metalloproteinase-2 activation and TIMP modulation,” vol. 1762, pp. 431–439, 2006.
[223] I. Lema, T. Sobrino, J. A. Dura, D. Brea, and E. Dı, “Subclinical keratoconus and inflammatory molecules from tears,” pp. 820–824, 2009.
[224] I. Lema, “Inflammatory Molecules in the Tears of Patients with Keratoconus,” pp. 654–659, 2005.

Appendix – Codes for electric cell stretcher

```
#include <Servo.h>
Servo myservo;  // create servo object to control a servo
// twelve servo objects can be created on most boards
int pos = 82;    // initial position
stop pos = 81;
void setup() {
  myservo.attach(9);  // attaches the servo on pin 9 to the servo object
}
void loop() {
  myservo.write(pos);
}
```